AD NUMBER
AD901525
LIMITATION CHANGES
TO: **Approved for public release; distribution is unlimited.**
FROM: **Distribution authorized to U.S. Gov't. agencies only; Test and Evaluation; 14 JUL 1972. Other requests shall be referred to Naval Air Systems Command, Washington, ATTN: AIR-330E, DC 20360.**
AUTHORITY
NAVAIR ltr dtd 16 Oct 1975

DESIGN AND DEVELOPMENT OF SUPERSONIC TURBINE NOZZLES

By F. W. Lipfert and I. Fruchtman

February 1972

For the Period October 1970 - October 1971

FINAL ENGINEERING REPORT NO. 767

Prepared Under Contract N00019-71-C-0194

for the

Department of the Navy
Naval Air Systems Command
Washington, D. C. 20360

Prepared by

General Applied Science Laboratories, Inc.
An Affiliate of CCI Corporation
Merrick and Stewart Avenues
Westbury, New York 11590

[redacted]

DESIGN AND DEVELOPMENT OF SUPERSONIC TURBINE NOZZLES

By F. W. Lipfert and I. Fruchtman

February 1972

For the Period October 1970 - October 1971

FINAL ENGINEERING REPORT NO. 767

Prepared Under Contract N00019-71-C-0194

For the

Department of the Navy
Naval Air Systems Command
Washington, D. C. 20360

DISTRIBUTION LIMITED TO U.S. GOVERNMENT AGENCIES ONLY;
- ☐ FOREIGN INFORMATION
- ☐ PROPRIETARY INFORMATION
- ☒ TEST AND EVALUATION
- ☐ CONTRACTOR PERFORMANCE EVALUATIO

DATE: 7 - 14 - 72
OTHER REQUESTS FOR THIS DOCUMENT MUST BE REFERRED TO COMMANDER, NAVAL AIR SYSTEMS COMMAND, AIR-330E

Prepared by

General Applied Science Laboratories, Inc.
An Affiliate of CCI Corporation
Merrick and Stewart Avenues
Westbury, New York 11590

[redacted]

Approved by: L. M. Nucci
Louis M. Nucci
President

ABSTRACT

A nozzle (stator) component for a supersonic turbine stage has been designed and tested. The design was three-dimensional, with the nozzle exit Mach number varying from 1.68 at the hub to 2.23 at the tip, according to simple-radial-equilibrium theory. The hub/tip ratio was .83, and the aspect ratio .35, with a 1-inch blade height. The supersonic contour was based on the Busemann sharp-edged-throat concept.

The nozzle was tested over a range of pressure ratios from 1.9 to 10.5 and Reynolds numbers from $.65 \times 10^6$ to 3.8×10^6, based on exit conditions and the blade chord. A blow-down wind tunnel was used, with atmospheric discharge. The performance of the nozzle corresponded well to theoretical predictions in the regions of the exit flow that were traversed and along the walls where pressure taps were installed. The test program was terminated before a complete map of the exit flow had been obtained, because of vibratory cracks in some of the blades.

TABLE OF CONTENTS

LIST OF ILLUSTRATIONS

LIST OF ILLUSTRATIONS (continued)

LIST OF ILLUSTRATIONS (concluded)

NOMENCLATURE

A	area
ℓ	length
M	Mach number
$\dot{m}$	mass flow rate
P	pressure, blade pitch
q	dynamic pressure ($\frac{1}{2}\rho V^2$)
r	radius
S	streamwise length
T	temperature
t	probe length
u	velocity
V	velocity
x	length
δ^*	boundary layer displacement thickness
α	flow angle, from axial
β	ratio of hot/cold mass flows
γ	specific heat ratio
ν	Prandtl-Meyer angle, kinematic viscosity
ψ	angle between probe axis and stem
θ	circumferential coordinate angle
μ	Mach angle = $\sin^{-1} \sqrt{1-M}$

Subscripts

amb	ambient
c	cold
h	hot
m	mixed
o	stagnation

Subscripts

1	free stream nozzle exit
2	behind normal shock (nozzle exit)
H	hub
t	tip
u, θ	tangential
r	relative to rotor blade
x	axial

Superscripts

*	sonic conditions

I. INTRODUCTION

The supersonic turbine is well known for its high stage loading capability, and has been investigated for various applications by several authors. Its use for propulsion applications has been given new impetus by recent trends in engine technology:

- use of high bypass, high pressure ratio cycles, requiring larger work extraction from the gas generator and many turbine stages (when conventional blading is used)

- identification of the "air pump" VTOL cycle, requiring high pressure ratio tip turbines to drive lift fans

- continued striving for higher turbine inlet temperatures, emphasizing the advantage of the supersonic stage's reduced cooling air requirements and compatibility with transpiration cooling techniques.

The general design features, capabilities, application details, and cooled rotor blade cascade performance have been investigated by GASL in previous efforts supported by the Naval Air Systems Command, and are reported in References 1 to 4.

This report covers initial efforts towards the hardware development and demonstration of a supersonic turbine stage, and is concerned with the design and testing of the nozzle component for that stage.

The aerodynamic design study (Reference 1) of the supersonic turbine showed that although high performance has been measured in (previous) two-dimensional nozzle cascades, a number of problem areas associated with the blading design in a real turbine stage remained. These areas included:

a) three-dimensional blading design

b) wake mixing

c) off-design performance

d) effects of thick trailing edges

In general, these effects can only be quantified through experimental demonstration. An annular cascade was selected as the means for this demonstration; this cascade would then later serve as the stator component of the complete supersonic turbine stage to be developed.

II. TURBINE NOZZLE AERODYNAMIC DESIGN

The function of the turbine nozzle is to turn the flow and accelerate it to the desired rotor entrance velocity. In many applications, the supersonic turbine is located immediately downstream of the combustor so that the nozzle entrance flow may be taken as uniform with zero swirl.

The nozzle blade flow field is considered in three parts: a subsonic region where the bulk of the turning occurs; a constant area throat section; and finally, a supersonic section, where complete expansion occurs within the guiding walls, to prevent shock losses.

As shown in Reference 1, design of the blading must include three-dimensional effects because of the large magnitude of the design exit swirl-velocity component. It was indicated there that failure to appreciate the importance of flow property variations along the blade height was responsible for the relatively poor performance of some previous supersonic turbine designs.

Conventional turbomachine design practice assumes that a three-dimensional blade can be designed by straightforward stacking of two-dimensional segments. Three-dimensional supersonic flow computations,Reference 5, have shown that the magnitude of the generated cross flows is small for properly designed blading, thus lending credence to the concept of stacking two-dimensional blade elements. This technique was adopted for the present design.

The following sections describe these blade design techniques, the stacking method necessary to satisfy radial equilibrium, and the corrections applied to account for boundary layer build-up.

A. <u>SELECTION OF DESIGN TYPE</u>. As pointed out in the general discussion of supersonic turbine design (Reference 1), there is a premium on length and wetted area for both rotor and nozzle. The general nozzle type having minimum length features a sharp-edged throat, from which a centered, Prandtl-Meyer expansion wave emanates. This type of nozzle, shown schematically in Figure 1, has been referred to as a Busemann nozzle.

(a) Busemann sharp-edged throat nozzle

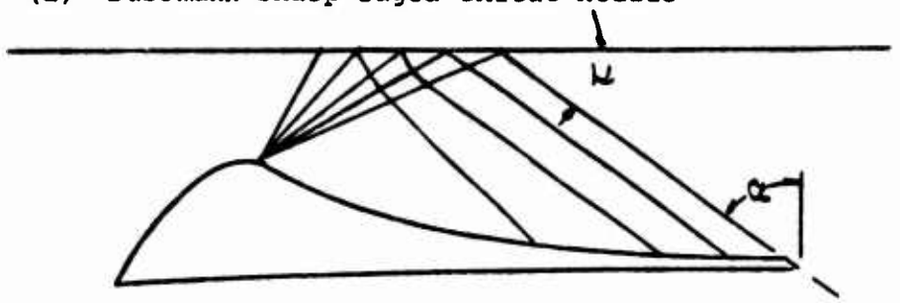

(b) Full Nozzles

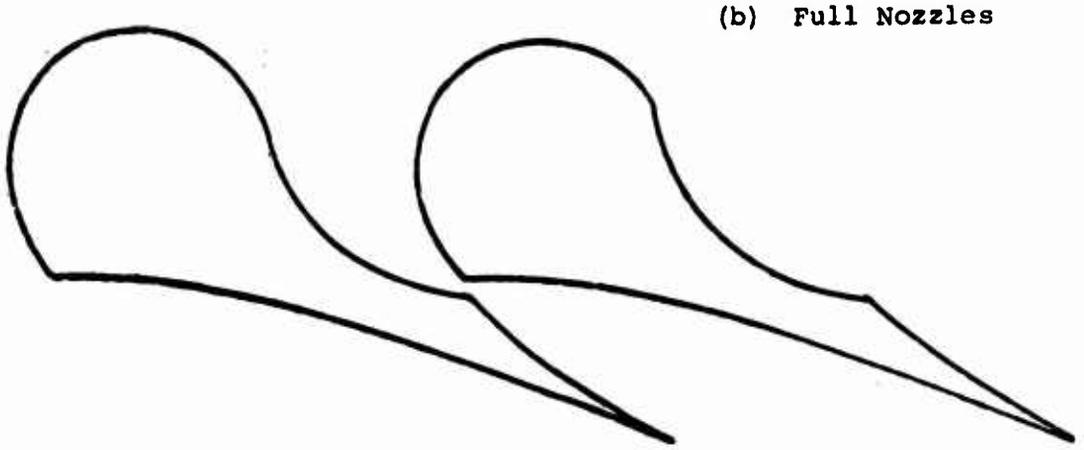

(c) Half Nozzles

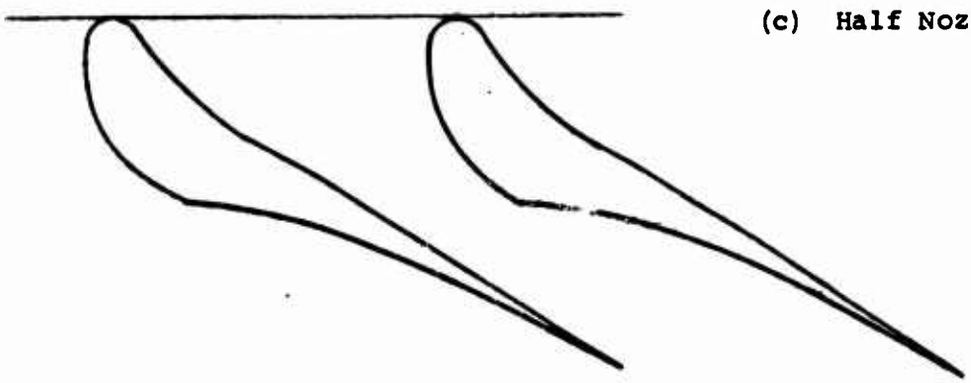

TR-767 Figure 1. - Supersonic Nozzle Design Types

However, the need to stagger the nozzles at an angle α for turbomachinery applications presents problems. In most previous works, full nozzles were used (Figure 1b) in which case the suction surface must be extended because of the stagger. In Reference 6, for example, a situation of nonuniform flow including shocks was shown to exist on this extended surface, which is also,of course, a source of additional boundary layer losses. Both of these effects are undesirable and contribute to the poor performance shown for these designs.

In contrast, use of a half-nozzle (Figure 1c) allows a shortening of the flat (pressure) surface because of stagger. This surface represents the line of symmetry for the two-dimensional full nozzle, and its limiting length is given by the location of a Mach line intersecting the adjacent blade trailing edge. Thus, when the Mach angle μ is greater than the complement of the stagger angle ($\mu > 90-\alpha$), the blade must be extended (by means of a straight addition to the contoured suction surface side).

Nevertheless, a considerable savings in nozzle length results from the use of half nozzles. Figure 2 presents the non-dimensional axial length ℓ/d^* for both full nozzles and half nozzles as a function of design Mach number and stagger angle, and length savings up to around 75% are seen.

B. TWO-DIMENSIONAL NOZZLE CONTOUR SPECIFICATION.

B.1 Subsonic Approach Region. In the blade entry region the flow must be turned to the desired swirl angle and accelerated to sonic velocity with minimum losses. Losses are generated here as a result of four main effects:

a) skin friction-profile losses

b) boundary layer separation

c) shock losses

d) secondary flows

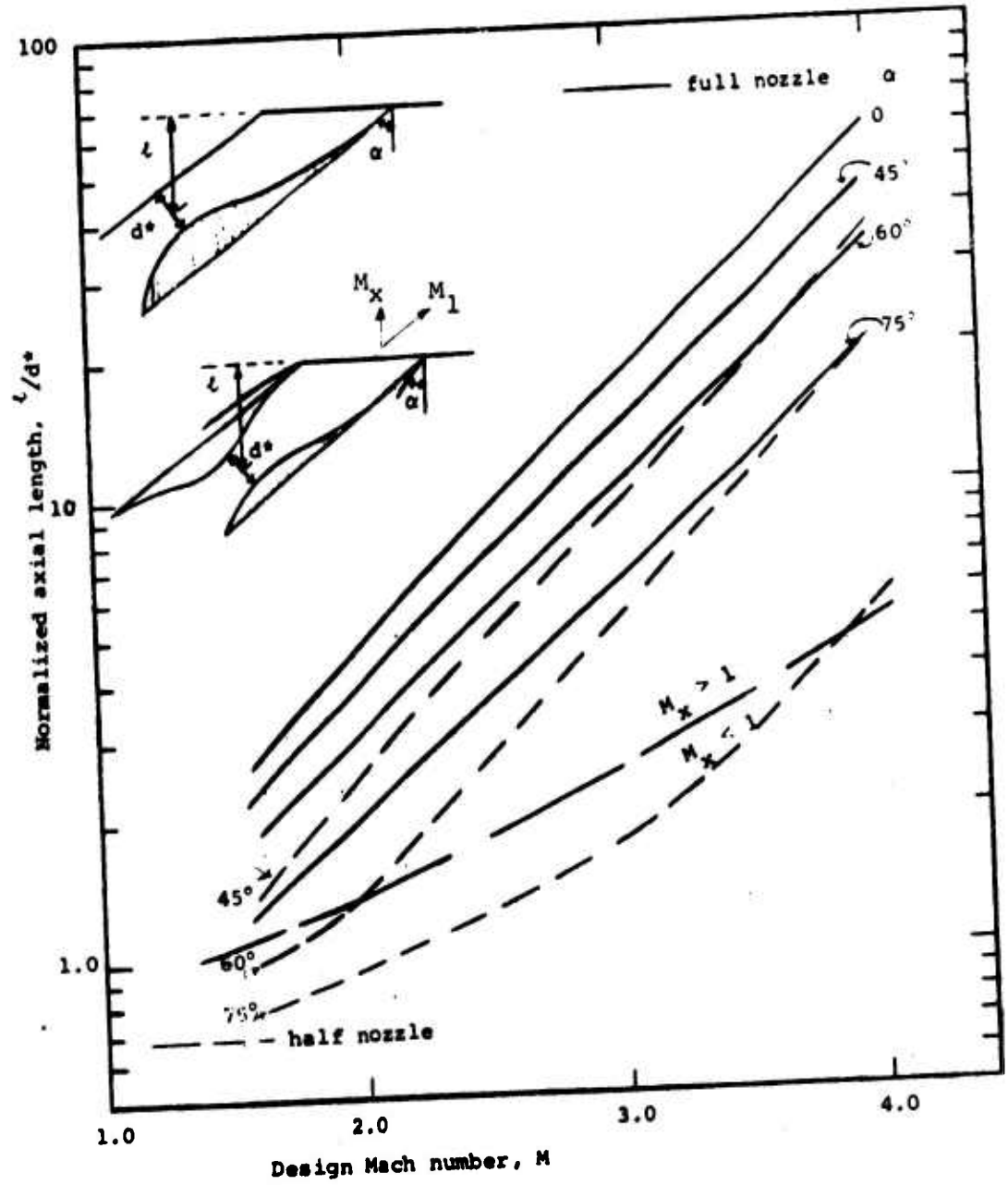

Figure 2. - Comparison of Full and Half Nozzle Length Requirements

Skin friction losses are the inevitable result of wetted surface areas; to minimize them a short profile is desired with minimum length in the high speed regions. Boundary layer separation can occur from either adverse pressure gradients (from overexpansion or shock-wave impingement) or from excessively small radii of curvature. Subsonic region shocks can only result from overexpansion. Thus the ideal subsonic contour will offer a compromise between length and radius of curvature, with particular attention to minimum curvature in the near-sonic regions (to prevent unwanted premature shock formation). Secondary flows are a function mainly of aspect ratio and hub tip ratio, and thus choice of the two-dimensional subsonic profile shape has little influence.

The contour of the blade inlet region was based on a proven blade series development described in Reference 7 . By prescribing the turning and the maximum thickness, the design procedure, described in Reference 7, allows layout of both the camber line and thickness distribution. Since only the inlet region was important for the present nozzle blade design, the referenced design technique was modified by choosing a (subsonic) turn angle much greater than desired for the final supersonic nozzle. That portion of the subsonic blade design aft of the camber angle actually desired was then replaced by the throat region and supersonic portion of the blading. Sufficient blade thickness is thus available so that the extension of the pressure surface is a straight line while the suction surface includes the entire supersonic contour. Figure 3 shows the blade features described above. It was found that prescribing the maximum thickness-to-chord ratio at 20% and turning equal to 120°, acceptable inlet blade contours resulted.

B.2 Throat Region. Design of the supersonic portion of the blade requires a straight sonic line. Among other things, this requires the existence of parallel flow with zero blade surface curvature in the throat region extending a sufficient length upstream of the throat. In order to satisfy these conditions in the present blade layout technique, a throat region with $\ell/d = 1$ was specified. This is in accordance with common wind tunnel nozzle design practice, and avoids the problem of overexpansion and shock formation, albeit at the expense of skin friction. This length then represents an element of conservatism in the blade design that might be optimized for future performance improvement.

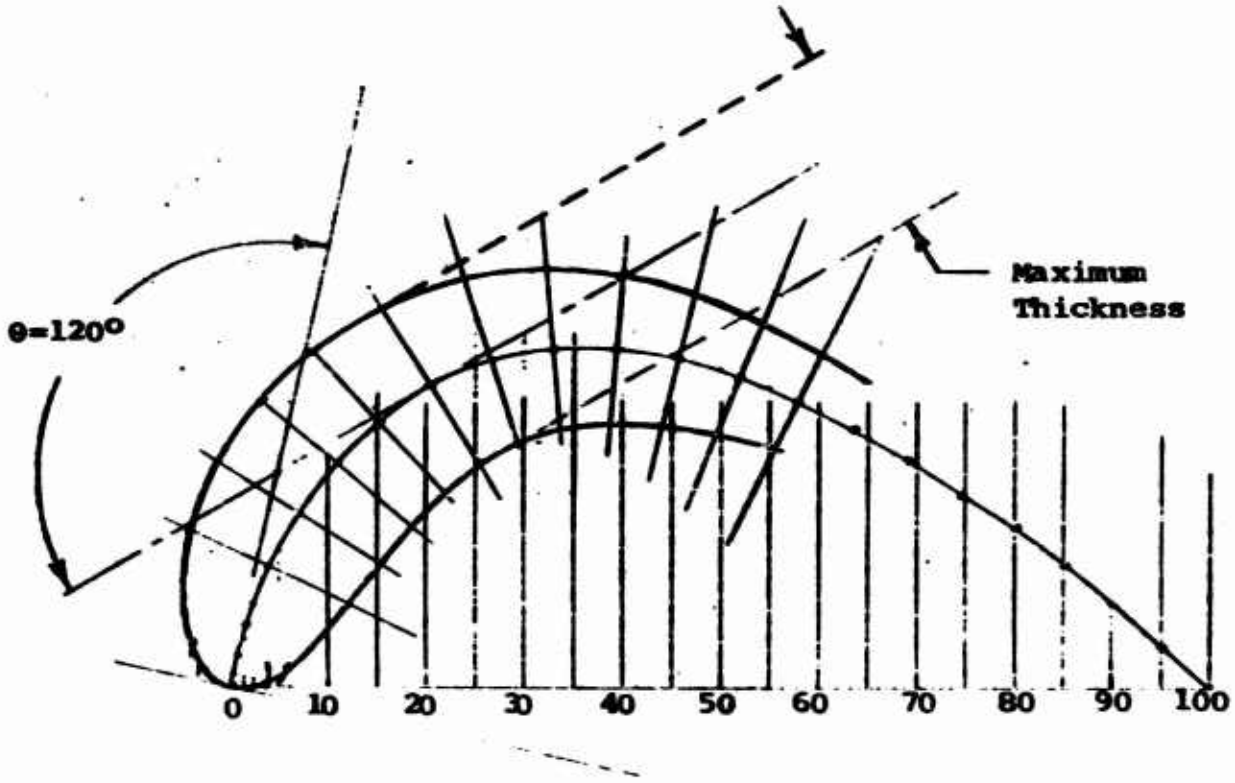

Figure 3. - Inlet Region of the Blading

B.3 Supersonic Contour. As discussed above, the sharp-edged minimum length nozzle concept was prescribed for the supersonic contour of the blading in order to minimize boundary layer build-up on the blade, hub, and shroud surfaces. The coordinates and hence layout of a nozzle are a function only of the desired exit Mach number and the specific heat ratio (for a perfect gas, which was assumed here), and have long been established (c.f. References 8 and 9). The computer code of Reference 9 was used in this instance.

Since the half nozzle design concept was to be used, only the suction surface of the nozzle blades was contoured. The pressure surface, representing the line of symmetry of the full, two-dimensional nozzle, was flat. As also discussed above, the blade suction was extended to allow full expansion on the pressure surface ($M_x < 1$).

C. THREE-DIMENSIONAL EFFECTS AND BLADE STACKING

C.1 Radial Equilibrium. The swirl component of the nozzle exit flow generates a large centrifugal acceleration. In order to prevent radial cross-flows, a balancing radial pressure gradient must be applied. This radial equilibrium of forces implies a significant variation of flow properties in the radial direction.

Considering the case of zero radial cross-flow at an inter-row station, the radial flow properties can be computed from (see Reference 1 for the derivation):

$$-\left[\frac{1}{1+\frac{\gamma-1}{2}M_1^2}\right]\frac{dM_1}{M_1} = \sin^2\alpha\,\frac{dr}{r} \qquad (1)$$

and assuming that the stagnation conditions are constant.

This equation may be solved by specifying another relationship between any two of the three variables. For the present design a free vortex type of distribution was selected, given by the relation:

$$V_\theta \cdot r = \text{constant} \qquad (2)$$

With the free vortex constraint the radial Mach number distribution is:

$$\left(\frac{M}{M_H}\right)^2 = \frac{1}{\left(\frac{1 + \frac{\gamma-1}{2} M_H^2}{\cos^2\alpha_H\left[1+\left(\frac{r_H}{r}\right)^2\tan^2\alpha_H\right]}\right) - \left(\frac{\gamma-1}{2} M_H^2\right)} \tag{3}$$

and the nozzle outlet flow angle distribution is

$$\alpha = \tan^{-1}\left[\frac{r_H}{r}\tan\alpha_H\right] \tag{4}$$

Previous systems considerations for typical engine applications have indicated the desired blade speed and flow conditions at the hub. Using these values in Eqs. (3) and (4) , Table I was prepared which describes the flow property variation along the blade height for both nozzle outlet and rotor inlet.

TABLE I

r/r_H	α^o	P/P_H	M_1	M_{1r}	M_u
1.00	69	1.0	2.23	1.6	.685
1.05	67.9	1.32	2.05	1.43	.691
1.10	67.0	1.65	1.91	1.3	.702
1.15	66.1	2.01	1.78	1.17	.72
1.20	65.4	2.34	1.68	1.07	.73

It should be noted that the above analysis is conventionally called simple radial equilibrium, or, "SRE" because no entropy variations or radial flow gradients are admitted. This technique was adopted for the following reasons:

a) Zero entropy gradient - The blade design concept is such that there are very small profile losses, and no generated shocks. Entropy production is therefore manifested only in the blade and end wall boundary layers which take up a small fraction of the interblade flow field. Since mixing of these high entropy regions with the mass flow is slow, and since the main concern for blade design is the blade row section - and not the downstream, mixed-out region - the entropy gradient is ignored. However, mixing of the nozzle blade wakes should be accounted for when choosing the rotor blade configuration.

b) Zero radial velocity - The main reason for this constraint on the supersonic portion of the nozzle blade is to allow the utilization of exact 2-D blade contours. Constant blade height along the chord is another result so that the radial mass flow gradient introduced from free vortex conditions must be generated in the subsonic portion of the blading. It was reasoned that allowing the turning and the mass flow variation to be produced upstream of the blade-throat would result in a more efficient design since, in general, the losses are proportional to the local stream kinetic energy.

Using the previously described design techniques, blade contours at 5 radial stations were generated. These are shown in Figures 4a through 4e, where $r/r_H = 1.0$ and $r/r_H = 1.2$ represent the hub and tip cylindrical sections, respectively.

C.2 Stacking. Arrangement of the 2-D blade elements to form a complete 3-D blade was predicated upon satisfying radial equilibrium requirements at the throat region, adjusting the blade thickness and camber distribution (following the technique previously described) so that each leading edge was tangent to a plane perpendicular to the axial direction, and allowing the supersonic contour to reach complete expansion. A stacking point was taken at the center of each throat making the throat region of the three-dimensional blade a trapezoidal shaped section. Because of radial equilibrium effects and the variation of the flow angle, the stacking line down through each stacking point is curvilinear.

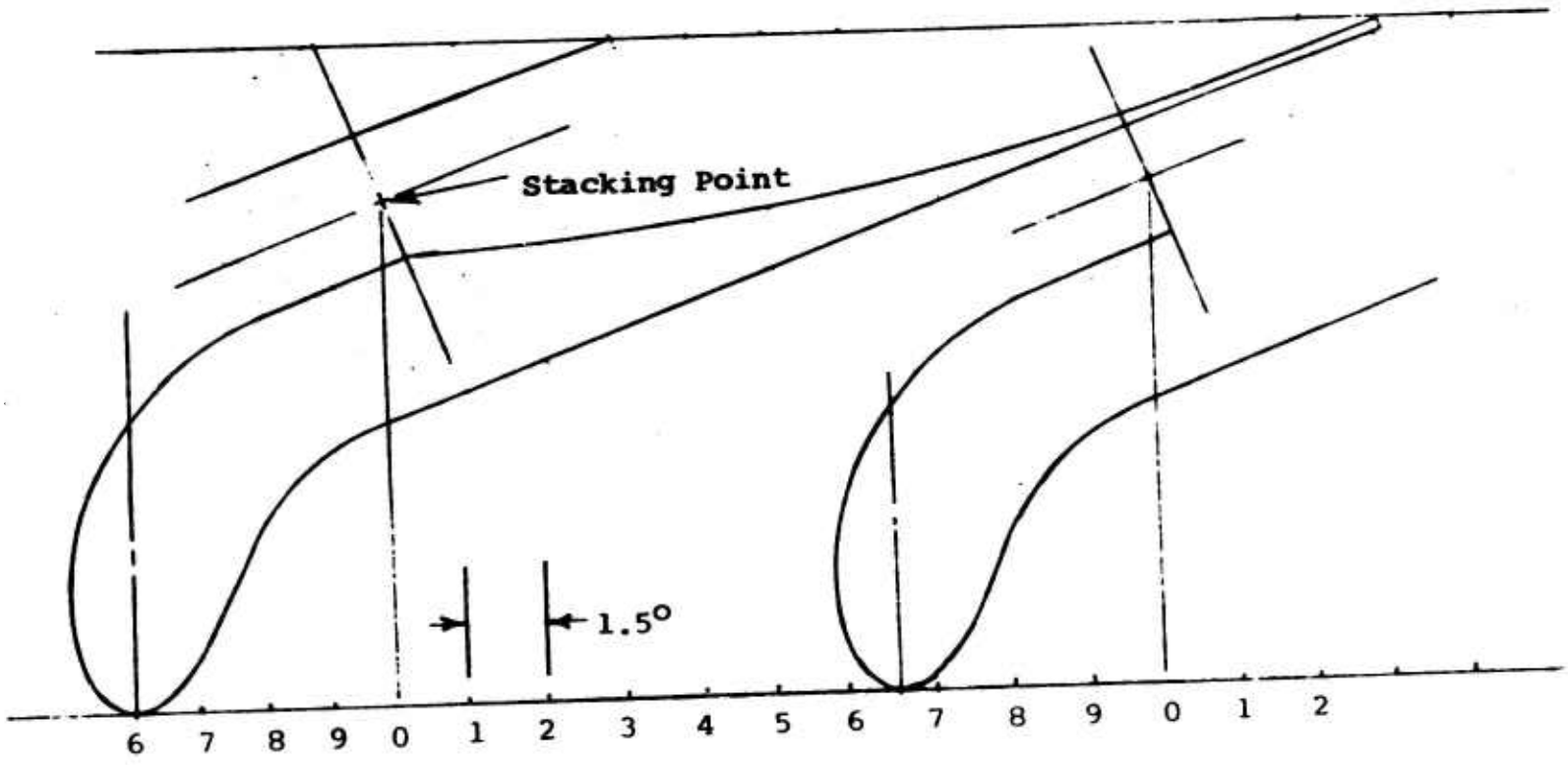

Figure 4a. - Blade Contour, r/r_H = 1.0 (Hub), M_1 = 2.23

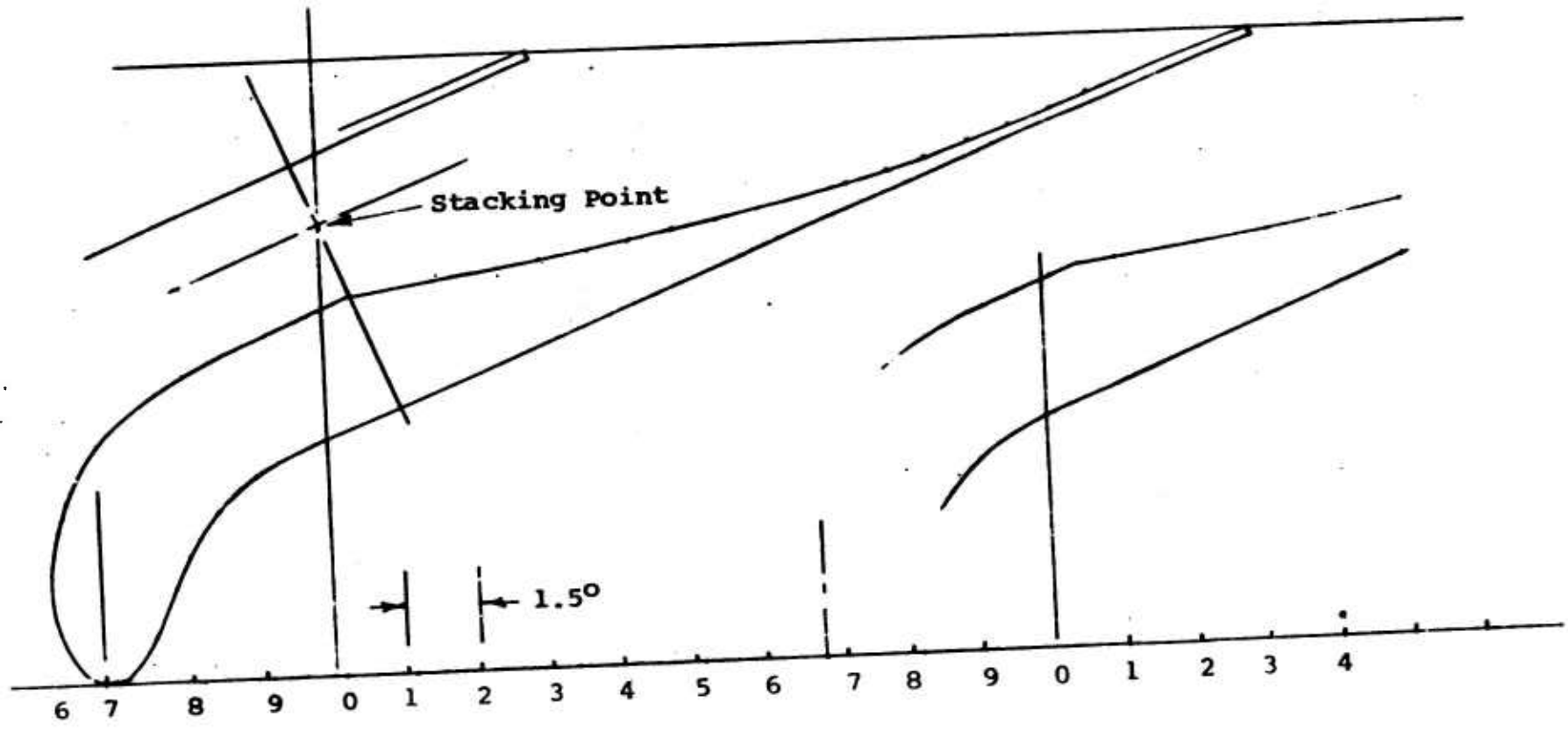

Figure 4b. - Blade Contour, $r/r_H = 1.05$, $M_1 = 2.05$

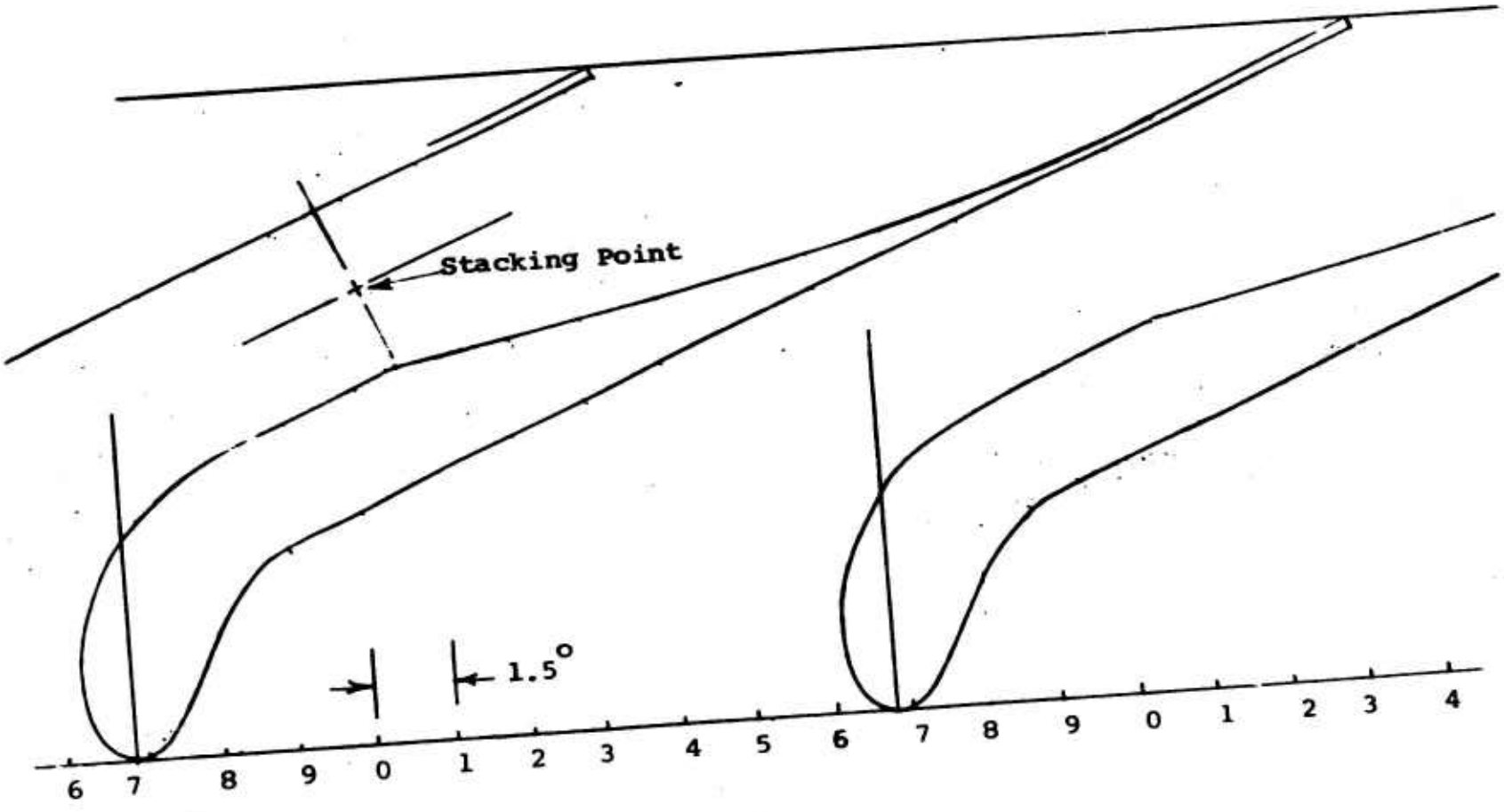

Figure 4c. - Blade Contour, $r/r_H = 1.10$, $M_1 = 1.91$

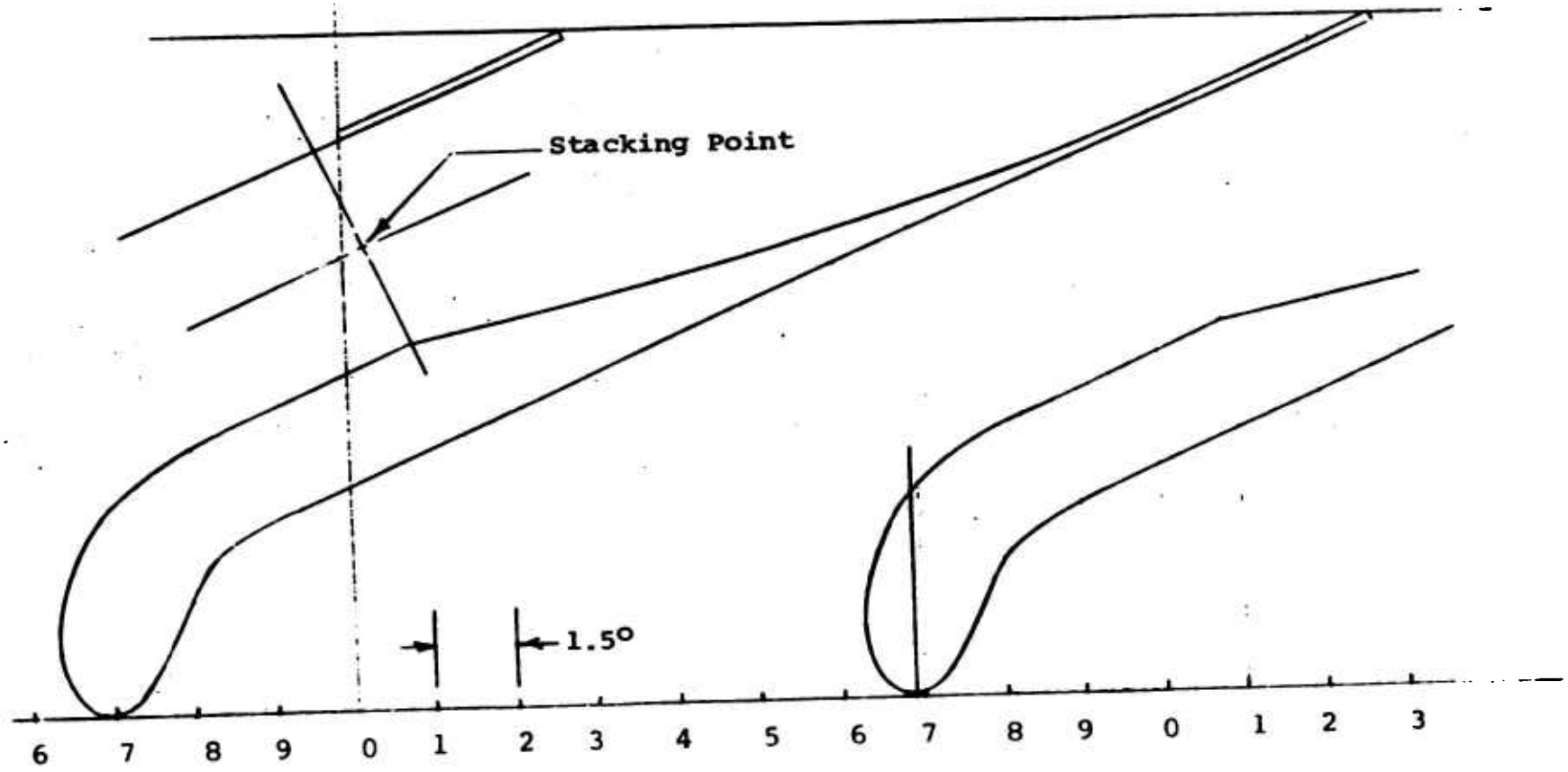

Figure 4d. - Blade Contour, $r/r_H = 1.15$, $M_1 = 1.78$

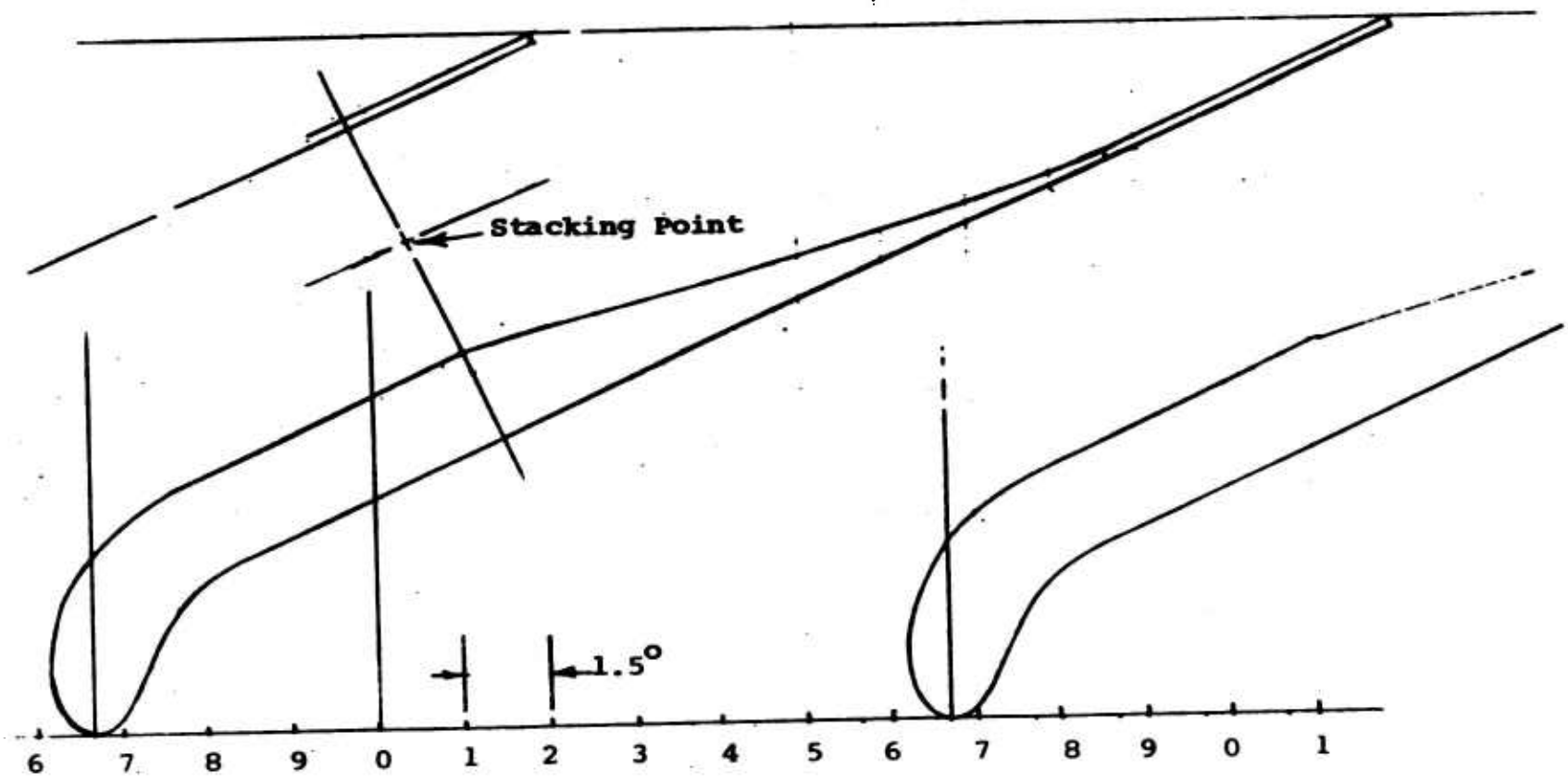

Figure 4e. - Blade Contour, r/r_H = 1.20 (Tip), M_1 = 1.68

In order to satisfy radial equilibrium at the throat it was assumed that the flow in the transonic region could be considered as quasi-one-dimensional. By displacing the throats of radially adjacent blade sections the proper radial pressure gradient is attained. The analysis used to determine the displacement of each blade section is as follows:

First, the pressure which must be maintained along the radial direction is obtained from integrating the radial equilibrium equation holding the absolute Mach number equal to unity, or

$$\frac{P}{P_H} = \left(\frac{r}{r_H}\right) \gamma \sin^2 \alpha \qquad (5)$$

Since the stagnation pressure is constant and equal to the inlet value, the values of P/P_o and A/A^* are known. Note that the pressure must increase with increasing radial distance so that the upper blade element must be displaced in the downstream direction relative to the lower blade section.

At the throat a Busemann-type supersonic contour is cusped-shaped at an angle relative to the flow direction equal to half the overall supersonic turning angle. Therefore, the area just downstream of the throat is:

$$A = A^* + (\Delta x) \tan (\nu/2) \qquad (6)$$

Solving Eq. (6) for Δx gives the required displacement of each blade section since the flow area and the turn angle are defined.

Defining the blade elements, shown in Figures 4a through 4e, as being true surfaces in the circumferential plane, and using the stacking technique defined above the complete 3-D blading was developed.

D. <u>BOUNDARY LAYER CORRECTIONS</u>. The problem of designing a suitable supersonic nozzle contour for any specified Mach number is usually reduced to a computation of the nozzle contour coordinates on the basis of perfect fluid flow theory plus a determination of the rate of boundary layer growth along the nozzle walls and

a modification of the potential flow contour to compensate for the boundary layer effects. The modification is usually based on the boundary layer displacement thickness, i.e., the equivalent mass flow criterion.

It is generally assumed in turbomachine work for medium and larger size engines that blade boundary layers will be turbulent. However, there is considerable experimental evidence, for example, with rocket nozzles (c.f. Reference 10), of substantial reductions of skin friction and heat flux in rapid expansion nozzles downstream of the throat. This situation is sometimes referred to as relaminarization, and is generally limited to situations where the nozzle throat Reynolds number is less than about a million. Using the throat hydraulic diameter to account for the trapezoidal throat shape, this Reynolds number would correspond to a stagnation pressure of 6 atm. for the supersonic nozzle design under consideration; thus design point operation of the nozzle with the hub fully expanded (11 atm.) would correspond to turbulent flow.

In this connection it is worthwhile to recognize the differences between the suction and pressure surfaces of the blading that result from stagger. Back, in Reference 11 , ascribes differences in the tendency to "laminarize" to the nozzle convergence angle in the subsonic region; the higher the convergence angle, the higher the critical throat Reynolds number. Thus on the pressure side of the blading which is quite straight near the throat and hence has a low acceleration parameter, the critical Re_B would be around 0.5×10^6 and turbulent flow would be expected for pressures in excess of about 3 atm. On the other hand, the rapid acceleration of the suction side might allow laminar flow up to 12-13 atm.

The turbulent boundary layer growth along the nozzle walls can be computed by numerical integration using the semi-empirical relation for boundary layer displacement thickness deduced by Ruptash (Reference 12)

$$\frac{\delta^*}{x} = \frac{1}{67}\left(\frac{\nu_1}{u_1 x_1}\right)^{.14} M_1^{0.75} \qquad (7)$$

It should be noted that the predicted linear growth of the boundary layer and value of δ^* are in good agreement with experimental results. For these conditions, the laminar values of δ^* are not greatly different.

Boundary layer displacement thickness development for each blade section is shown in Table II, as a function of the supersonic pressure surface length (x). The results are all normalized with respect to a throat height of 1.0. For ease of reference the nozzle height dimension (y) is given also at each pressure surface station.

TABLE II

$M_e = 2.23$ $\quad \delta^*/x = 4.1104^{-3}$

X	Y	δ^*
0.0	1.0	0.0
.6962	1.2030	7.711^{-4}
1.0165	1.2958	1.1113^{-3}
1.4216	1.4108	1.575^{-3}
1.8164	1.5165	2.012^{-3}
2.2159	1.6141	2.455^{-3}
2.6174	1.7014	2.789^{-3}
3.0221	1.7783	3.348^{-3}
3.4147	1.8427	3.783^{-3}
3.8288	1.9004	4.242^{-3}
4.2374	1.9475	4.694^{-3}
4.6388	1.9849	5.138^{-3}
5.0296	2,0135	5.572^{-3}
5.9450	2.0359	6.032^{-3}
5.8459	2.0501	6.48^{-3}
6.2273	2.0574	6.898^{-3}
6.4933	2.0590	7.193^{-3}

$M_e = 2.05$ $\quad \delta^*/x = 3.883 \times 10^{-3}$

X	Y	δ^*
0.0	1.0	0.0
.6694	1.1653	8.845^{-4}
.97735	1.2408	1.266^{-3}
1.2720	1.3119	1.681^{-3}
1.5882	1.3846	2.099^{-3}
1.8839	1.4477	2.490^{-3}
2.1728	1.5037	2.871^{-3}
2.4750	1.5561	3.271^{-3}
2.7770	1.6020	3.670^{-3}
3.0859	1.6423	4.078^{-3}
3.3790	1.6746	4.465^{-3}
3.6843	1,7023	4.869^{-3}
3.9744	1.7233	5.252^{-3}
4.2780	1.7399	5.654^{-3}
4.5641	1.7509	6.032^{-3}
4.8636	1.7576	6.426^{-3}
5.14185	1.7598	6.795^{-3}

TABLE II (Cont.)

M_e = 1.91 $\quad \delta^*/x = 3.661^{-3}$

X	Y	δ^*
0.0	1.0	0.0
.6471	1.1368	1.055^{-3}
.9448	1.1992	1.546^{-3}
1.0436	1.2197	1.701^{-3}
1.2296	1.2577	2.004^{-3}
1.4347	1.2081	2.338^{-3}
1.6260	1.3338	2.650^{-3}
1.8456	1.3721	3.008^{-3}
2.0476	1.4044	3.337^{-3}
2.2419	1.4327	$3,654^{-3}$
2.4336	1.4578	3.966^{-3}
2.6495	1.4828	4.319^{-3}
2.8438	1.5025	4.635^{-3}
3.0418	1.5197	4.957^{-3}
3.2445	1.5344	5.288^{-3}
3.4528	1.5466	5.628^{-3}
3.6404	1. 5552	5.933^{-3}
3.8335	1.5616	6.248^{-3}
4.0324	1.5657	6.572^{-3}
4.2677	1.5676	6.955^{-3}

M_e = 1.78 $\quad \delta^*/x = 3.494 \times 10^{-3}$

X	Y	δ^*
0.0	1.0	0.0
.6234	1.1107	1.159^{-3}
.9101	1.1612	1.693^{-3}
1.0052	1.1777	1.870^{-3}
1.18415	1.2082	2.202^{-3}
1.3466	1.2349	2.504^{-3}
1.5363	1.2644	2.857^{-3}
1.7246	1.2915	3.207^{-3}
1.8967	1.3141	3.528^{-3}
2.0837	1.3362	3.876^{-3}
2.2663	1.3552	4.215^{-3}
2.4476	1.3715	4.552^{-3}
2.6297	1.3853	4.891^{-3}
2.7910	1.3954	5.191^{03}
2.9784	1.4047	5.539^{-3}
3.1701	1.4116	5.896^{-3}
3.3419	1.4154	6.216^{-3}
3.5693	1.4174	6.639^{-3}

M_e = 1.68 $\quad \delta^*/x = 3.399 \times 10^{-3}$

0.0	1.0	0.0
.6044	1.0915	1.162^{-3}
.8825	1.1331	1.697^{-3}
.9747	1.1468	1.874^{-3}
1.1927	1.1781	2.293^{-3}
1.3725	1.2025	2.639^{-3}
1.5456	1.2243	2.972^{-3}
1.7228	1.2445	3.313^{-3}
1.9099	1.2634	3.672^{-3}
2.0891	1.2789	4.017^{-3}
2.2650	1.2917	$4,355^{-3}$
2.4403	1.3020	4.693^{-3}
2.6166	1.3098	5.032^{-3}
2.7954	1.3153	5.375^{-3}
2.9775	1.3183	5.726^{-3}
3.09335	1.3189	5.948^{-3}

III. NOZZLE FABRICATION AND MECHANICAL DESIGN

Various methods for fabrication were considered in the mechanical design of the nozzle ring. The thrust load on the ring is substantially greater than in conventional turbines because of the large pressure drop across it. The entire center disk sees statgnation pressure on the upstream side and hub static pressure on the discharge side, a difference of 10 atmosheres. This load must be transferred through the blades to the outer ring from which the turbine is supported, if struts are to be avoided in the gas stream.

The methods of fabrication considered were:

(1) detachable individual blades

(2) contour - milled blades, with detachable outer shroud

(3) integral assembly - blades formed by electro-discharge machining the passages from a solid piece of material

Method (1) was eliminated because of the problem of designing a blade attachment system with sufficient "wrap around" (25° at the hub, for example) and because of the reduced capability of the blades as load carrying members when attached in this fashion.

Method (3) was to be preferred from a strength standpoint, but was rejected by the fabrication vendor as technically unworkable for these blade contours.

Method (2) was thus selected, and offered the advantages of improved accessibility to the blade passages for static pressure tap instrumentation and the capability for subsequent modification of the blades for coolant passages for later heat transfer studies, in addition to providing some load capacity through the outer ring attachment screws.

The mechanical design was based on 24 blades, with hub and tip diameter of twelve and ten inches, respectively. The trailing edge thickness was set at .025 in., which was only marginally safe to withstand the gas bending loads when calculated as an unsupported plate. It was felt that the trailing edges would in fact gain some support from contact with the outer shroud.

The turbine nozzle ring was fabricated by THERM, Inc., Ithaca, New York, under subcontract, from 410 stainless steel material. Master drawings were made 10 x size, in 4 plane sections. A master blade passage was constructed from these, which was used for profile milling of the diaphragm. The outer ring was then screwed on using 48 small screws fastened directly into the blades. This procedure was to be preferred over welding or brazing because of the unpredictable nature of the thermal distortion inherent in these processes. Photographs of the ring are shown in Section IV. The table of coordinates used and the plane section drawings are given in Appendix A. The following fabrication tolerances were held, as obtained from the vendor's inspection of the completed part.

1. 12 inch outside diameter measures 11.998 inches

2. 12 inch shroud diameter measures 12.0005 inches

3. Airfoil master within .001 band of nominal mylar charts

4. Blades within plus/minus .003 inches of nominal contour except for localized areas to .008 for areas not exceeding .375 wide

5. Throat within plus/minus .004 of .294 at A5, .269 at A4, .258 at A3, .230 at A2 except 1 Vane to minus .015 from nominal

6. Trailing edge thickness within .025/.039 except 1 Vane as in Item 5

7. 10 inch diameter to bottom of vane passage is within plus/minus .005 inches of nominal depth

In order to reduce the loading on the outer shroud screws and to minimize distortion of the ring under test, a central sting was provided (through the hole in the spinner) and was pre-loaded by means of threaded rod and nuts. The attachment of this sting to the outer vessel was accomplished well upstream of the nozzle in order to minimize flow disturbances.

IV. TEST APPARATUS AND INSTRUMENTATION

A. AIR SUPPLY. The overall arrangement of the turbine nozzle test rig is shown in the layout drawing, Figure 5. The GASL Vertical Pebble Bed heater was used as the basic air supply, augmented with additional cold air as shown in the double throat detail, Figure 6. This dual air supply system had been used on several other test programs and it had been shown that adequate mixing of the hot and cold supplies is obtained. Figure 7 is a typical test calibration result, from Reference 3 showing that the same stagnation temperature profile is obtained with hot and cold air mixed as with hot air alone.

The use of this additional cold air extends the nozzle test envelope substantially, as shown in Figure 8. By varying the stagnation temperature and pressure independently, tests could be run at varying pressure ratio across the nozzle with constant Reynolds number, as seen from Figure 9. This capability is important since boundary layer effects may be expected to play a dominant role in off-design nozzle operation.

The maximum pressure which may be supplied to the turbine nozzles is limited by the throat opening of the air supply nozzle and the characteristics of the Vertical Pebble Bed heater. This heater has a limiting pressure of 1500 psia, which results in a maximum pressure in the turbine nozzle plenum chamber of about 300 psia with maximum cold air flow, more than adequate for these tests. The air supply nozzle, shown in the layout, is of course operated with subsonic flow.

B. NOZZLE DISCHARGE CONDITIONS. The nozzle was operated with atmospheric pressure discharge. The exit flow was received by a conical duct which was connected to an elbow and a vertical discharge stack. A 4-inch long cylindrical extension was added at the tip radius to guide the flow into the discharge duct, prevent outward expansion, and facilitate exit flow traversing.

The original plans for this test rig called for an annular discharge diffuser, in order to maintain the radial pressure gradient in equilibrium at the nozzle discharge plane. This idea, while theoretically correct, was dropped because of practical difficulties.

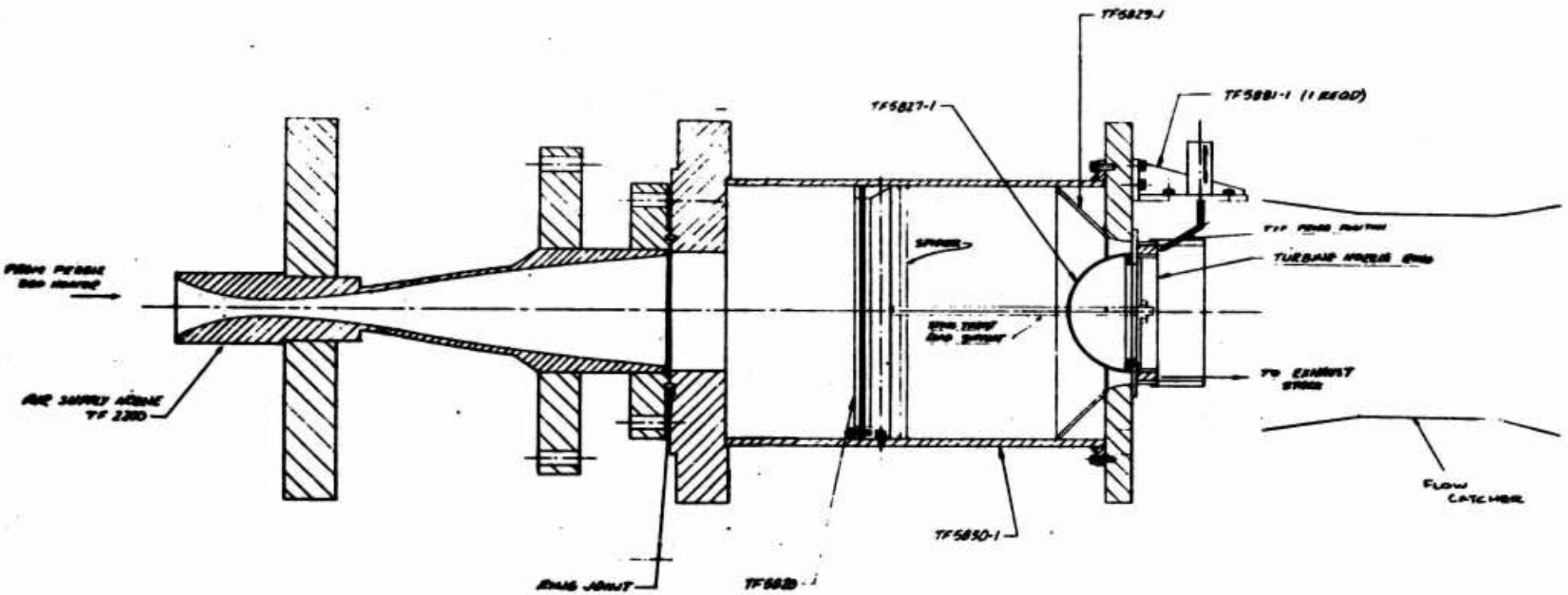

FIGURE 5. - Test rig layout

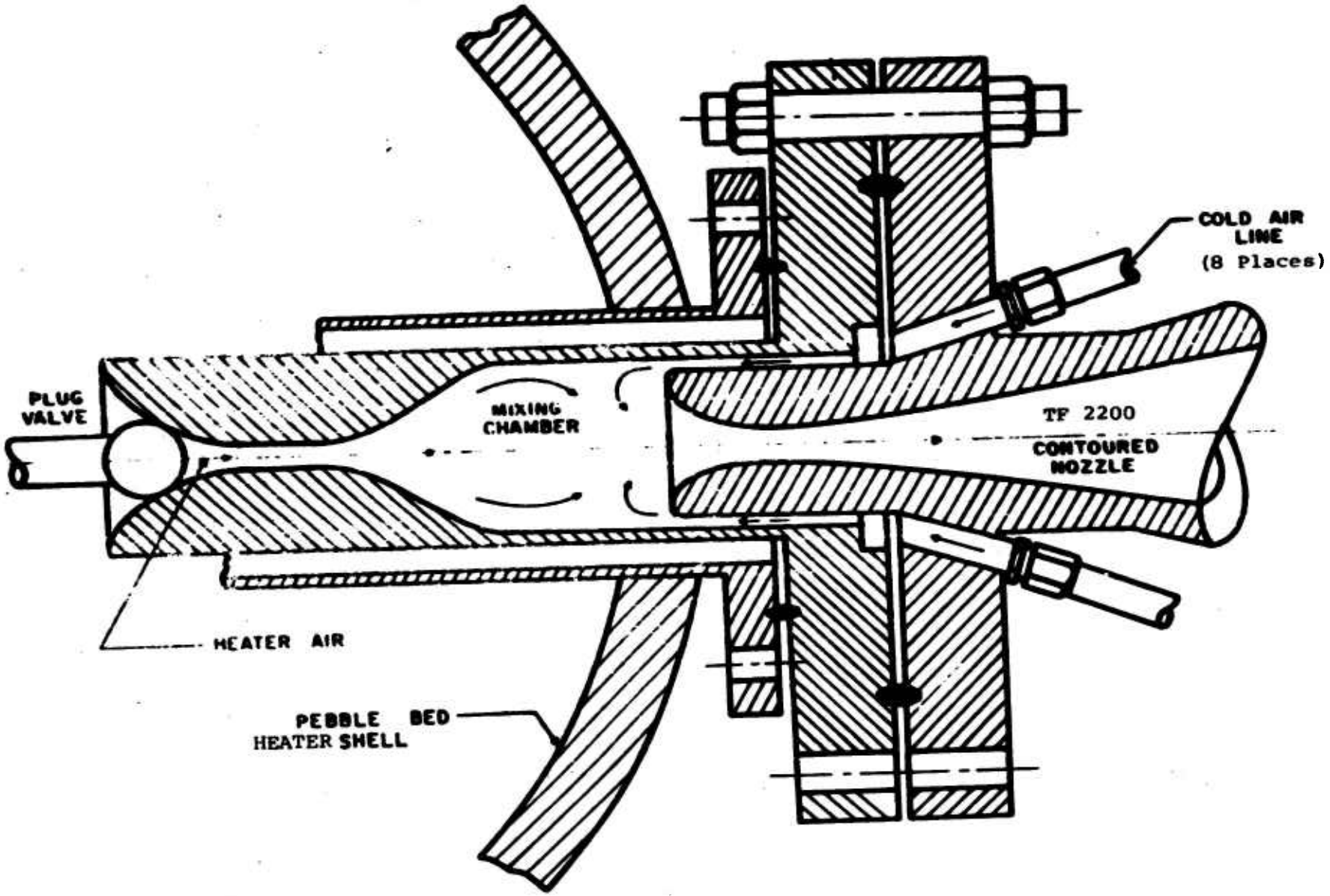

FIGURE 6. - Double throat detail

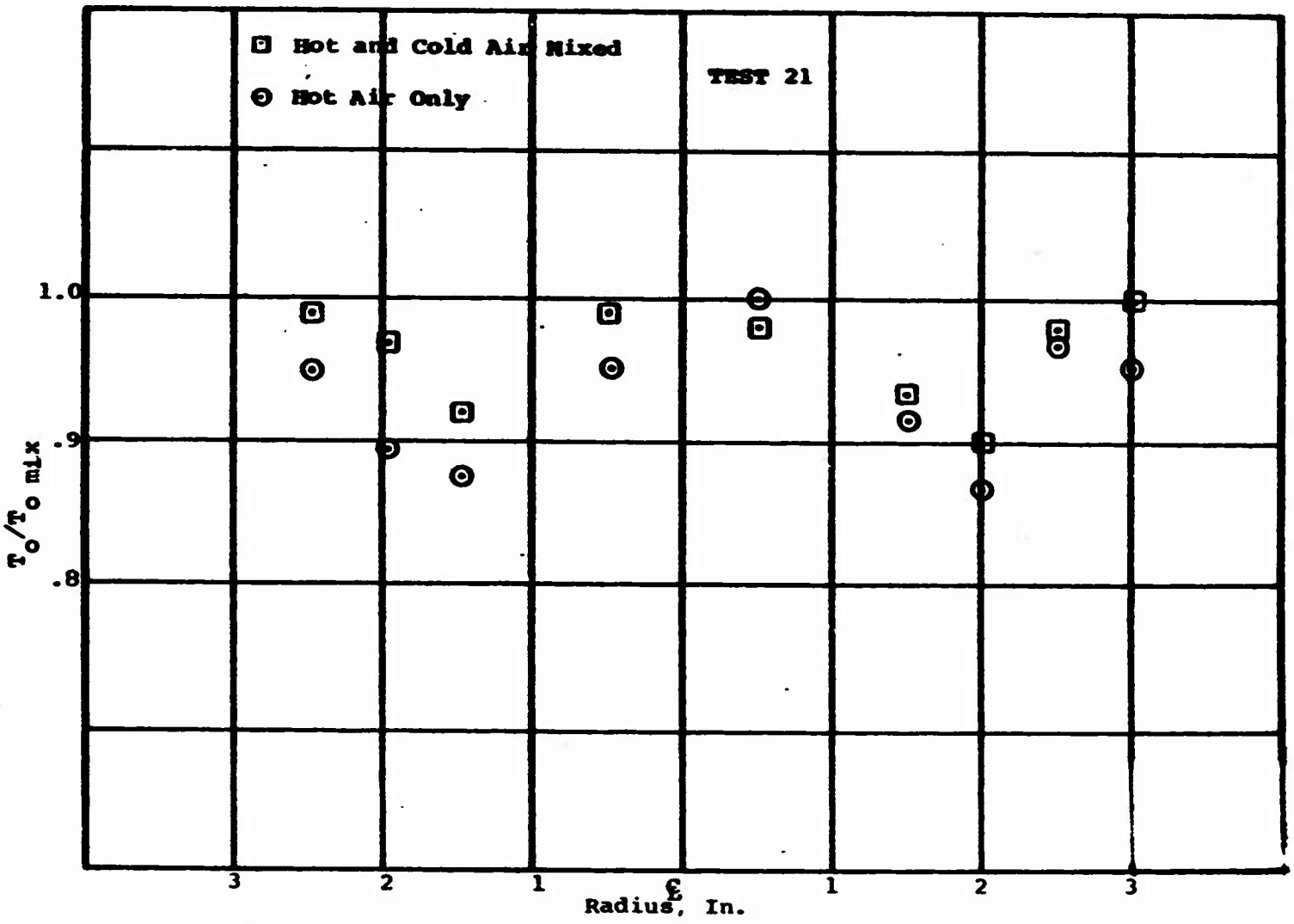

FIGURE 7(a). - Typical test section stagnation temperature distribution (Reference 13)

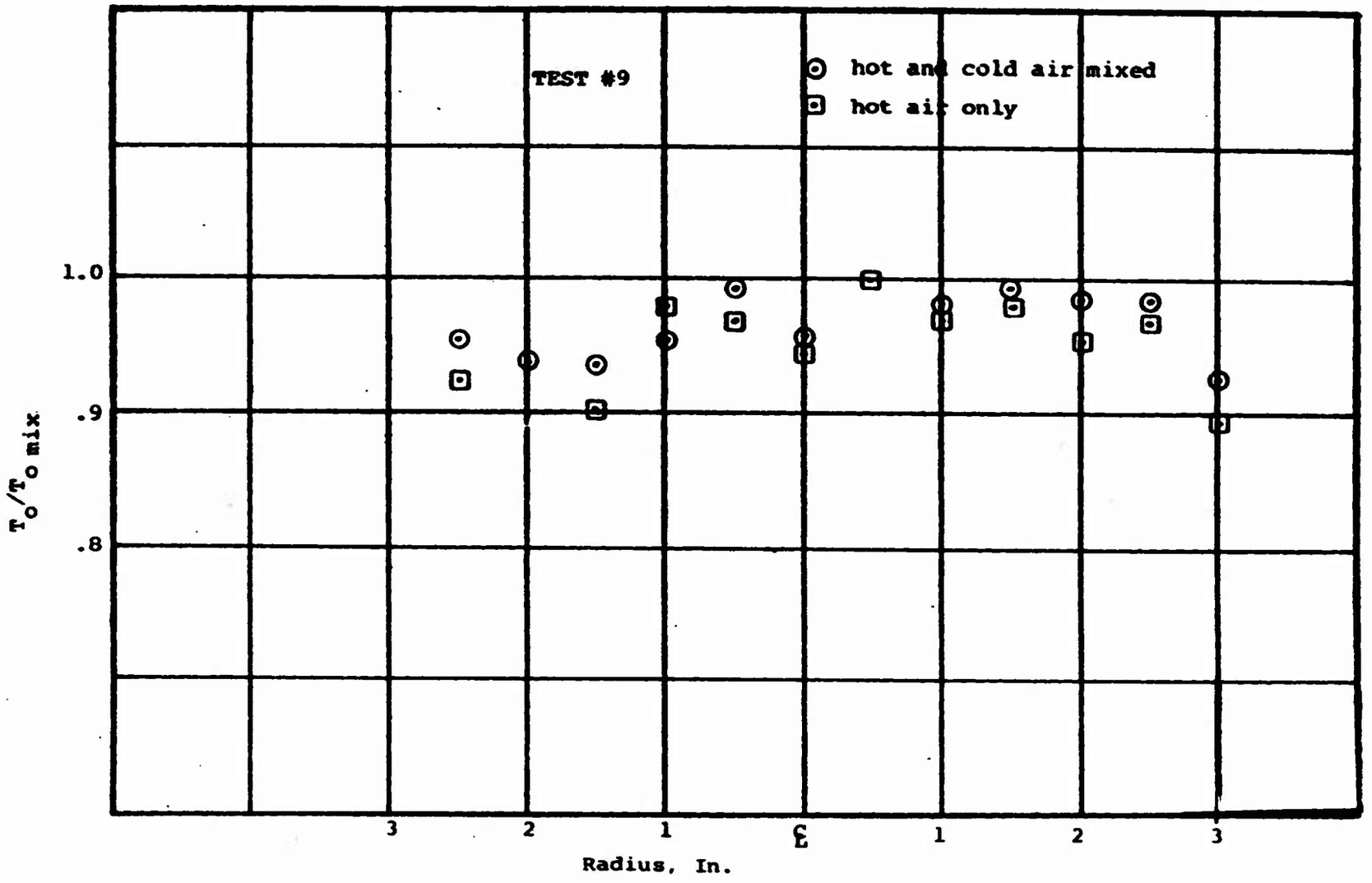

FIGURE 7(b). - Typical test section stagnation temperature distribution (Reference 13)

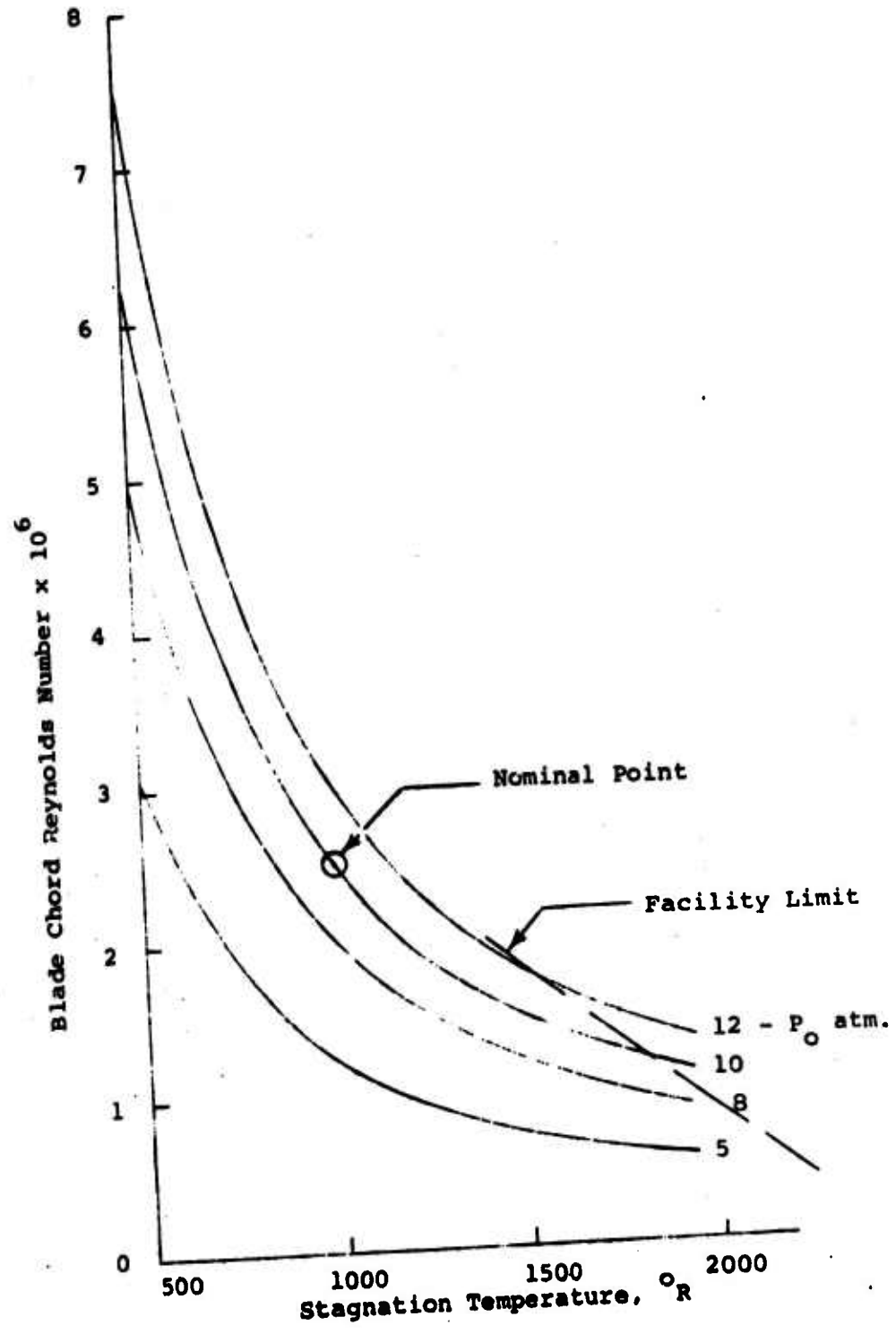

FIGURE 8. - Test Reynolds number envelope

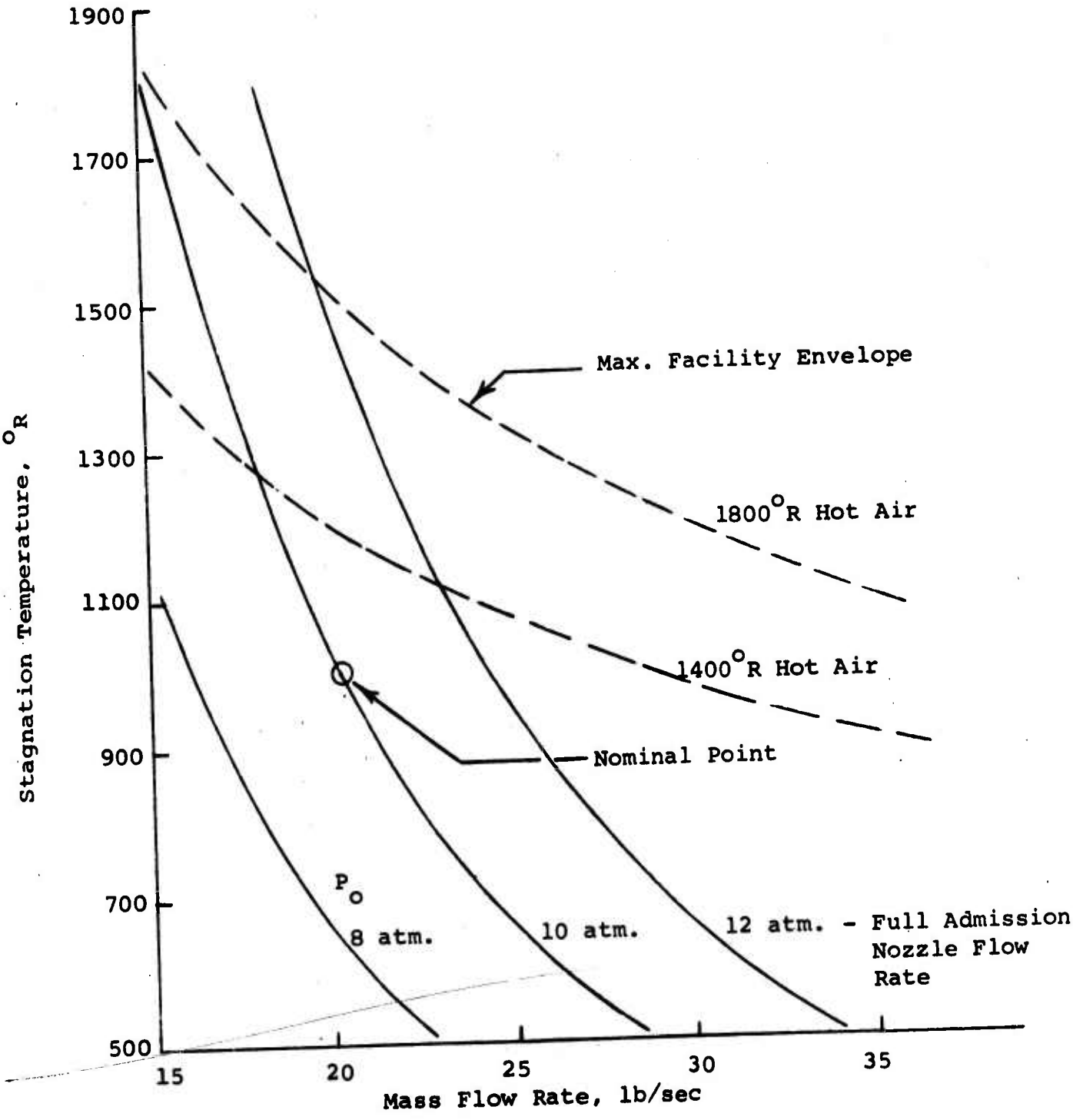

FIGURE 9. - Test rig capability envelope

First of all, boundary layer computations showed that the narrow annulus required to decelerate the flow would be nearly completely filled by boundary layer flow at the exit. This corresponds to a fully developed pipe flow of sorts, and has the overall result that the diffuser would introduce new problems while solving the blade exit radial pressure gradient problem. The diffuser performance would be Reynolds number sensitive and might have flow separation problems of its own. In addition, the problem of access to the nozzle exit plane for traversing is greatly compounded through the use of a diffuser.

The decision to eliminate the exit diffuser had important ramifications with respect to the back pressure imposed on the blading. As discussed previously, the design requires a pressure ratio of 2.3 between tip and hub stations. Since the axial Mach number is subsonic, there is a feedback effect present, as shown in the sketch below where μ represents the Mach angle defining the zone of influence from a given point.

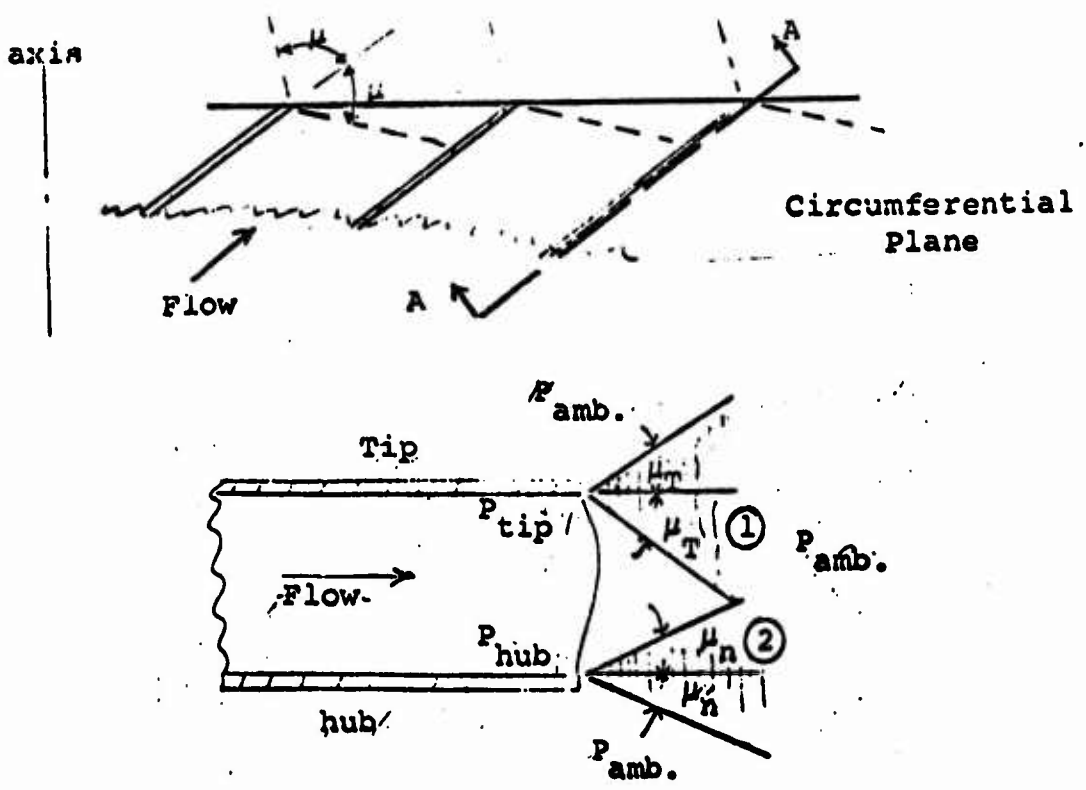

Section A-A

The feedback results from the Mach cones from hub to tip trailing edge (pressure side) falling inside the passage, a consequence of the subsonic axial Mach number. This results in the ambient pressure downstream of the cascade being felt over a region of the suction side blade, which is shaded in the sketch above. The extent of the region varies slightly from hub to tip because of the stacking arrangement chosen.

When the blading is operated with the theoretical hub exit static pressure equal to ambient, this region of the blading will be subject to a favorable pressure gradient, (region 1 is an expansion fan) and no adverse effects should occur. At the other extreme, when the tip static pressure is matched, the hub will be overexpanded, and some flow separation may occur (region 2 is a compression). The test schedule and instrumentation were planned to explore the performance of the blading under this full range of extremes of operation.

C. INSTRUMENTATION. Instrumentation for the nozzle tests fell into three groups:

(1) air supply instrumentation
(2) nozzle blade pressure distribution
(3) exit flow traversing

1. Air Supply. In order to determine incoming flow properties, measurements of the stagnation temperature and pressure are required. These parameters were measured in the large tank between the settling screens and the nozzle. The mass flow rate passing through the cold air supply was measured independently through a venturi. This allows an independent check of the effective throat areas of the system.

2. Nozzle Blade Pressure Distributions. A large number of static taps (57) were provided in the nozzle blading, centered around one particular flow passage and its neighbors. Taps in the hub and shroud (cylindrical surfaces) were drilled in a straightforward manner. Taps in the blade pressure and suction surfaces were more difficult, since two intersecting holes were required. Electric discharge machining was used for some of the less accessible locations. A few taps were installed in identical locations in adjacent flow passages as a check on flow uniformity. Most of the holes were .040 in. diameter, with some of the more difficult locations at .032 and .020 inches.

3. Exit Flow Traversing. Because of the supersonic nature of the exit flow, special probes are required to obtain meaningful measurements of the nozzle exit flow. The parameters desired are total pressure, static pressure, and flow direction angle. Point measurements are desired, and care must be taken that the probe stem not introduce blockage effects or measurement errors. This rules out use of a conventional cylindrical probe, in common use in subsonic situations, with which measurements are taken at nearly the axis of alignment of the probe.

The most common sensing head in use for diagnosis of supersonic flows is a cone, with pressure taps at the nose (stagnation) and at several (usually four) independent locations around the cone surface. This allows independent measurement of the Mach number and the three dimensional cone angle of attack, which may then be resolved into the desired components for the coordinate system, i.e., swirl and radial flow angles. Reference 14 contains a detailed calibration of such a probe over the Mach number range 1.5 - 3.5. An iterative procedure is required to finally determine both Mach number and flow angle. First, the average of the four cone static pressures is used to compute P_c/P_{t_2}, from which a trial estimate of Mach number and the ratio q/P_{t_2} are found (Figure 10) then the pressure differences between diametrically opposed orifices are used to find the ratios $(\Delta P/q)_c$ and $(\Delta P/q)_r$. The corresponding flow angles may then be read from Figure 11. Note the weak dependence on Mach number. Reference 14 contains correction factor curves to correct P_c for angularity effects, enabling a new determination of M and q/p_{t_2} to be made from Figure 10. The corrected values should then be used with Figure 11 for a final determination of flow angle, but for small angles the first try is sufficiently accurate.

This is a relatively straightforward procedure in relatively uniform flows and in two-dimensional flows, neither of which apply here. The high degree of swirl is particularly troublesome, when one considers that the cone axis must lie on a local tangent surface. If the probe stem or direction of traverse is to be radial, then the angle between the cone axis and the radial direction will not, in general, be 90°, as shown in the sketch below. The angle will be given by the relation (the derivation is given in Appendix B)

$$\cos \psi = \sin \alpha \sin \left(\frac{\pm \sin \alpha}{r} \right) \qquad (8)$$

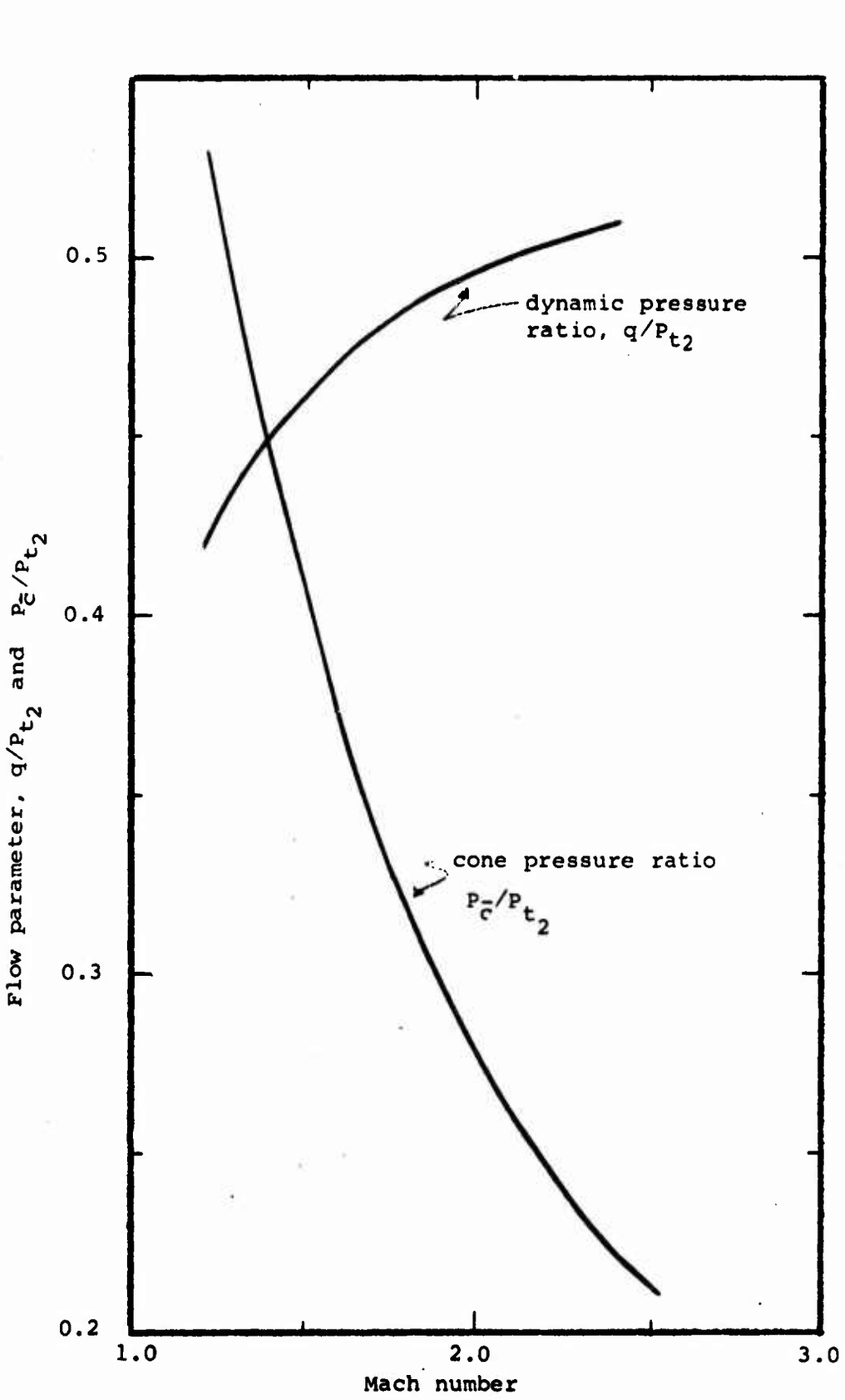

FIGURE 10. - 15° Half angle cone parameters

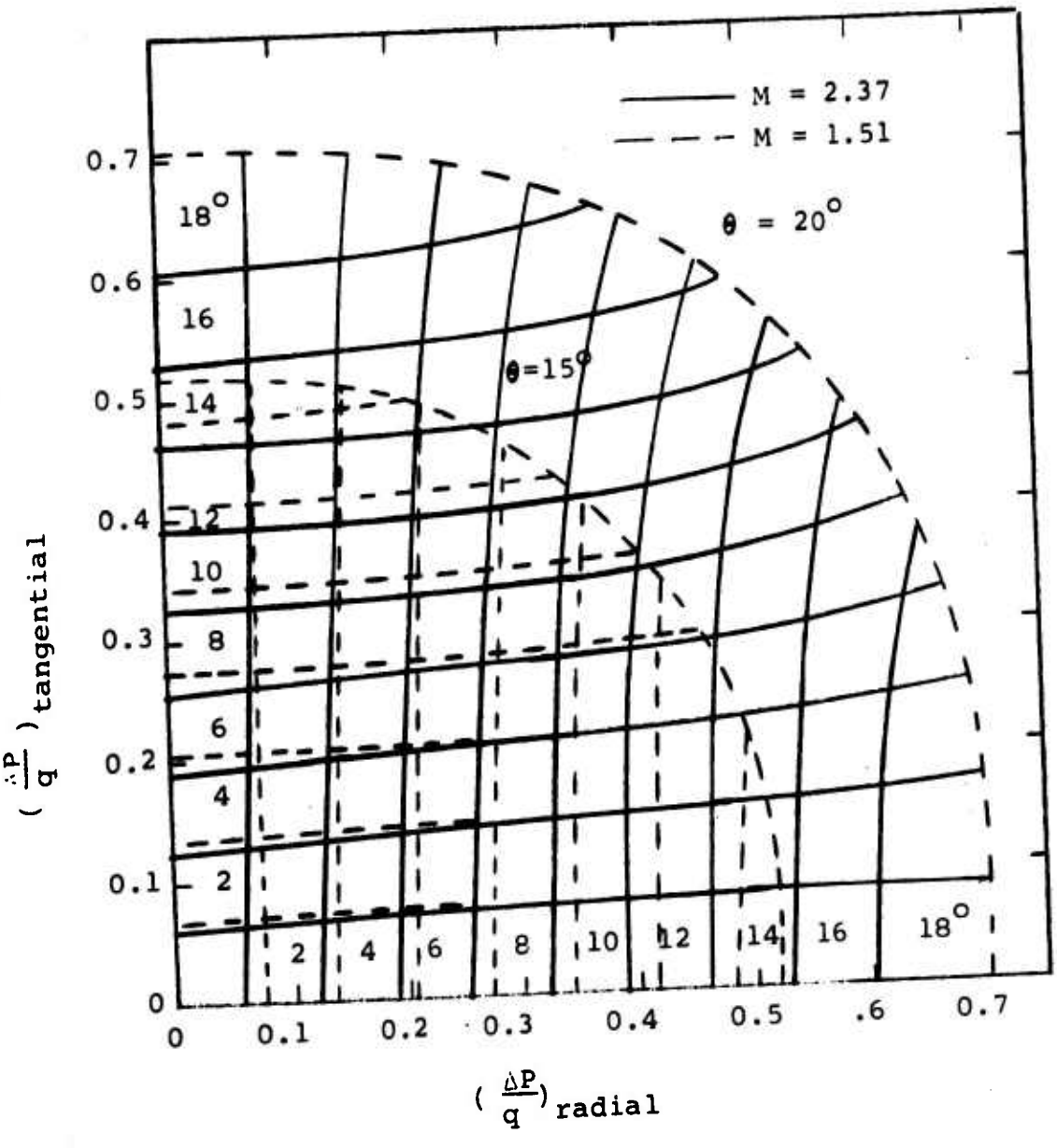

FIGURE 11.- 15° Half angle cone angle of attack data

and is a function of the swirl angle, radius, and distance of the probe stem back from the probe tip at which tangency is desired.

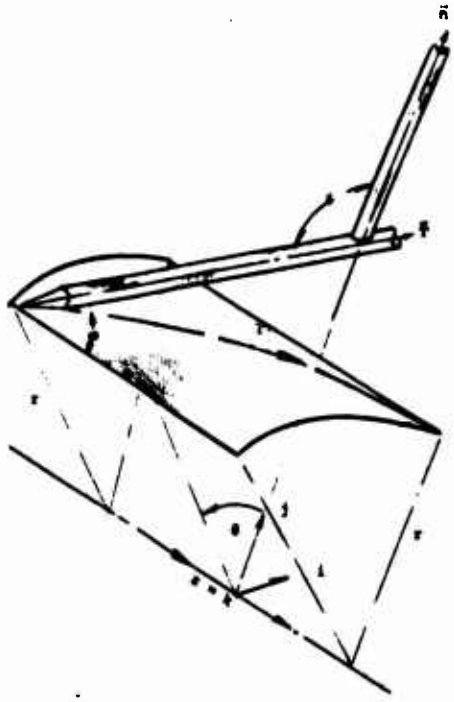

Traversing Probe Alignment Geometry

Two different probes were used in conjunction with a radial traversing drive. This drive had a stroke of 0.9 - 1.0 in. and a linear speed of about 0.2 in/sec. One probe had a base diameter of 0.25 in., a nose diameter of .030 in., a semi-vertex angle of 6.5°, and only one cone surface static pressure indication - an average of two diametrically opposed taps. This probe was used for initial checkout and for test runs where there was fear of physical probe damage.

The other cone probe was a commercially-obtained 5-hole probe having 15° half-angle, a base diameter of .125 in., a nose tip diameter of .025 in. with pitot tap, and 4 independent core surface taps. This probe was intended for the actual traversing measurements. It was reinforced by mounting in a .25 in. diameter tube (making the two probes interchangeable) as shown in Figure 12.

In general, combination conical total/static probes are subject to two kinds of errors; effects due to tip bluntness and those due to boundary layer build-up changing the effective cone angle. For the small probe, the latter effect amounted to an increase in effective cone angle of 0.25° and 0.35° for test pressures of 10 and 5 atmospheres, respectively. This trend is compensated by the overexpansion around the blunt tip, which is shown in Reference 15 to result in about a 5% underestimation of the sharp cone surface pressure (at 5 nose tip diameters downstream) at $M_\infty = 3$.

The response of the pressure measuring system was also checked to determine if the .020 in. capillary tubing was unduly restrictive. A characteristic time of .04 sec. was calculated, which was deemed sufficiently small for the traverse speed used.

4. Measurement Systems. The exit flow traversing pressures were each read by means of a strain gage transducer whose output was recorded on an oscillograph. The steady parameters, i.e., nozzle static pressures and air supply pressures were recorded by means of rotary scanning valves. Three such scanners were used, having full scale pressures of 25, 250, and 1500 psia.

Temperatures were sensed by means of chromel/alumel thermocouples whose output was also recorded on oscillograph charts.

A 10-turn precision potentiometer was used to indicate the traverse probe position, which as displayed in the test control room in addition to being recorded.

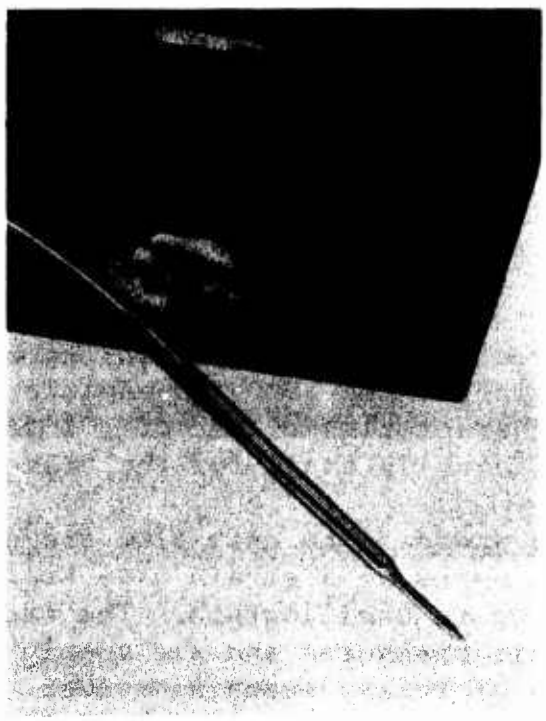

Figure 12. - 15° Half-Angle, 5-Hole Cone Probe, Mounted in Traverse Mechanism

V. TEST RESULTS

A. GENERAL RESULTS. Testing of the nozzle ring was conducted over a range of pressure ratios from 1.9 to 10.5, and Reynolds numbers from .65 - 3.5 x 10^6. Table III summarizes the test conditions. Exit traversing with the 5-hole cone probe was accomplished on test series 9 and 10.

After the initial shakedown tests, it was determined that an outer shroud was required to properly guide the exit flow and prevent radial expansions from unduly influencing the nozzle flow. Without this shroud, sub-atmospheric pressures were recorded at the blade passage exit plane, tip section, indicating expansion effects. An aluminum shroud, 4 in. long and 12 in. diameter,was then attached to the rig. An access slot was provided for the traversing probe, so that complete circumferential uniformity was not possible.

In general, the test results were as expected, with complete expansion being achieved at pressure ratios near or above the local theoretical requirement, and shocks and separated flow zones being present at lower pressure ratios. However, shocks formed by overexpansion at the hub tended to persist at the larger radii where correct expansion was possible, resulting in discharge pressure higher than ambient at the larger radii.

Following test series #10, mechanical damage to the blading was noted. The damage consisted of trailing-edge cracks at about $r/r_h = 1.05$, beginning parallel to the hub surface, and turning to the radial direction. Three blades were badly cracked and a piece was missing from one blade, the "thin" blade created by machining tolerance buildup discussed in Section III. The damage may be noted in Figure 13.

It was theorized that the blade trailing edge damage occurred as a result of flutter, and only the blades with a noticeable lack of contact with the outer shroud were affected. The contact between blade tips and the shroud was nonuniform because of machining tolerances and thermal distortions of the outer ring, caused by both the heating required for installation of pressure tap connections and by the actual testing.

TABLE III

TEST LOG

Test No.	$P_o/P_{amb.}$	T_{o_m} *^oR	T_{o_m} +^oR	$\dot{m}_h/\dot{m}_c$	$Re_c \times 10^6$	$\dot{m}$-lb/sec	Remarks
1-A	1.9	540	530**	0	1.10	5.2	Shakedown testing; large probe
1-B	2.94	525	530	0	1.77	8.4	
1-C	2.25	750++	910	∞	0.65	4.7	
1-D	4.54	670	694	.56	1.93	11.1	
2-A	3.66	540	530	0	2.1	10.	4 in. tip shroud installed no probe
2-B	6.33	710	693	.53	2.55	15.	
3-A	4.33	515	530	0	2.65	12.2	
3-B	6.2	650	655	.32	2.78	15.	
4-A	7.8	718	708	.47	3.09	18.6	Base pressure taps added
4-B	10.1	740	766	.81	3.80	23.	
5	7.7	730	705	.36	2.99	18.	Trouble shooting Traverse mechanism
6	7.35	650	650	.30	3.28	18.1	
7	7.7	686	682	.34	3.22	18.6	
8-A	4.73	522	530	0	2.82	13.4	
8-B	10.1	788	814	.98	3.44	22.2	
9-A	5.55	535	530	0	3.14	15.1	Small probe traverse 3/8 in. back from exit
9-B	8.	657	655	.23	3.49	17.6	
9-C	10.	820	790	.66	3.30	22.1	
10-A	5.58	535	530	0	3.20	15.8	Small probe traverse at exit plane
10-B	7.7	668	669	.24	3.50	18.6	
10-C	10.5	805	880	.73	3.48	23.5	

* Measured
\+ Deduced from Figure
** Assumed value
++ Unsteady value, increasing with time

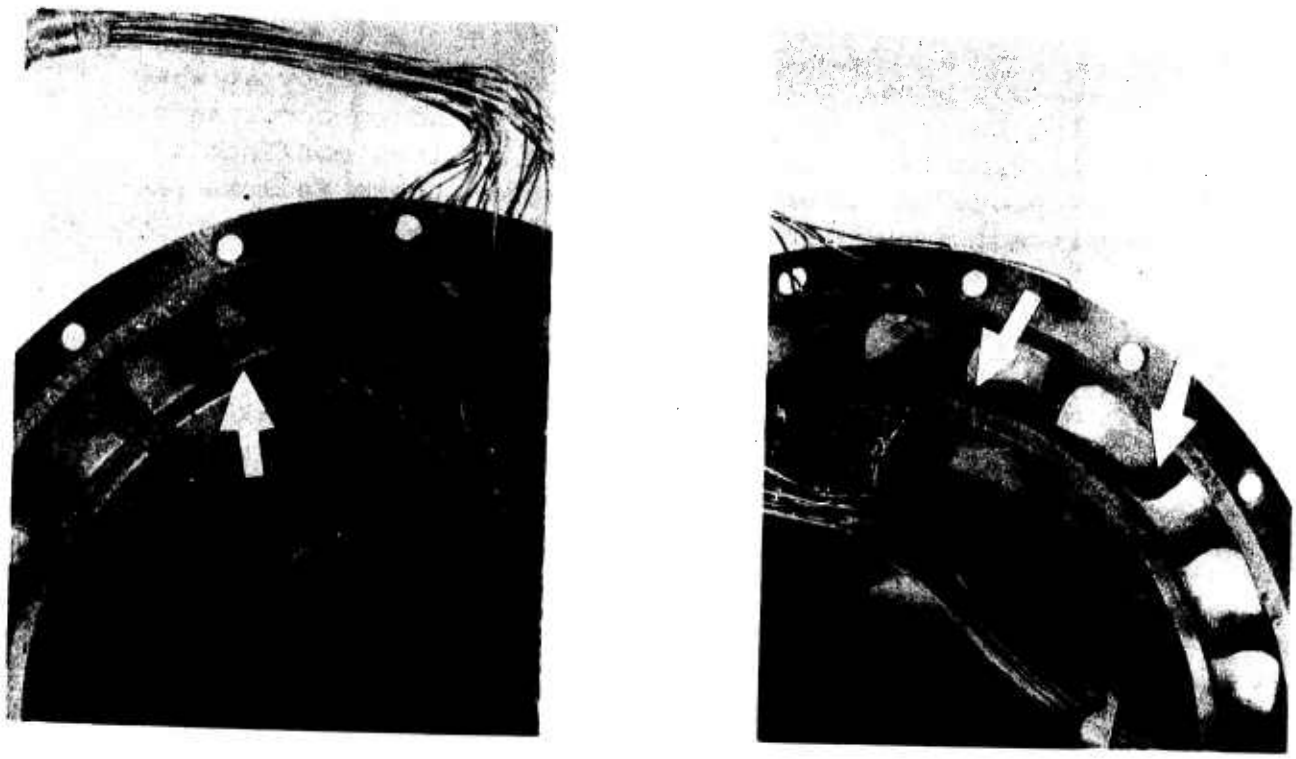

a) Cracked Blade

b) Cracked Blade and Blade with Piece Missing

Figure 13. Post-Test Blade Damage

After disassembly of the test rig and a more thorough inspection of the nozzle, it was noted that the trailing edge of the blading had taken a slight set in the direction of the pressure loading, more or less uniformly for all blades. The bending would have resulted in additional expansion along the pressure surface and reduced expansion along the suction surface, with a corresponding change in flow direction at the tip section.

It was not possible to determine with certainty at what point in the testing the cracking and/or bending occurred since inspections from test-to-test were more or less confined to instrumentation, and specific searches for these failure phenomena were not conducted prior to Test 10.

Finally, the deposits of dust and other particulate matter (presumably from the Pebble Bed Heater) on certain sections of the blading indicated the presence of local separated flow regions, as seen from Figure 14. Two such regions were noted: on the pressure side of the leading edge, and at the junction of the subsonic blade profile and the straight portion of the pressure surface where a relatively sharp corner existed.

B. SUPPLY CONDITIONS. Since direct measurements of the hot mass flow were not possible (because of the lack of choked flow across the heater exit throat), it was necessary to solve for the theoretical mixed flow conditions, using the equations of continuity through the turbine nozzle throat and an energy balance for both cold and hot flows. Figure 15 is a nomograph for this purpose, where temperatures have been normalized with respect to the cold air temperature. The small scatter of the data for cold-flow-only about the line $(1 + \beta)\sqrt{\frac{T_{om}}{T_{om}}} = 1$ indicates the validity of these measurements. The heater outlet temperatures (hot flow) were obtained from a previous calibration of the heater under similar flow conditions. The theoretical mixed temperatures are compared to the measured values in Table III, and reasonable agreement is seen. The thermocouples used for these measurements had very poor response because of the low air velocity in the settling chamber; an aspirating type probe would have given better results.

Figure 14. - Post-Test View of Blading Showing Dirt Deposits Indicating Separated Flow Region

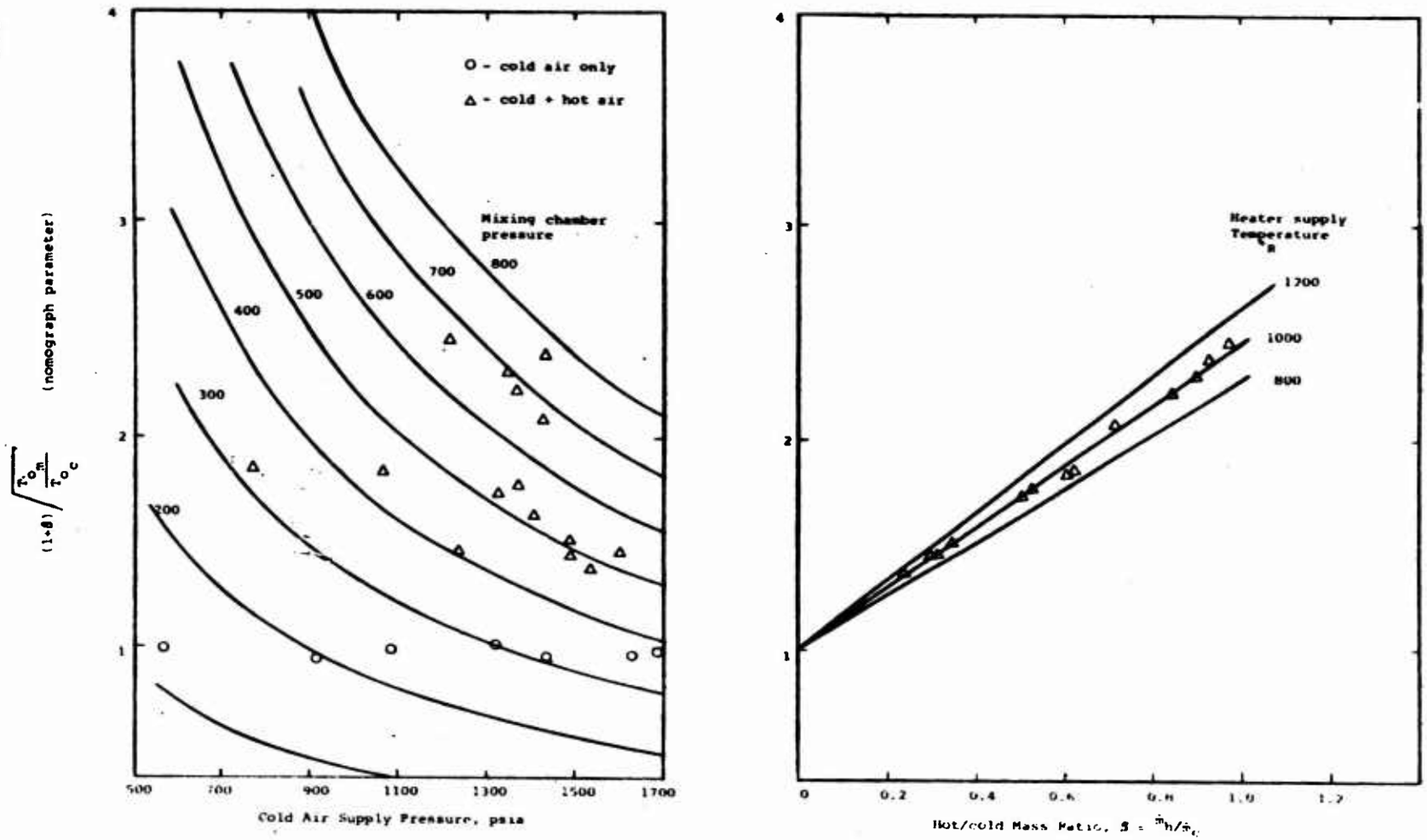

Figure 15. Nomograph to Find Ratio of Hot/Cold Air and Mixed Temperature

Towards the end of the test period a procedure was adopted for obtaining data at more than one set of supply conditions per run. This involved preloading the Pebble Bed Heater to the desired pressure, establishing the cold air flow, and taking data before and after opening the valve. The preloading was desirable in order to balance the pressure load across the valve. This test procedure resulted in nearly constant Reynolds number with varying pressure ratio, as noted in Table III. A different range of Reynolds numbers is obtained by changing the heater bed temperature. The Reynolds number range covered was somewhat lower than anticipated (Figure 8) because the test program was terminated (due to blade damage) before the full heater output had been obtained.

No evidence of changes were noted in the mass flow capacity of the nozzle ring which might have resulted from geometric throat changes due to blade bending.

C. STATIC PRESSURE DISTRIBUTIONS. The static pressure distributions in theblading are given in Figures 16 to 21. The data have been grouped according to the overall nozzle pressure ratio, $P_o/P_{ambient}$. The length coordinate is the streamwise length normalized with respect to the blade pitch. The results are as expected, in that agreement with theory at the throat and exit is quite good. The effects of overexpansion ($P_o/P_{amb.}$ < design) are most evident along the suction surface, as expected because of the subsonic axial Mach numbers. The upstream influence of back pressure beyond the location of the trailing Mach wave is of course due to the boundary layer, which may have become separated because of the adverse pressure gradient. Data in the subsonic region of the blading is shown as a band. This scatter is due in part to the normalizing procedure and in part to the effects of Reynolds number on the streamtube pattern in this section of the blading. This latter effect is particularly noticeable in Figure 17 in which streamline shifts are apparently seen at the lower pressure ratios.

The exit pressure distributions (circumferential) are shown in Figures 19 a and b, for hub and tip, respectively. At design conditions, a nearly uniform pattern at the correct level is seen. As the pressure ratio is decreased (increasing the amount of overexpansion) the suction side of the passage is affected first, and finally the entire passage. These cicumferential non-uniformities would, of course, dissipate due to viscous mixing downstream of the blade passage, with a corresponding shift in flow angle.

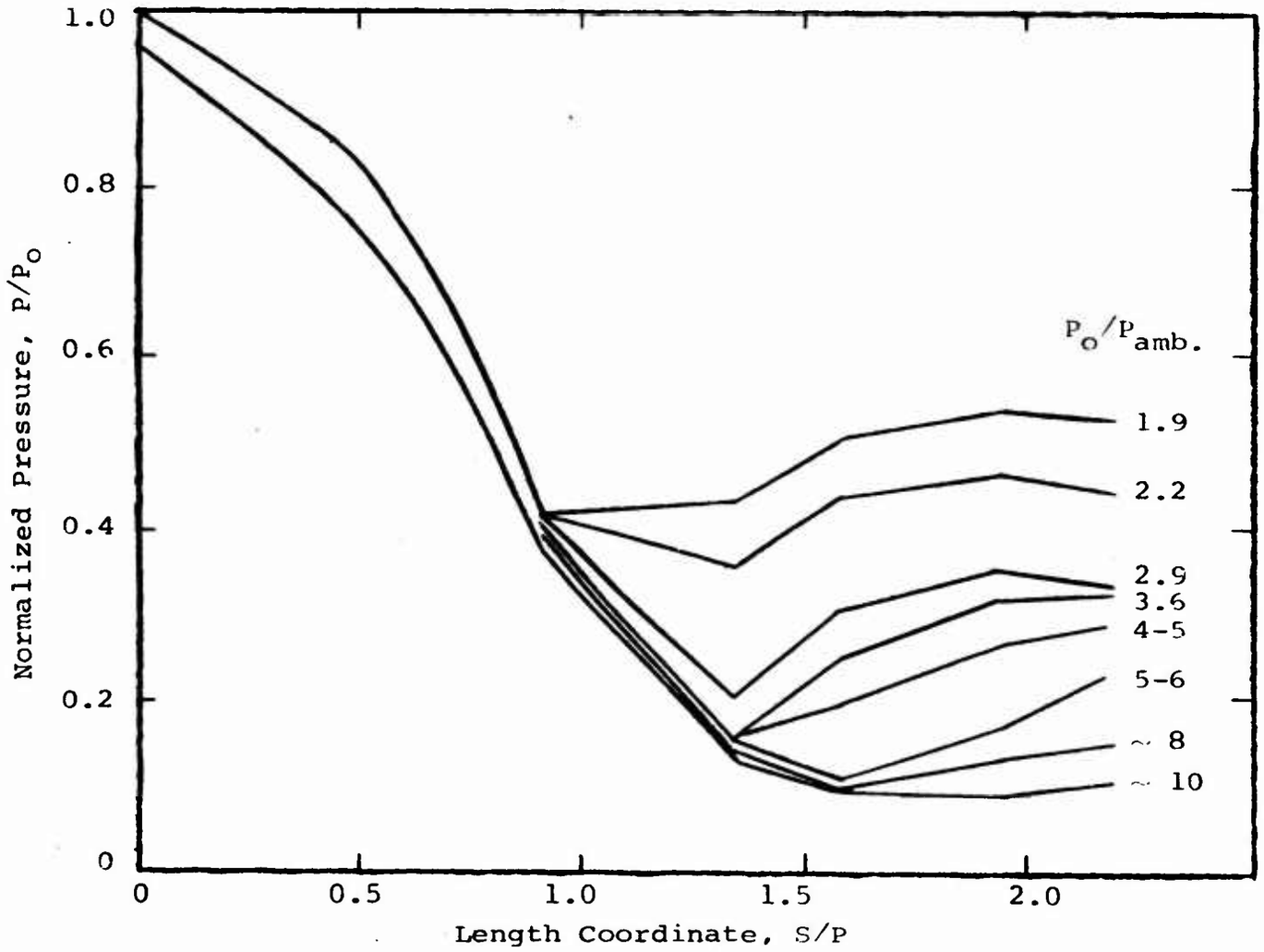

Figure 16a. - Hub Section Pressure Distribution, Suction Surface Side

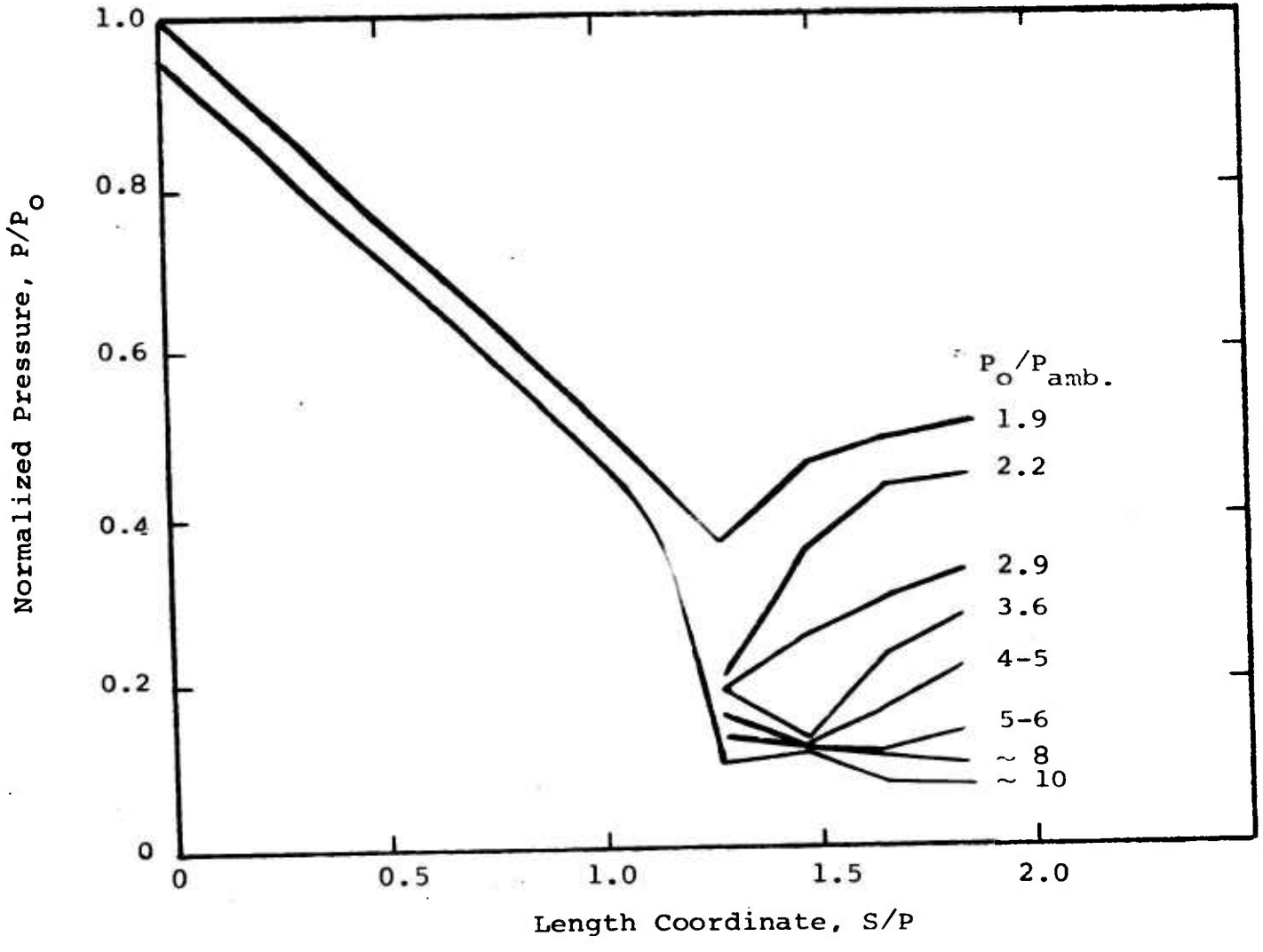

Figure 16b. - Hub Section Pressure Distribution, Mid-Channel

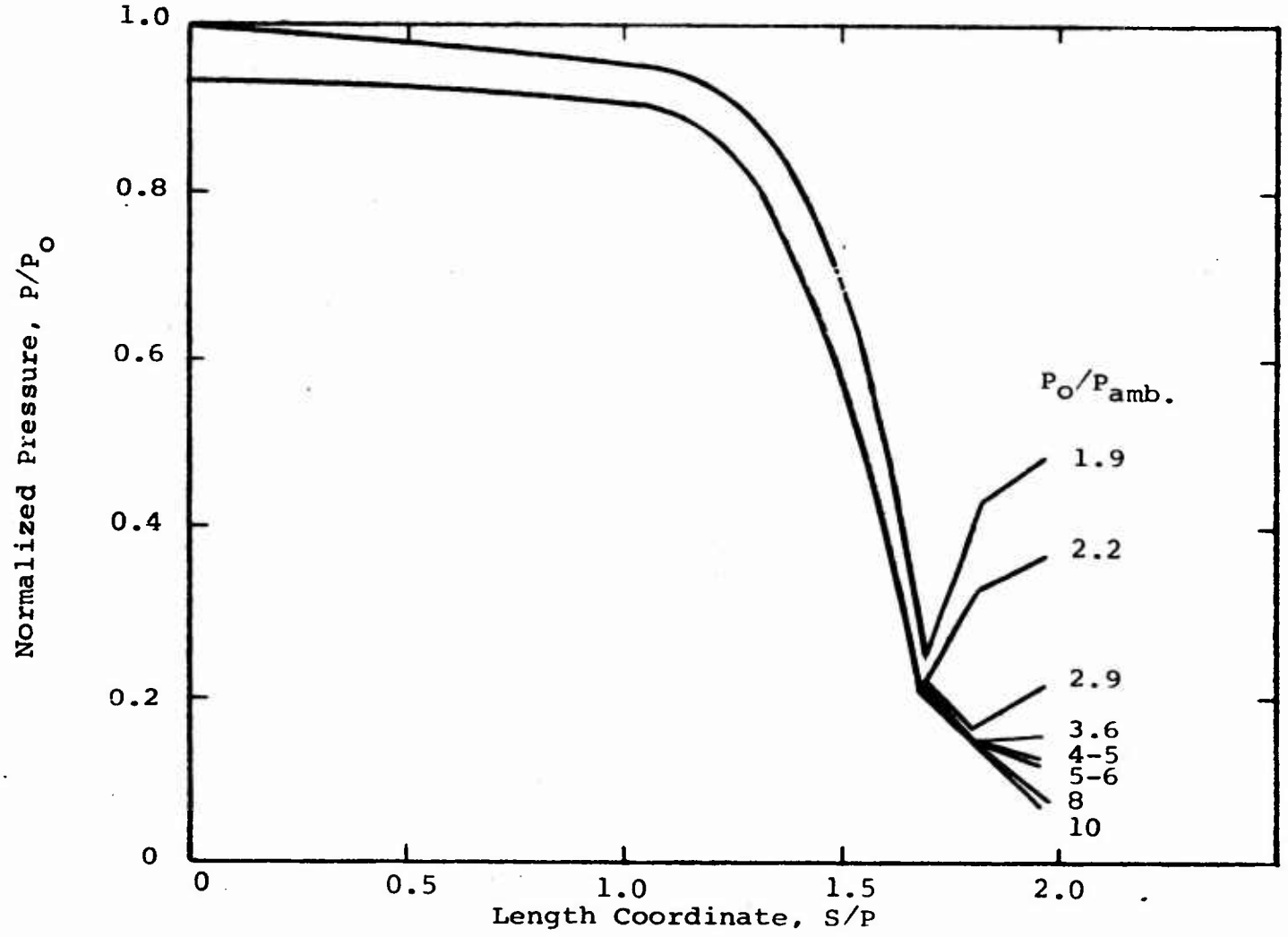

Figure 16c.- Hub Section Pressure Distribution, Pressure Surface Side

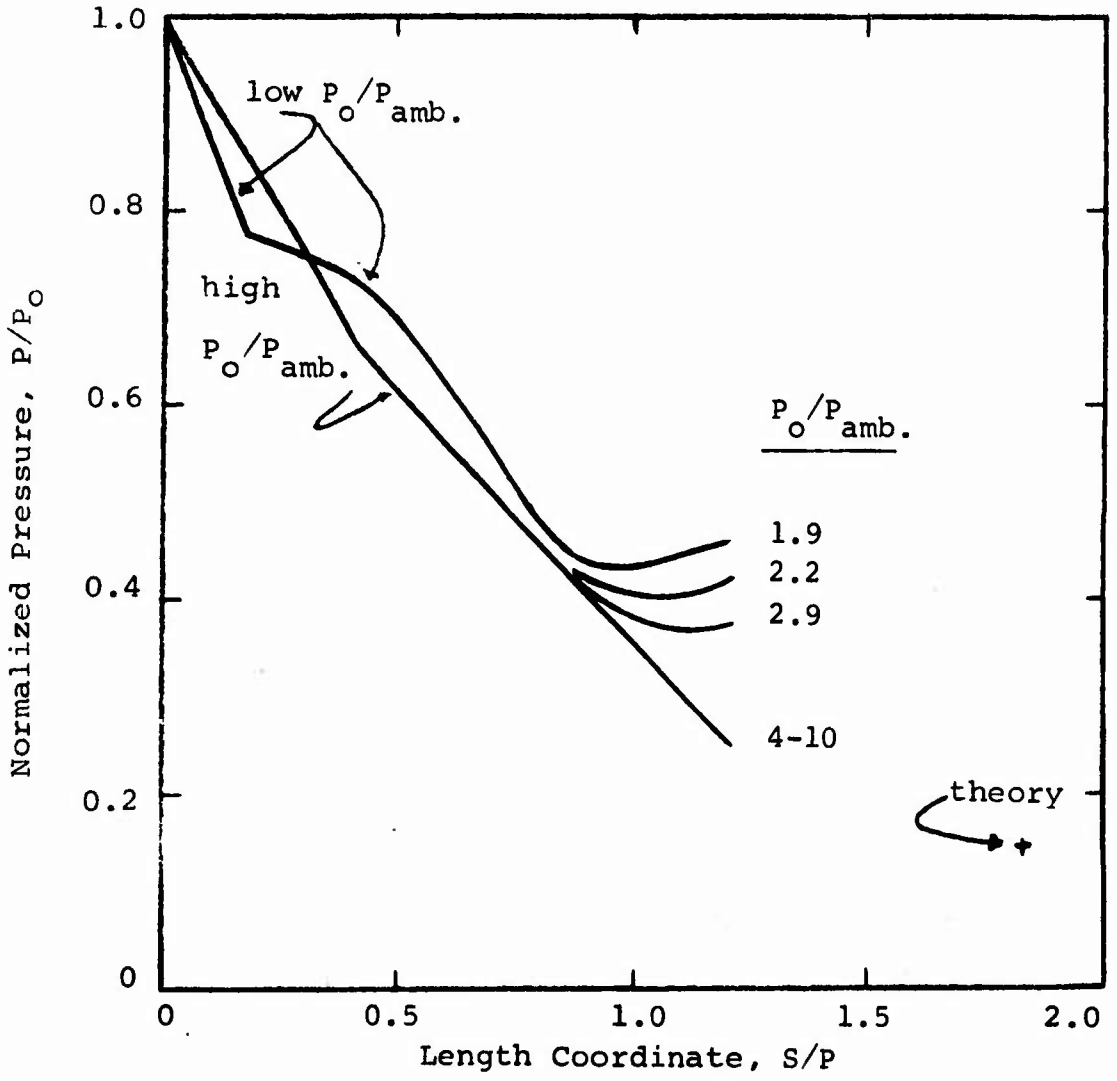

Figure 17. - Mid-Radius Pressure Distribution, Suction Surface

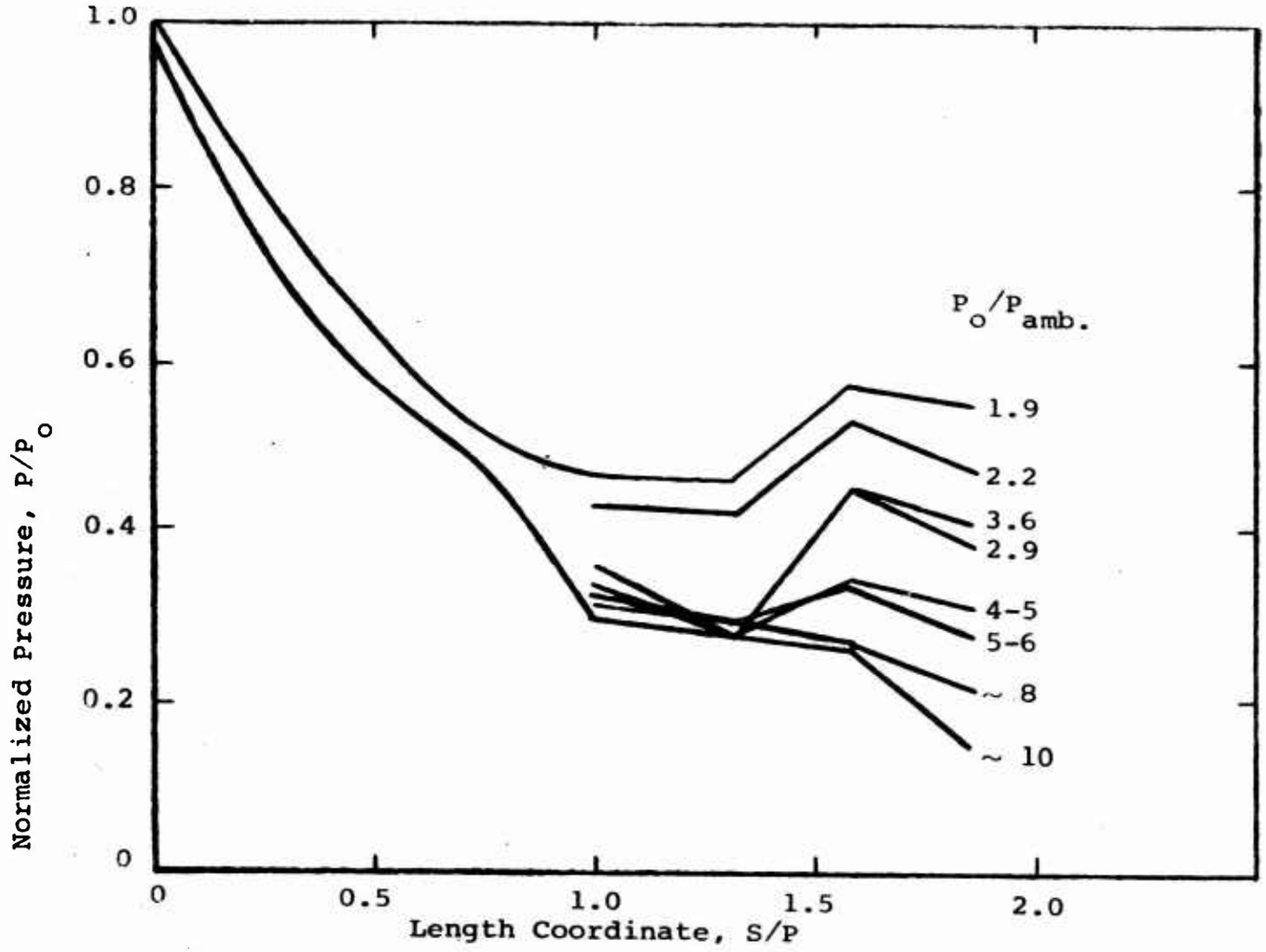

Figure 18a. - Tip Section Pressure Distribution, Suction Surface Side

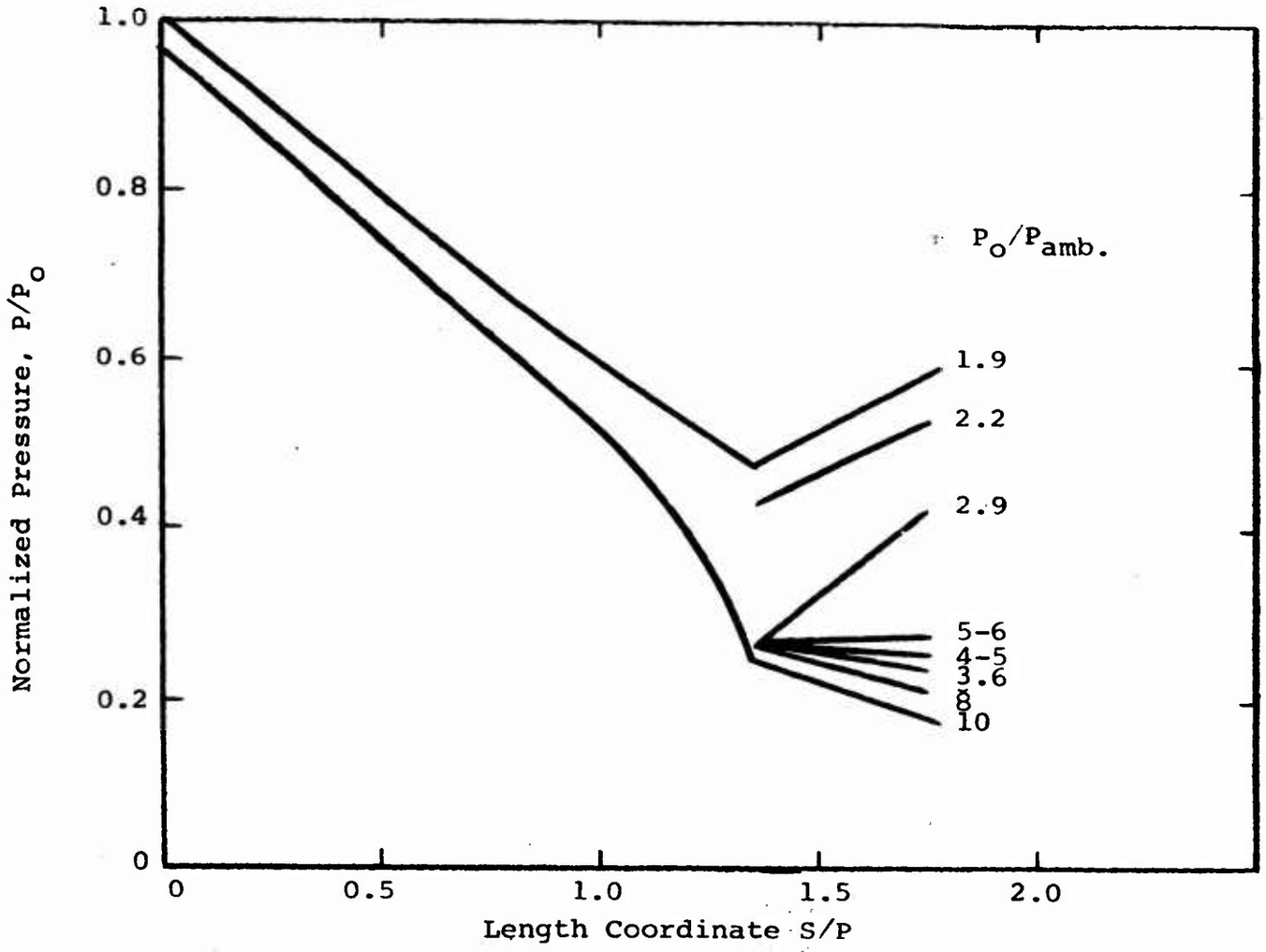

Figure 18b. - Tip Section Pressure Distribution, Mid-Channel

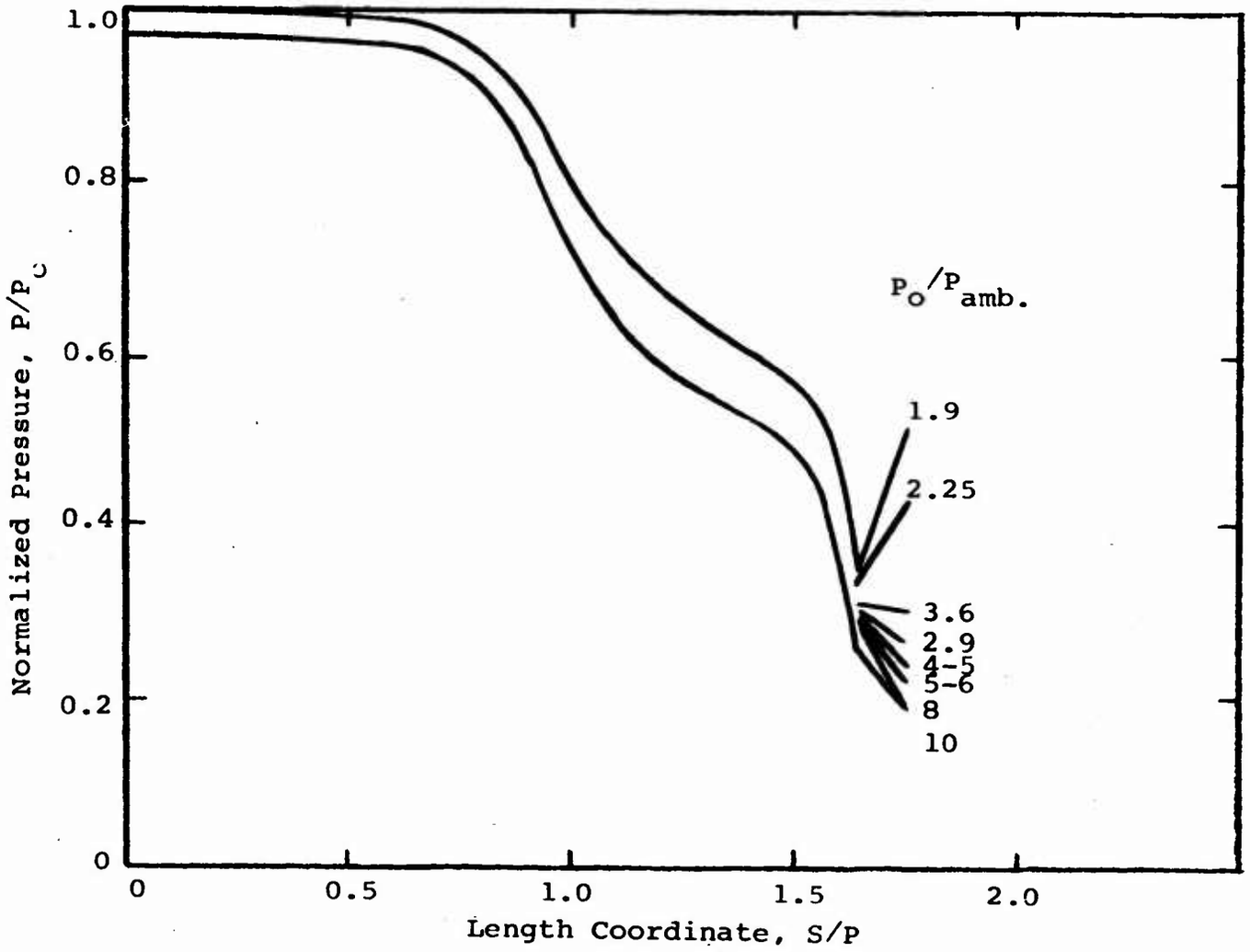

Figure 18c. - Tip Section Pressure Distribution, Pressure Surface Side

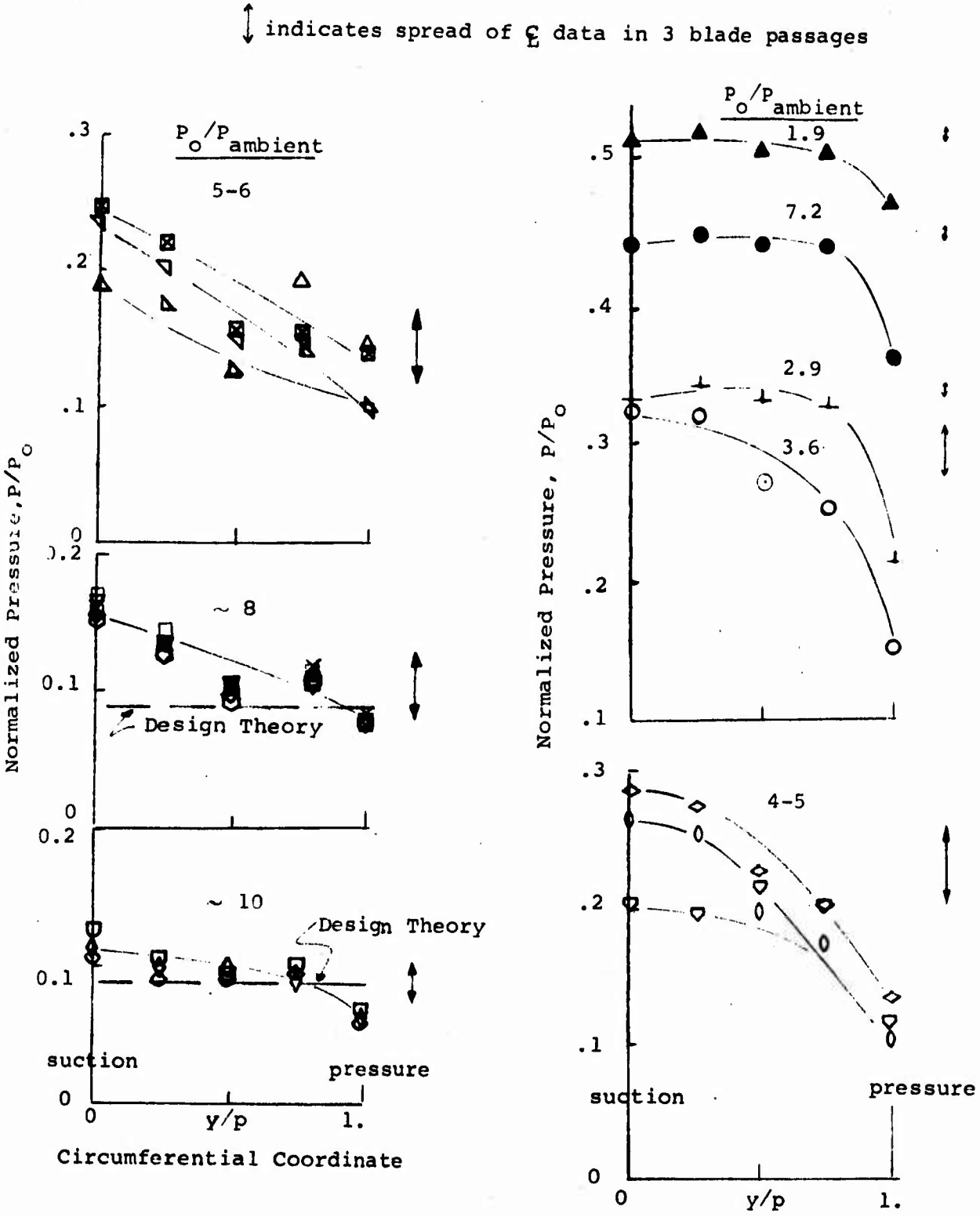

TR-76.7

Figure 19a. - Exit Pressure Distribution, Hub Section

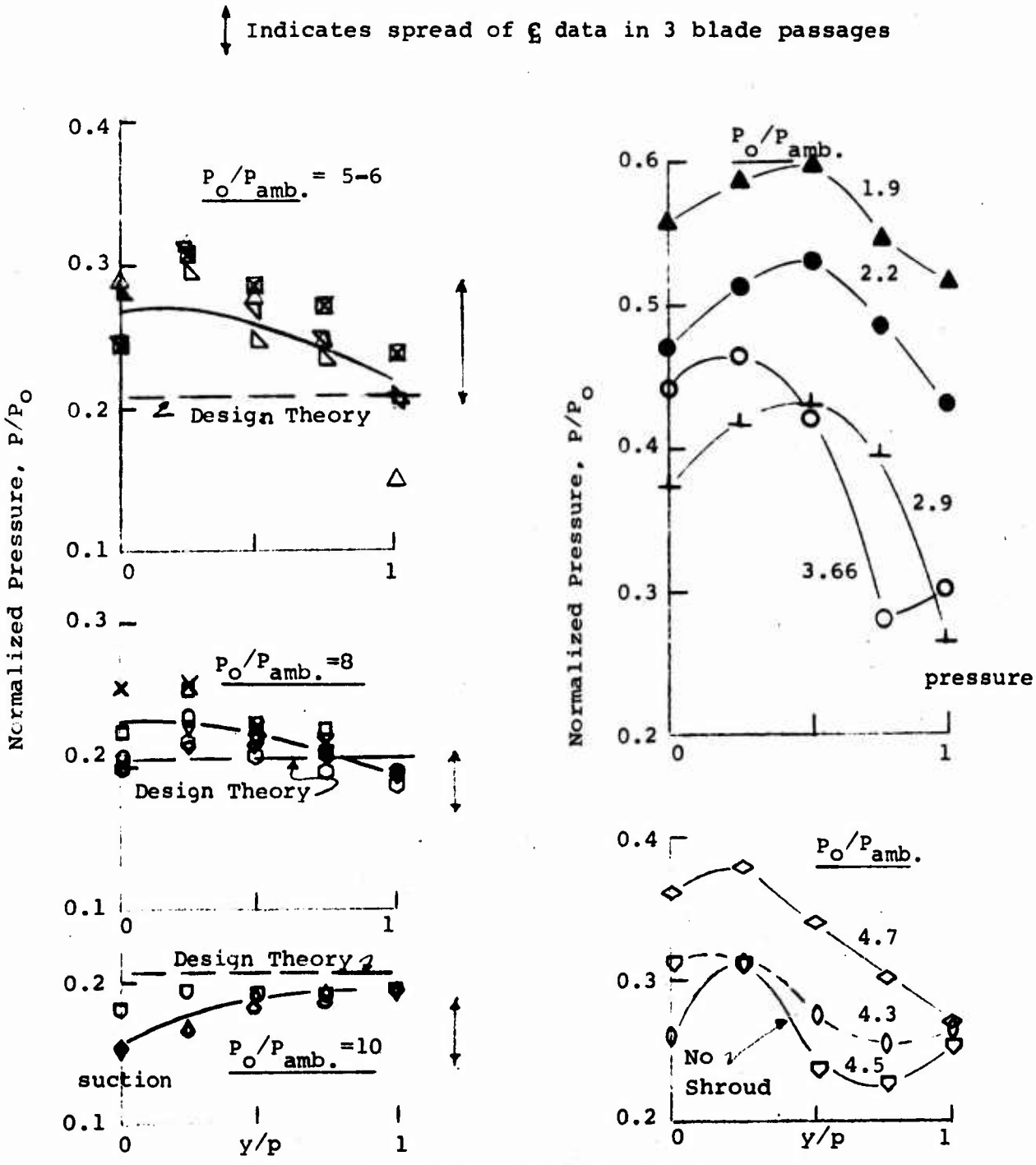

Figure 19b. - Exit Pressure Distribution, Tip Section

An idea of blade-to-blade uniformity may be obtained from the arrows shown in Figures 19a and b, representing the total spread of the reading of the centerline exit taps in 4 separate adjacent blade passages. Similar results were obtained at the passage inlets.

In general the data of Figure 19b (tip) exhibit more variability than Figure 19a (hub). This is due to the effects of tip shroud, seen in the lower right hand curve, and also of the blade bending previously discussed.

Cross plots of the exit pressure data vs overall pressure ratio are given in Figures 20a and b, for hub and tip section, respectively. It is seen that at the hub, some overexpansion may be tolerated before an increase in exit pressure ratio results, i.e., the nozzle will operate correctly at $P_o/P_{amb.} > 8$, compared to the theoretical values of 11. This may be explained by the pumping effect of the discharge jet on the central hub/base region. Two pressure taps were installed in this region, and their readings are presented in Figure 21. It is seen that the pressure in this region (outside the blading) is substantially lower than ambient.

D. BLADE TRAVERSE RESULTS.

Complete blade traverse data (Mach number, recovery, static pressure, and flow direction) were obtained for a total of six tests: three pressure ratios at each of two axial positions. The axial positions were at the nozzle ring exit plane and approximately .37 inch back from that plane, as indicated in Figure 22. The line of traverse was not radial, because of the complicated geometry of the probe, also as indicated in Figure 22. These traverse data are of course only a part of what had been intended for the original test program, which was terminated because of mechanical problems as discussed above. Nevertheless, they do serve as an indication of the adequacy of the blade design and the characteristics of the exit flow.

1. Exit Plane Traverses. Figure 23 gives the exit Mach number distribution at the nozzle exit plane (actually slightly downstream of the blade trailing edges, as shown in Figure 22). The agreement with theory is quite reasonable, particularly for

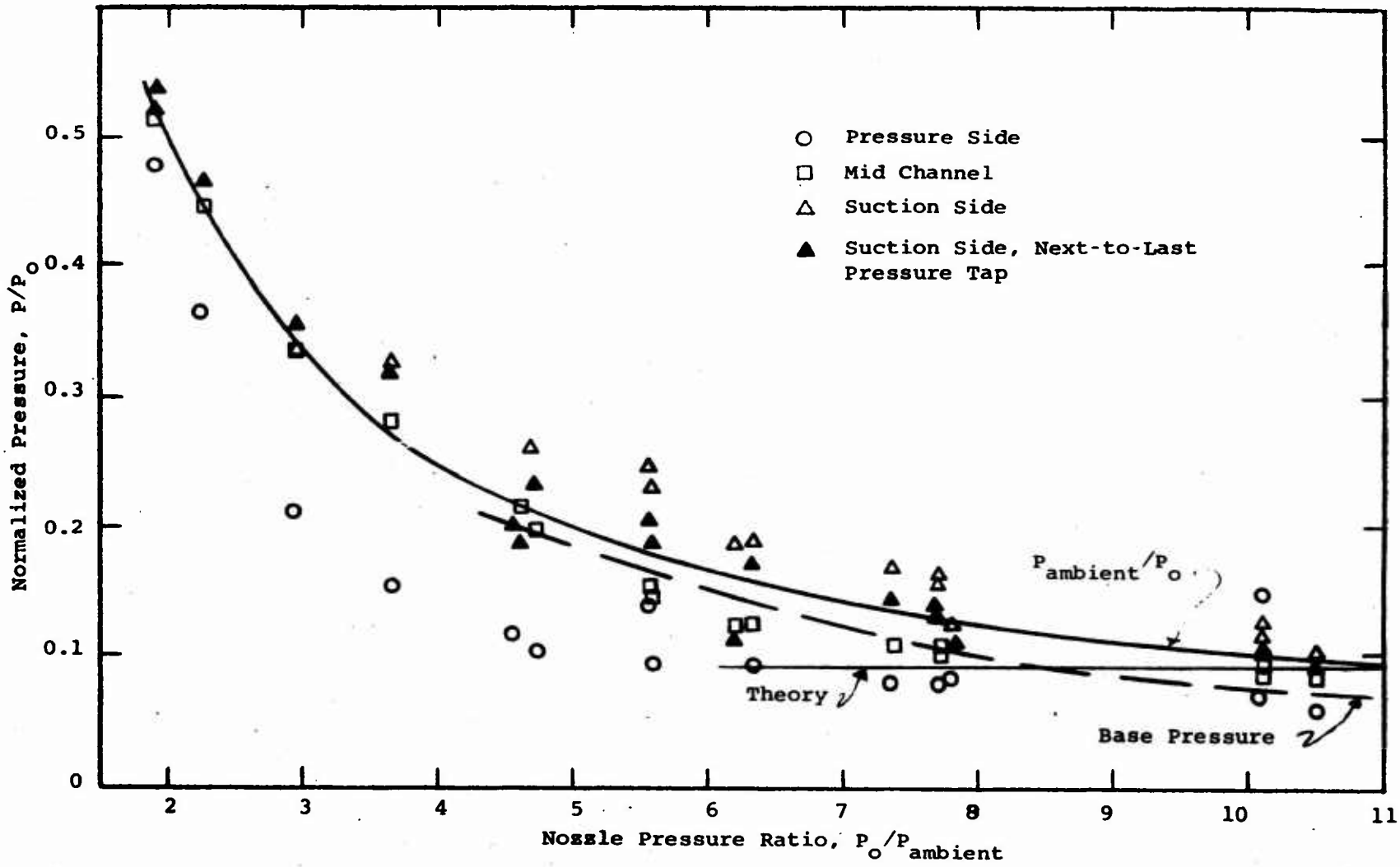

Figure 20a. - Nozzle Exit Pressure, Hub Section

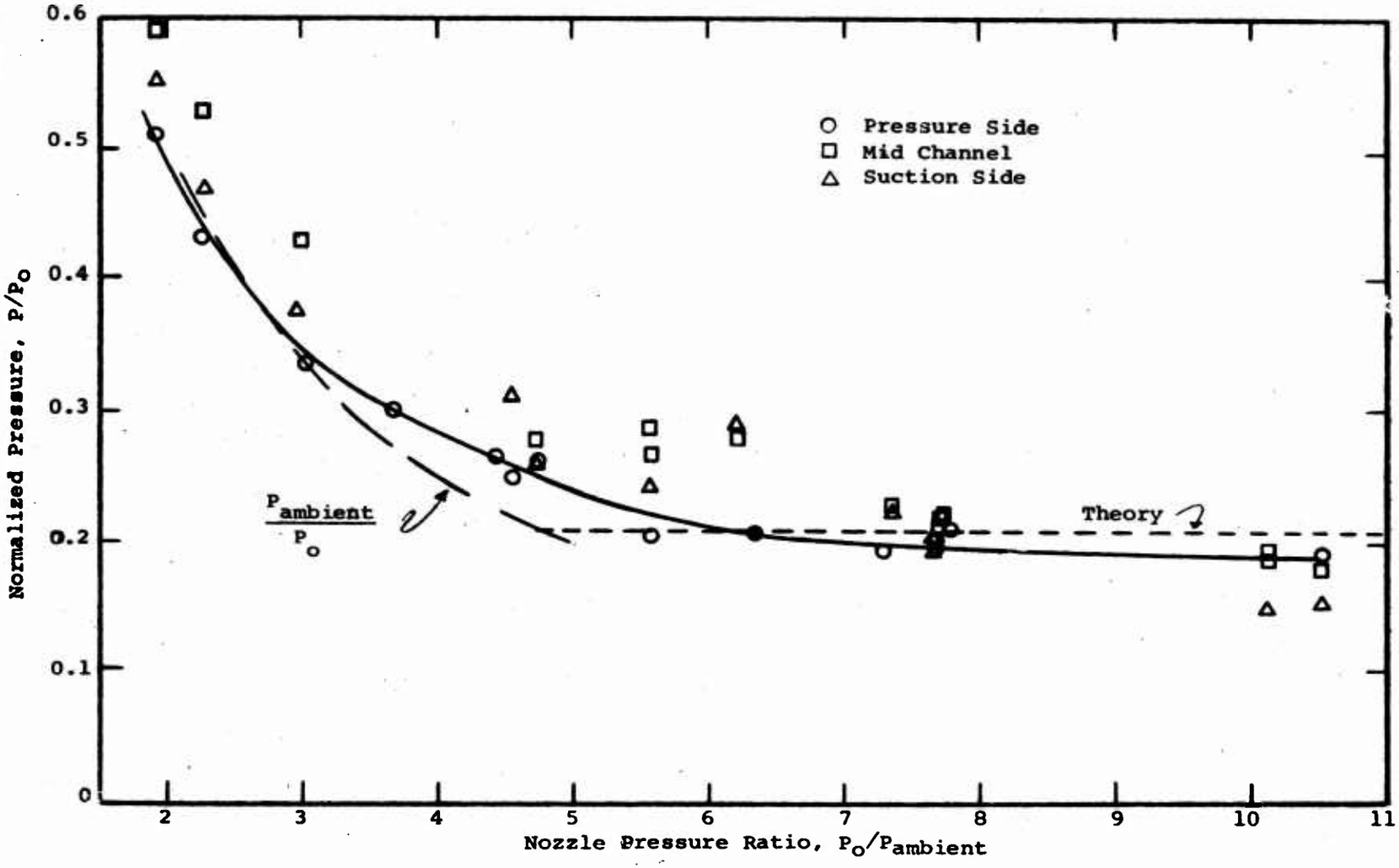

Figure 20b. - Nozzle Exit Pressure, Tip Section

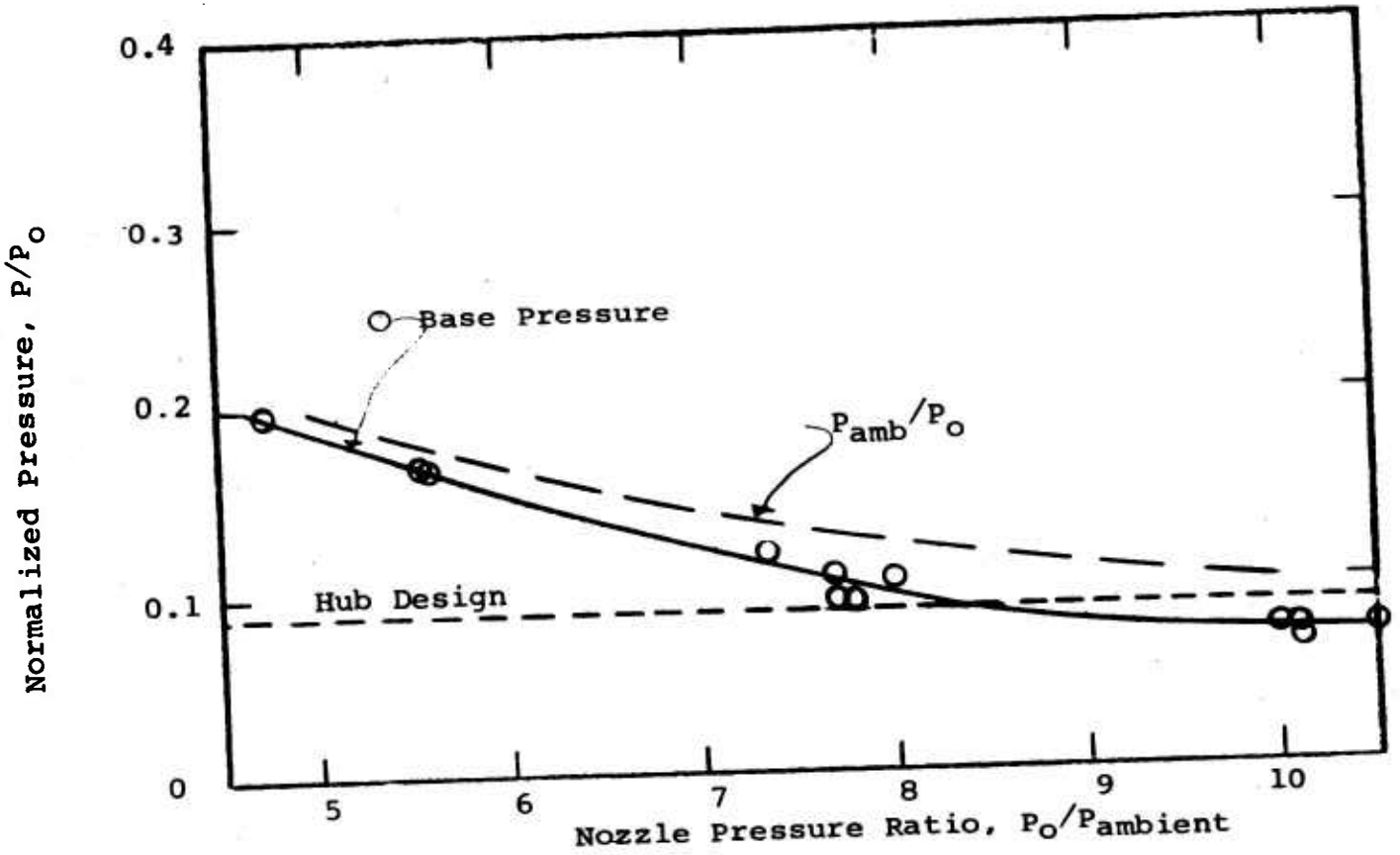

Figure 21. - Base Pressure Data

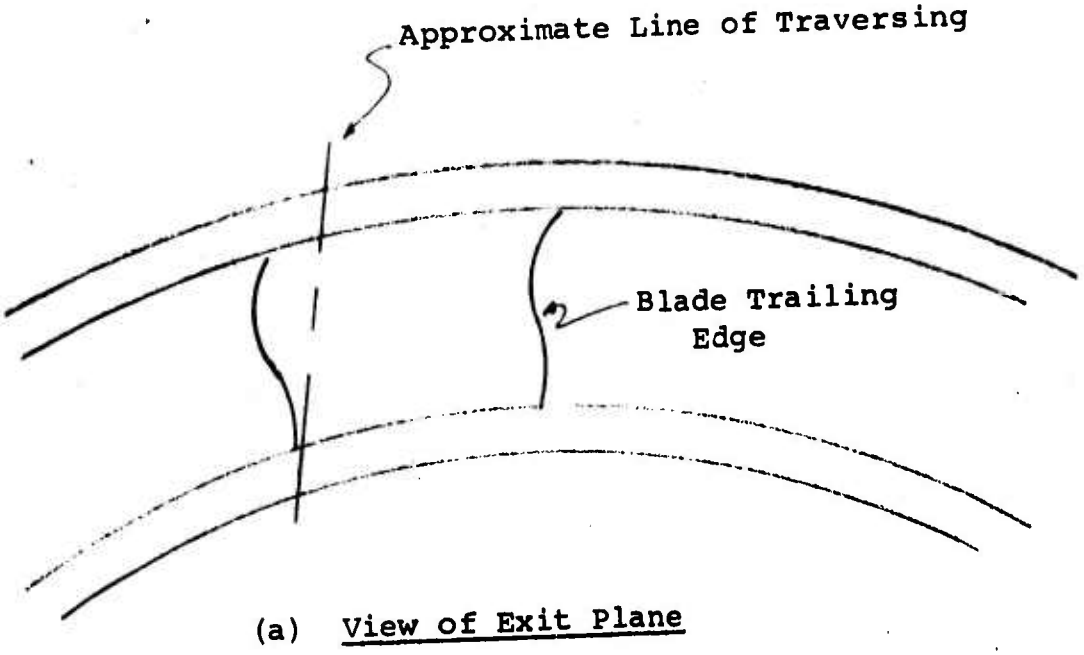

(a) View of Exit Plane

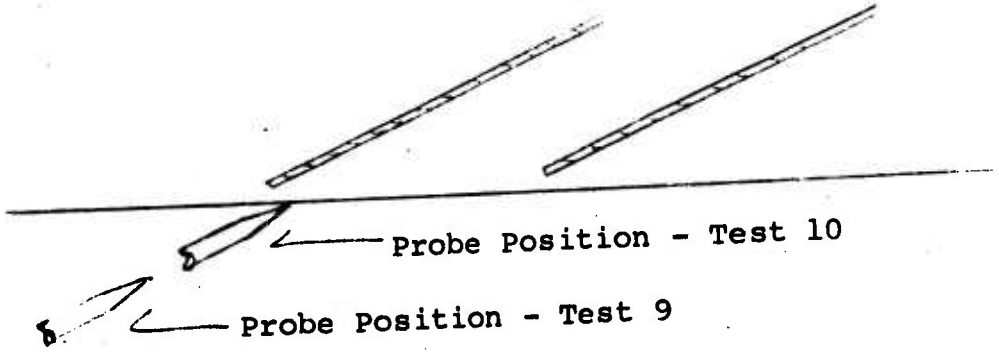

(b) Mid Radius Section

Figure 22. - Traversing Locations

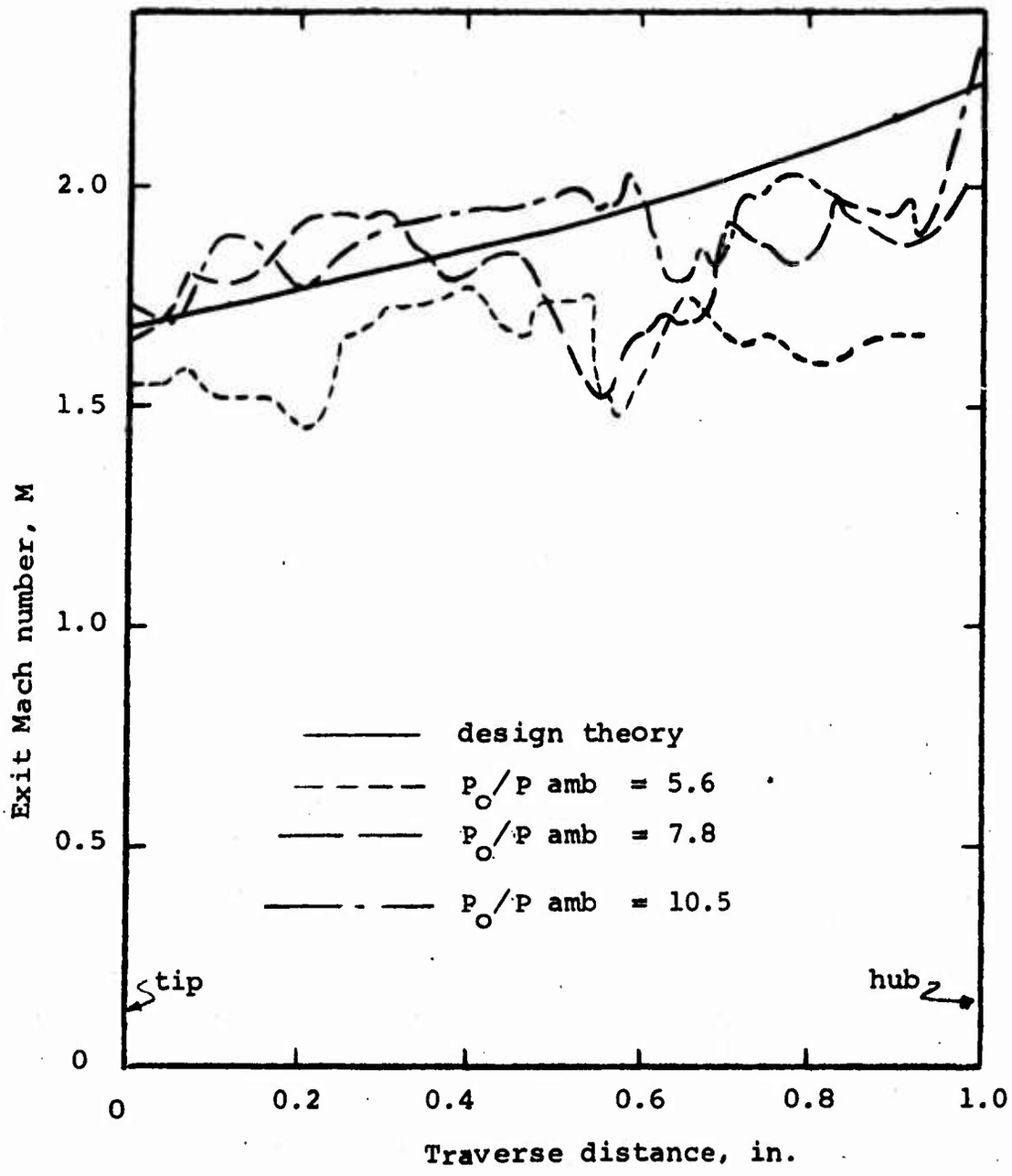

Figure 23. - Mach Number Data from Exit Plane Traverses (Test Series 10)

the higher pressure ratios. The effects of downstream expansion waves feeding in would have been expected for the high pressure ratios near the tip. Evidently this effect was compensated for by the distortion of the blades due to mechanical loading, since there is a general trend shown of higher tip Mach number for higher pressure ratio.

The dip in Mach number at about 0.6 - 0.7 or the radial traverse scale must be examined together with the total pressure recovery (Figure 24) and static pressure (Figure 25) curves. Since this region corresponds to nearly constant static pressure and a similar dip in recovery, it must be a region of viscous dissipation rather than a shock. Because of the lack of additional traverse data at other circumferential locations within the blade passage, no definite conclusion can be drawn. Yet, it appears that the traverse intersected a portion of the blade wake, whose location of course depends on the pressure gradient across the blade trailing edge. Since this "dip" has a different extent depending on pressure ratio, evidently the circumferential transport of the wake varies similarly.

The recovery curves, Figure 24, are also reasonable with the exception of the few points where greater than 100% recovery is indicated. The generally lower recoveries near the hub are believed to reflect the proximity of the traverse to the blade wake. The static pressure distribution (Figure 25) also reflects the design theory reasonably well, allowing for the presence of extraneous waves feeding upstream.

The flow angles, Figure 26a and b, are also what would be expected. The extreme hub and tip regions are subject to outside influences, but the agreement with theory in the mid radius region is reasonable. Note that some outward radial flow is expected near the tip because of the access slot in the shroud for the probe. The tendency for outward radial flow near the hub may result from the hub boundary layer.

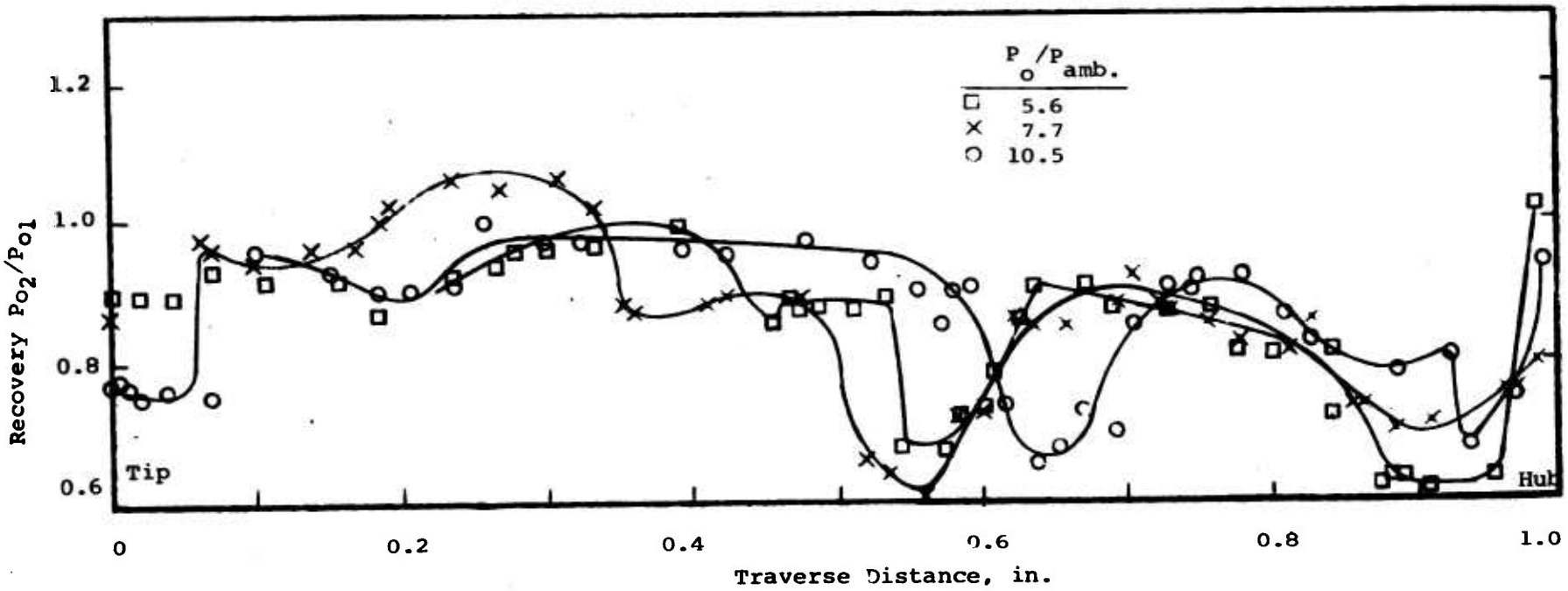

Figure 24. - Total Pressure Recovery at Exit Plane

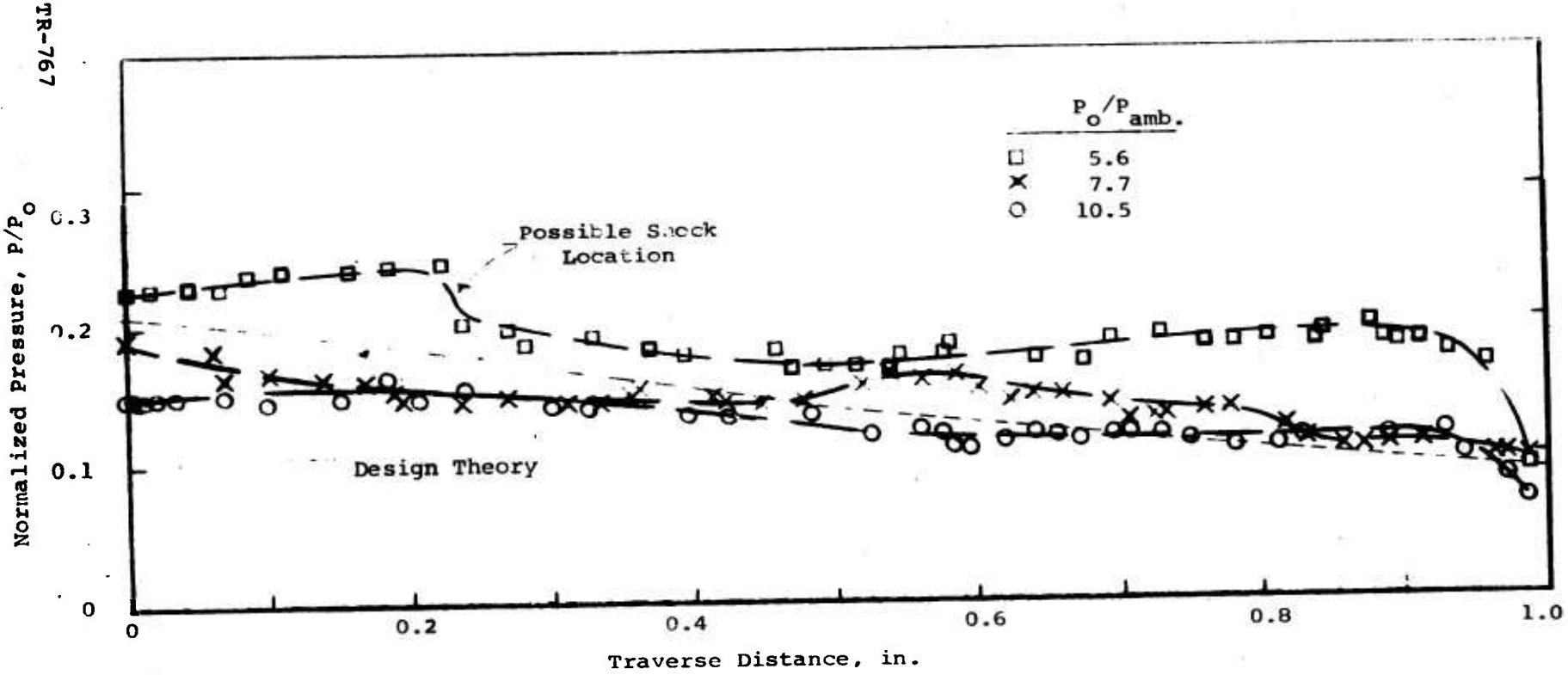

Figure 25. - Static Pressure Data from Exit Plane Traverse

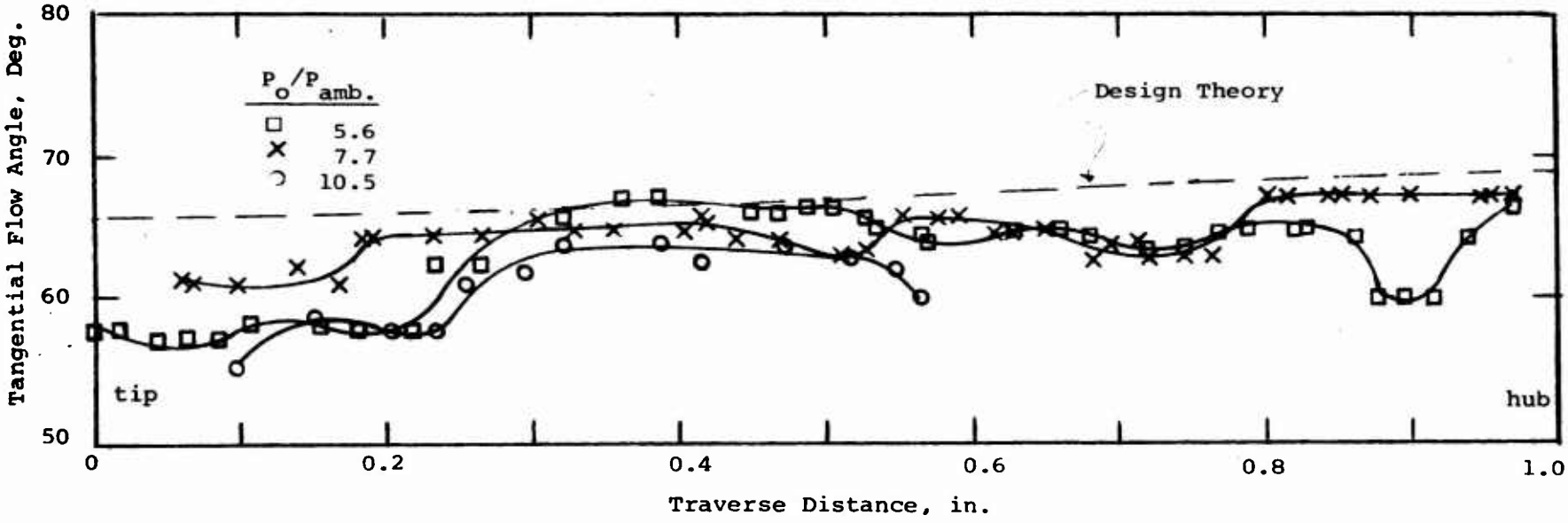

Figure 26a.- Nozzle Outlet Flow Angle (Tangential) at Exit Plane

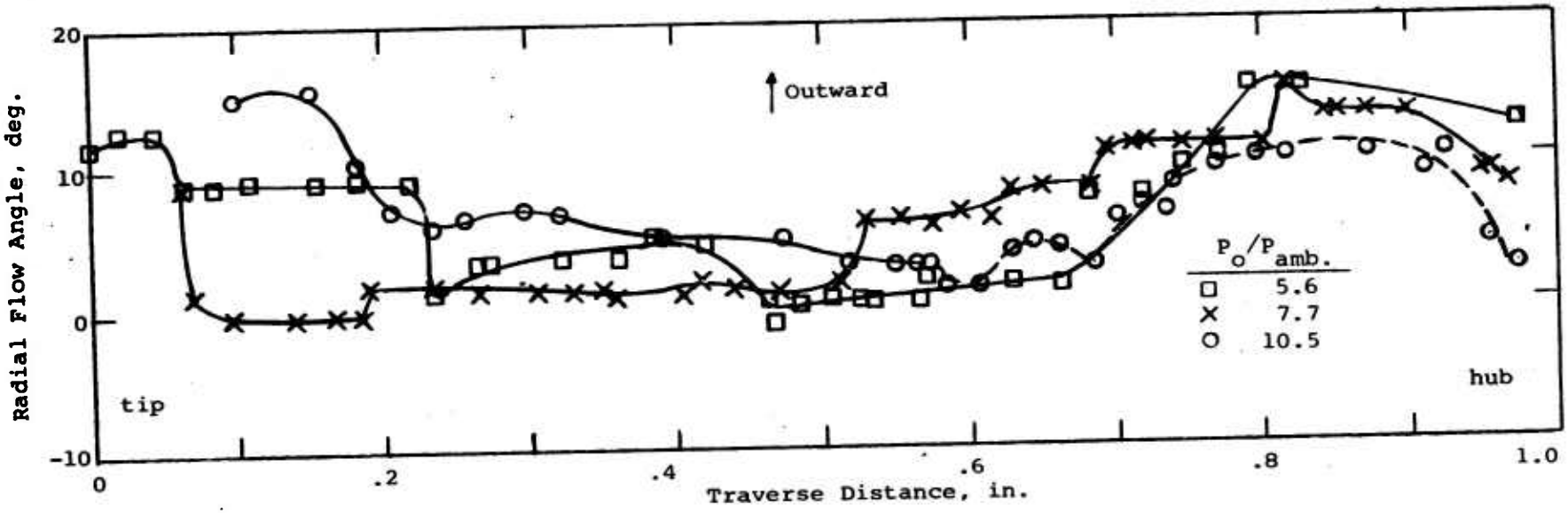

Figure 26b. - Radial Flow Angle at Nozzle Exit Plane

2. Downstream Traverses. The distribution of exit Mach number at the downstream location is shown in Figure 27. As might be expected, a leveling process has occurred, in that the tip values increased and the hub values decreased. The wake-like region is still present, and evidence of the hub boundary layer is seen. Evidently the jet has moved outward radially somewhat, in spite of the tip stroud.

The recovery data (Figure 28) reflect the mixing losses entailed in a free jet in that the values are generally lower than at the exit plane (Figure 24), particularly at the hub. Note that the 3/8" downstream distance corresponds to about 1" in the streamline direction, which is a significant mixing length.

The static pressures (Figure 29) correspond reasonably well to the radial equilibrium theory, again taking into account the effects of over and under expansion at tip and hub. The flow angles (Figures 30a and b) also agree well with theory. The high tangential angles at the hub correspond to the low recovery region there, which is different from the situation at the exit plane. The remaining data correspond reasonably well to the exit plane results.

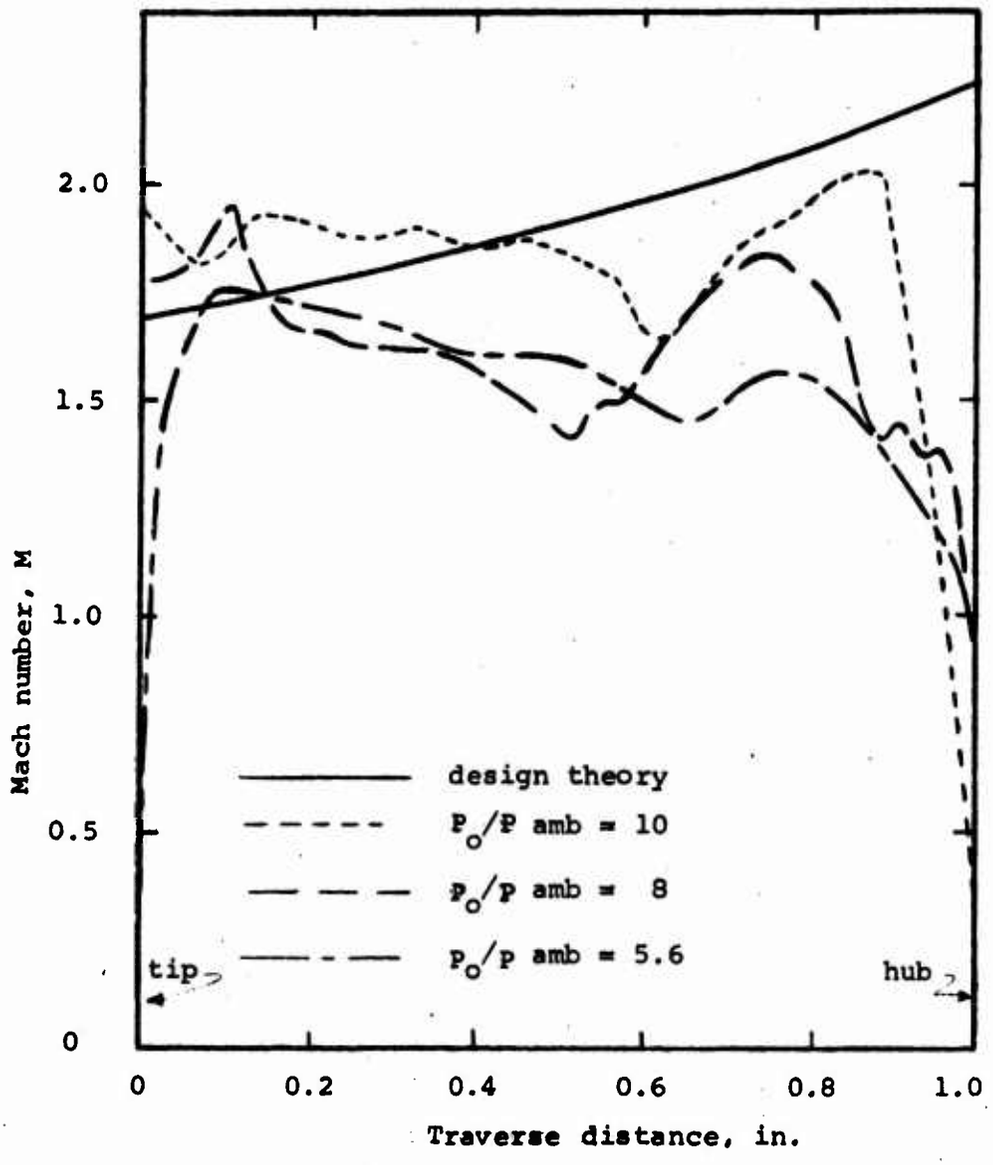

Figure 27. - Mach Number Data from Traverse 3/8 in. Downstream of Exit Plane (Test Series 9)

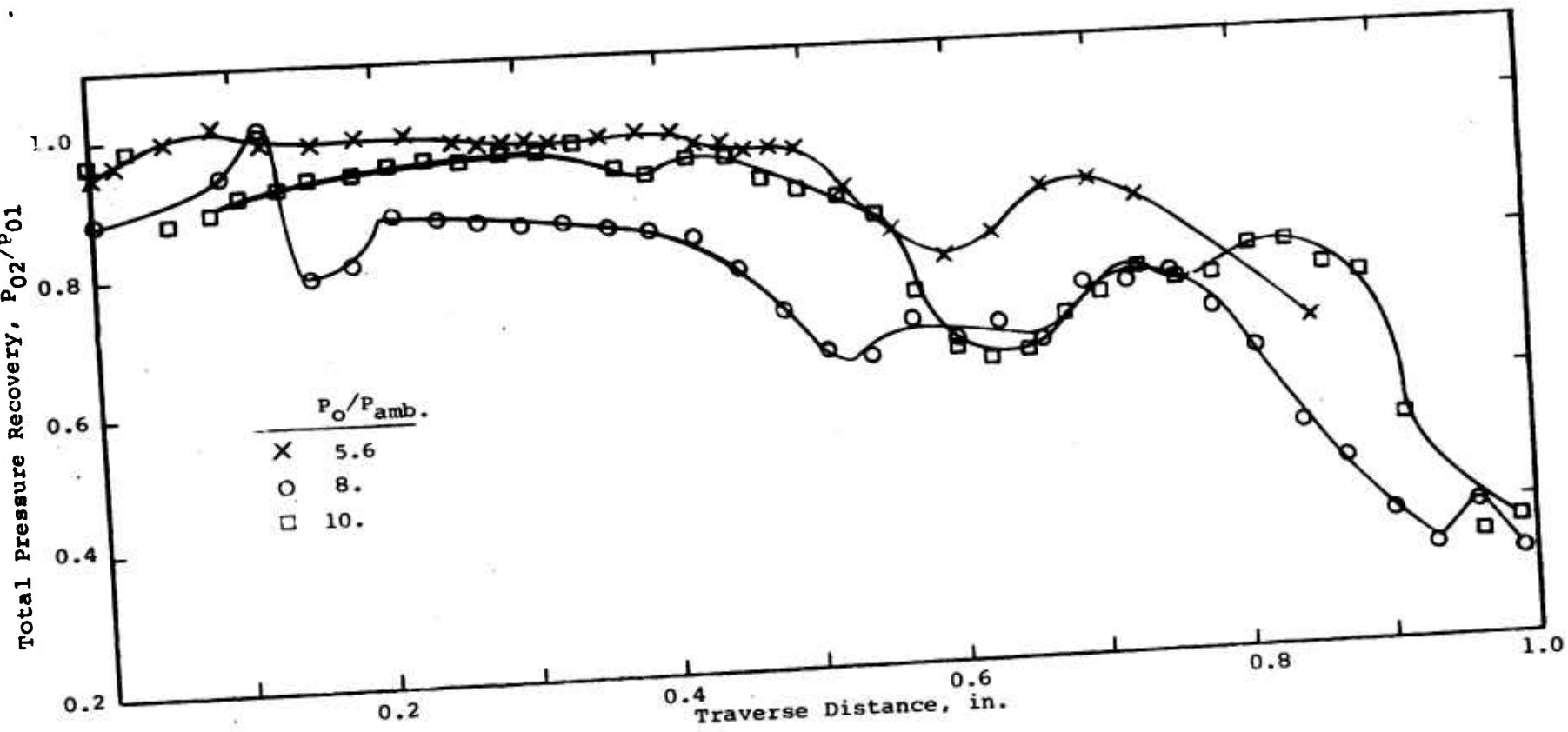

Figure 28. - Total Pressure Recovery 3/8 in. Downstream of Exit Plane

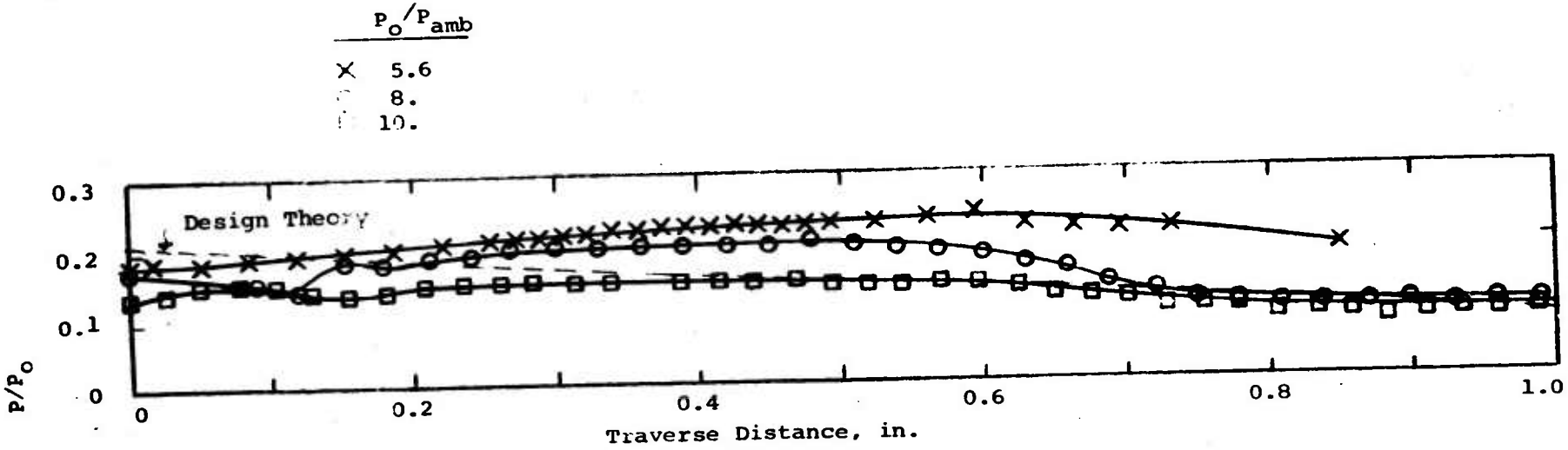

Figure 29. - Static Pressure Data from Traverse, 3/8 in. from Exit Plane

Figure 30a. - Nozzle Exit Flow Angle (Tangential) 3/8 in. From Exit Plane

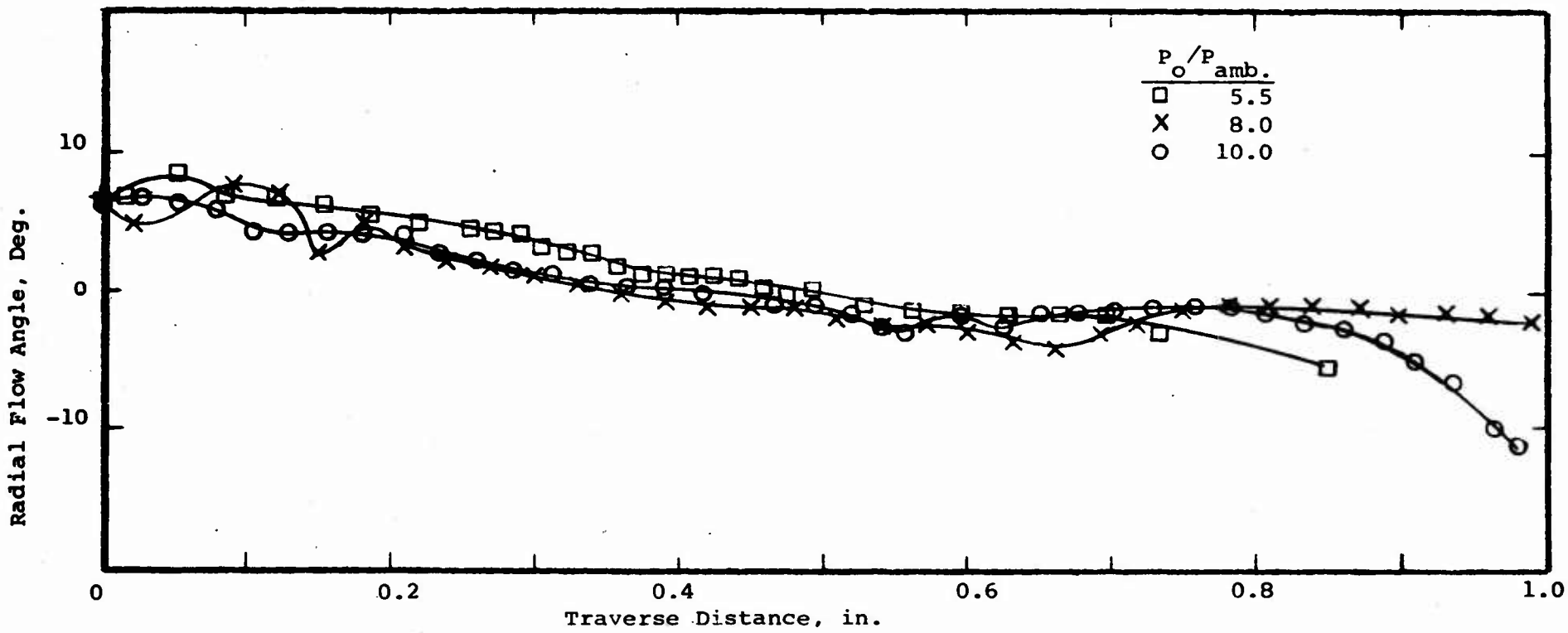

Figure 30b. - Radial Flow Angle 3/8 in. From Exit Plane

VI CONCLUSIONS

Two primary conclusions were reached as a result of this program:

1) Based on the data obtained, the supersonic nozzle design method appears adequate, and the performance of the nozzle was reasonable.

2) The structural design of the blading was inadequate, and the blade tips must be firmly attached to the outer shroud either by brazing or welding, particularly in the trailing edge region.

Secondary conclusions were reached with respect to the general task of obtaining meaningful outlet flow traverse data and of simulating appropriate nozzle discharge conditions:

3) With subsonic axial discharge Mach number, the feedback effect of the effect of the ambient conditions will obscure at least some portion of the true flow field at any nozzle pressure ratio.

4) Free jet operation is not practical and at least an outer shroud must be provided. An inner shroud would be desirable to eliminate base flow pumping effects in the hub region.

VII RECOMMENDATIONS

It is recommended that the nozzle design be adopted for use in a demonstrator supersonic turbine stage, with appropriate attachment of the blade tips. Static pressure instrumentation should be retained as a check on stator-rotor interaction.

APPENDIX A

TABLES, SPECIFICATIONS, AND DRAWINGS FOR BLADE CONTOURS

SECTION a^2

$\frac{r}{r_h} = 1.15$

	1	2	3	4	5	6	7	8	9
1	B.L.	Y	y_1	y_2		y_1	y_2		
2		[illegible]	x 3.4	x 3.4		in.	in.		
3									
4	C	-5.475	.555	.555		.163	.163		
5		-5.250	.205	.950		.060	.279		
6	LE (7')	-4.500	0	1.390		0	.409		
7		-3.750	.240	1.560		.071	.459		
8	8'	-3.000	.750	1.770		.221	.520		
9		-2.250	1.125	1.890		.331	.556		
10	9'	-1.500	1.270	2.020		.373	.594		
11		-0.750	1.398	2.125		.411	.625		
12	0	0	1.500	2.230		.441	.656		
13	1	1.500	1.730	2.430		.509	.714		
14	2	3.000	1.970	2.550		.579	.750		
15	3	4.500	2.180	2.670		.641	.785		
16	4	6.000	2.410	2.790		.709	.820		
17	5	7.500	2.600	2.940		.779	.864		
18	6	9.000	2.900	3.090		.847	.908		
19	7	10.500	3.110	3.280		.914	.964		
20	8	12.000	3.370	3.460		.991	1.017		
21	9	13.500	3.590	3.680		1.053	1.082		
22	10	15.000	3.820	3.930		1.126	1.155		
23	TE	16.500	4.120	4.200		1.211	1.235		

SECTION a^3

$\frac{r}{r_h} = \underline{1.10}$

			3	4	5	6	7	8	9
		θ	y_1	y_2		y_1	y_2		
		degrees	x 3.4	x 3.4		in.	in.		
	C	-5.610	.613	.613		.180	.180		
		-5.250	.083	1.253		.024	.368		
	LE	-4.66	0	1.530		0	.450		
	7'	-4.50	.010	1.570		.029	.462		
		-3.75	.250	1.780		.074	.523		
	8'	-3.00	.750	1.950		.221	.573		
		-2.75	1.154	2.063		.339	.607		
	9'	-1.50	1.370	2.180		.403	.641		
		-0.75	1.469	2.271		.432	.668		
	0	0	1.580	2.330		.465	.685		
	1	1.50	1.800	2.530		.529	.744		
	2	3.00	2.000	2.630		.588	.773		
	3	4.50	2.200	2.720		.647	.800		
	4	6.00	2.420	2.820		.711	.829		
	5	7.50	2.620	2.940		.770	.864		
	6	9.00	2.840	3.080		.835	.906		
	7	10.50	3.010	3.230		.885	.950		
	8	12.00	3.280	3.390		.964	.997		
	9	13.50	3.490	3.580		1.026	1.053		
	10	15.00	3.710	3.800		1.091	1.117		
	11	16.50	3.980	4.070		1.147	1.197		
	12	18.00	4.230	4.300		1.244	1.264		
	TE	19.09	4.400	4.480		1.294	1.317		

SECTION a^4

$\frac{r}{r_h} = 1.05$

	1	2	3	4	5	6	7	8	9
1	P.Y	θ	y_1	y_2		y_1	y_2		
2		degrees	x 3.4	x 3.4		in.	in.		
3									
4	C	-5.540	.660	.660		.194	.194		
5		-5.250	.053	1.430		.016	.420		
6	LE	-4.760	0	1.625		0	.478		
7	7'	-4.500	.025	1.710		.007	.503		
8		-3.750	.295	1.933		.087	.568		
9	8'	-3.00	.800	2.080		.235	.612		
10		-2.25	1.150	2.170		.338	.638		
11	9'	-1.50	1.350	2.280		.397	.670		
12		-0.75	1.475	2.368		.434	.696		
13	0	0	1.600	2.470		.470	.726		
14	1	1.50	1.800	2.600		.529	.764		
15	2	3.00	1.980	2.670		.582	.785		
16	3	4.50	2.160	2.730		.641	.803		
17	4	6.00	2.380	2.830		.700	.832		
18	5	7.50	2.560	2.920		.759	.858		
19	6	9.00	2.770	3.040		.814	.894		
20	7	10.50	2.970	3.170		.873	.932		
21	8	12.00	3.190	3.310		.938	.973		
22	9	13.50	3.390	3.480		.997	1.023		
23	10	15.00	3.610	3.690		1.061	1.085		
24	11	16.50	3.810	3.890		1.120	1.144		
25	12	18.00	4.070	4.160		1.197	1.223		
26	13	19.50	4.280	4.360		1.258	1.282		
27	TE	19.89	4.294	4.374		1.262	1.286		

SECTION a^5

$\frac{r}{r_h} = 1.00$

	1	2	3	4	5	6	7	8	9
1	RAY	θ	y_1	y_2		y_1	y_2		
2		degrees	x 3.4	x 3.4		in.	in.		
3									
4	C	-6.39	.675	.675		.198	.198		
5	G'	-6.00	.153	1.260		.045	.370		
6	LE	-5.25	0	1.675		0	.492		
7	7'	-4.50	.070	1.950		.021	.573		
8		-3.75	.400	2.150		.118	.632		
9	8'	-3.00	.820	2.320		.241	.682		
10		-2.25	1.263	2.404		.371	.707		
11	9'	-1.50	1.480	2.480		.435	.729		
12		-0.750	1.645	2.575		.484	.757		
13	0	0	1.730	2.650		.509	.779		
14	1	1.50	1.900	2.730		.559	.803		
15	2	3.00	2.070	2.750		.609	.809		
16	3	4.50	2.230	2.810		.656	.826		
17	4	6.00	2.400	2.870		.706	.844		
18	5	7.50	2.570	2.930		.756	.861		
19	6	9.00	2.740	3.020		.806	.888		
20	7	10.50	2.920	3.130		.858	.920		
21	8	12.00	3.100	3.240		.911	.953		
22	9	13.50	3.280	3.390		.964	.997		
23	10	15.00	3.480	3.570		1.023	1.050		
24	11	16.50	3.700	3.780		1.088	1.111		
25	12	18.00	3.900	3.980		1.147	1.170		
26	TE (13)	19.50	4.100	4.180		1.205	1.230		

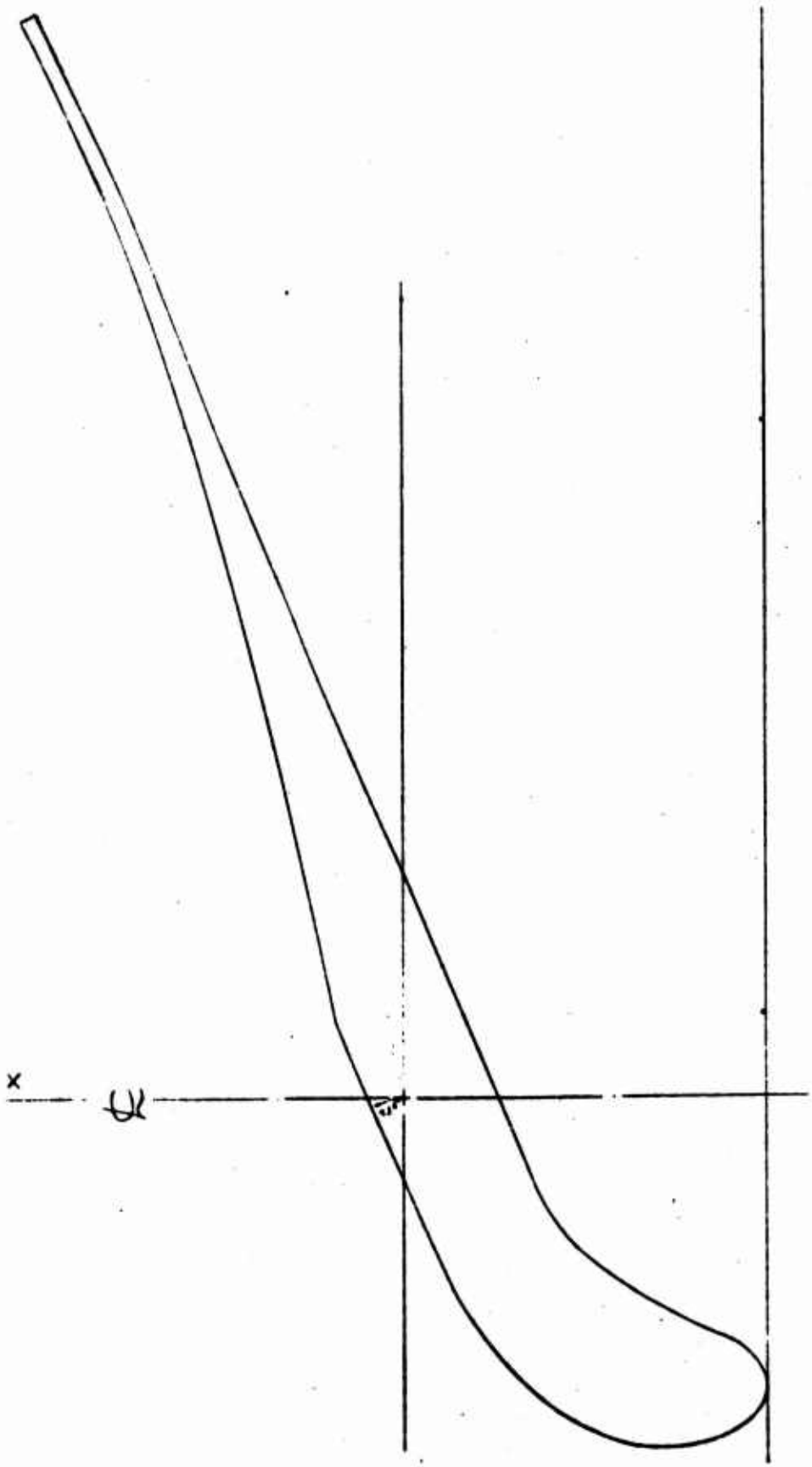

FIGURE A-1:PLANE SECTION, A-2 (Through $r/r_h = 1.15$)

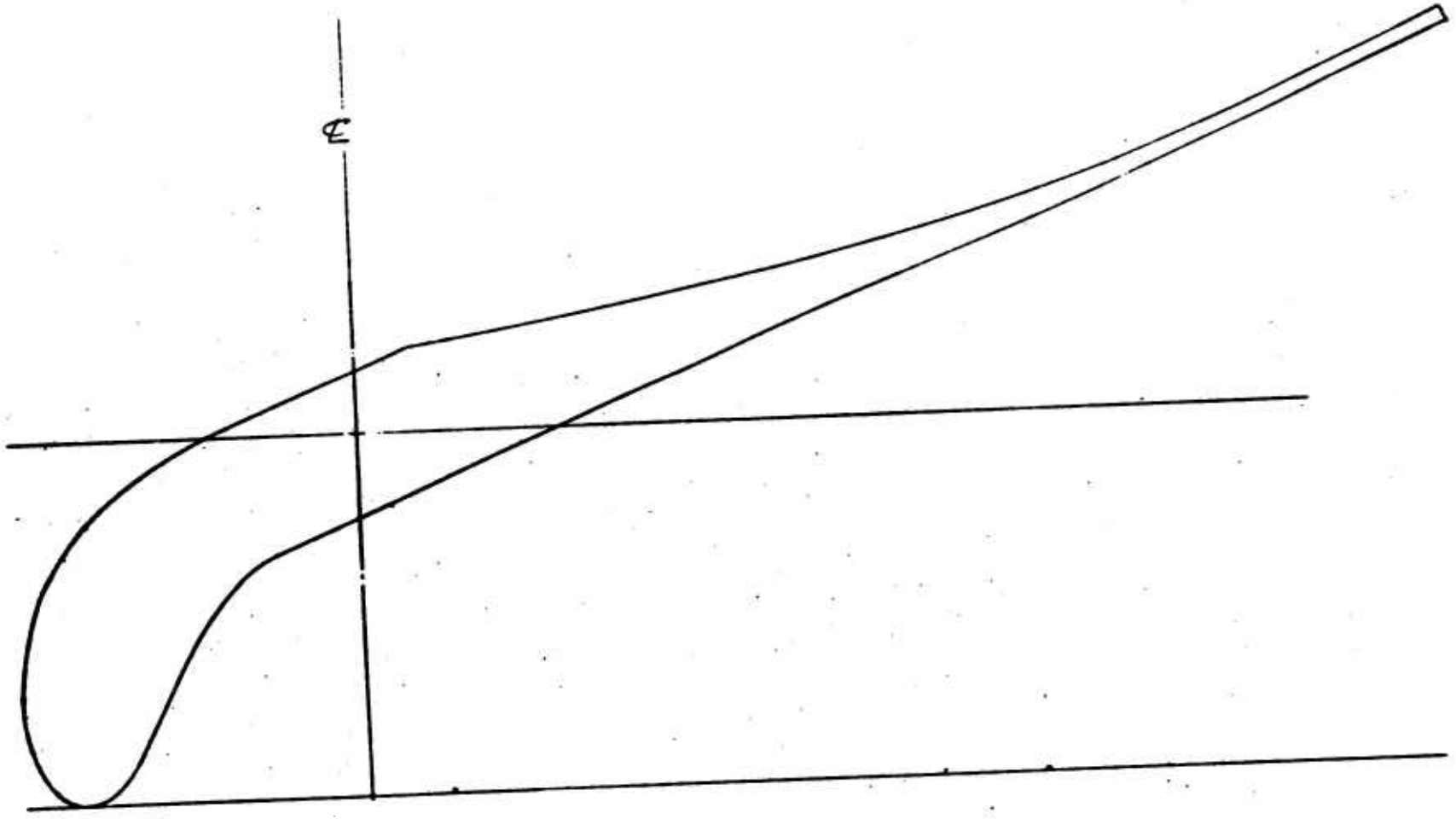

FIGURE A-2: PLANE SECTION, A-3 (Through $r/r_h = 1.10$)

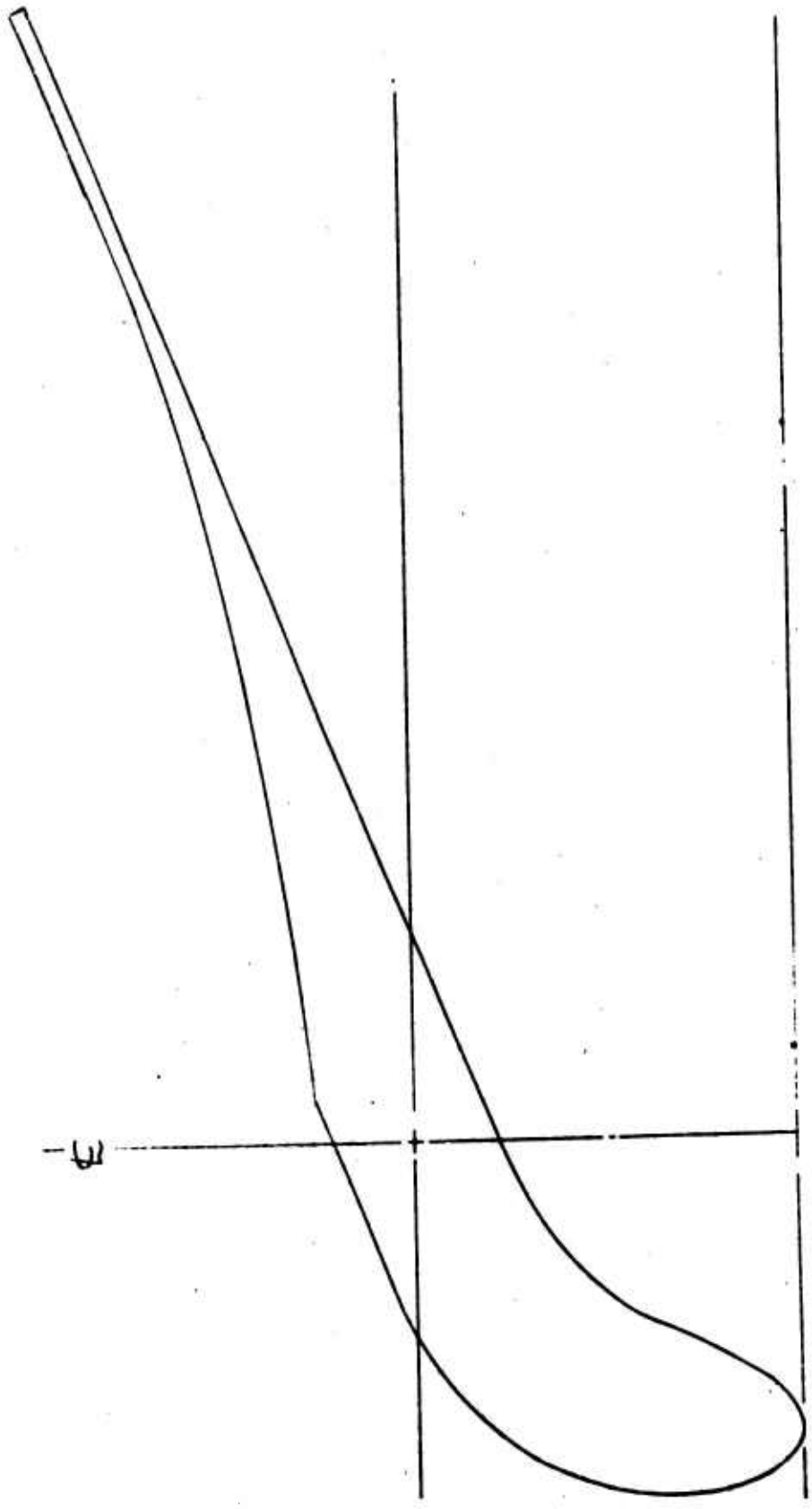

FIGURE A-3:PLANE SECTION, A-4 (Through $r/r_h = 1.05$)

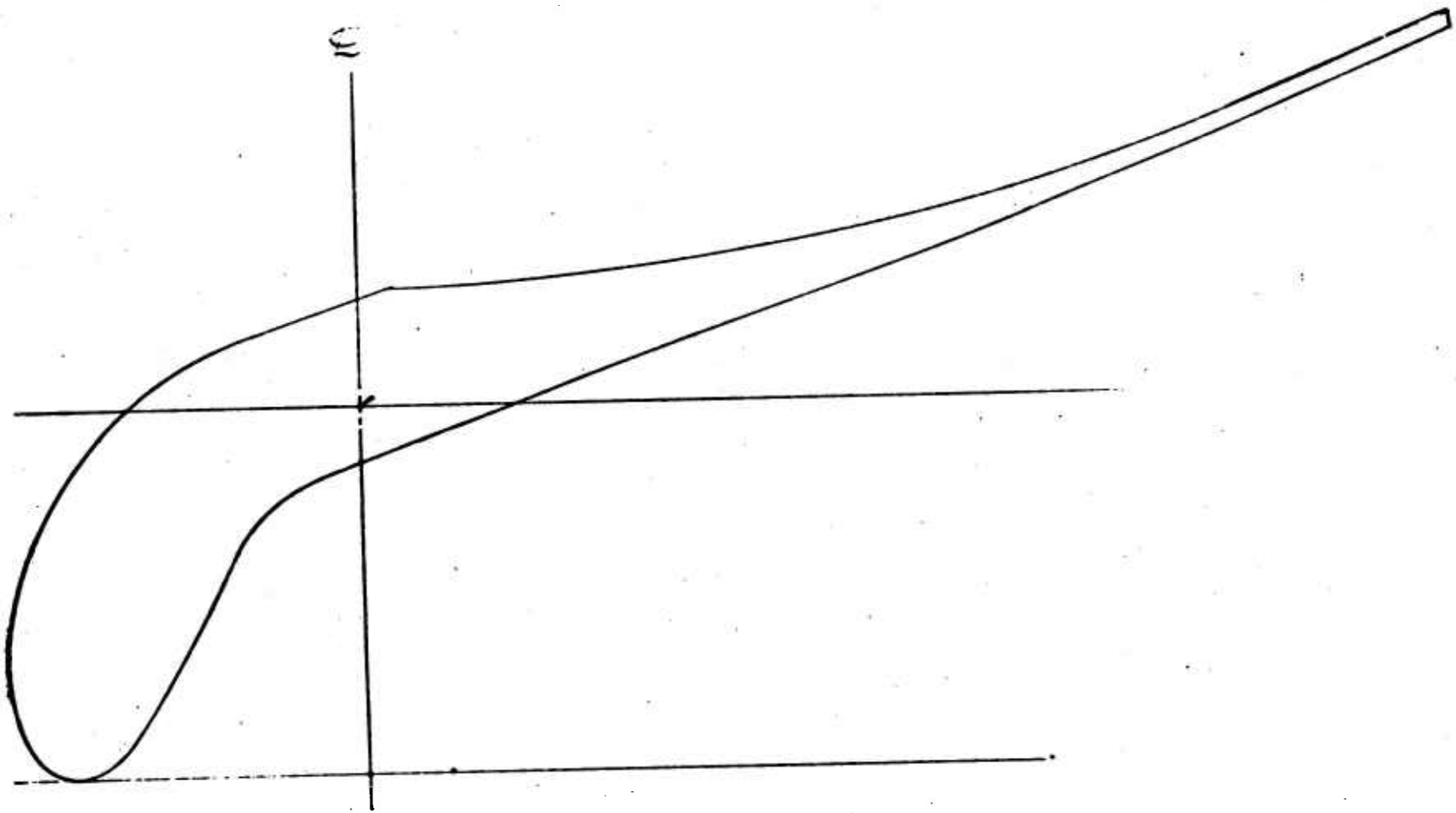

FIGURE A-4: PLANE SECTION, A-5 (Through $r/r_h = 1.0$)

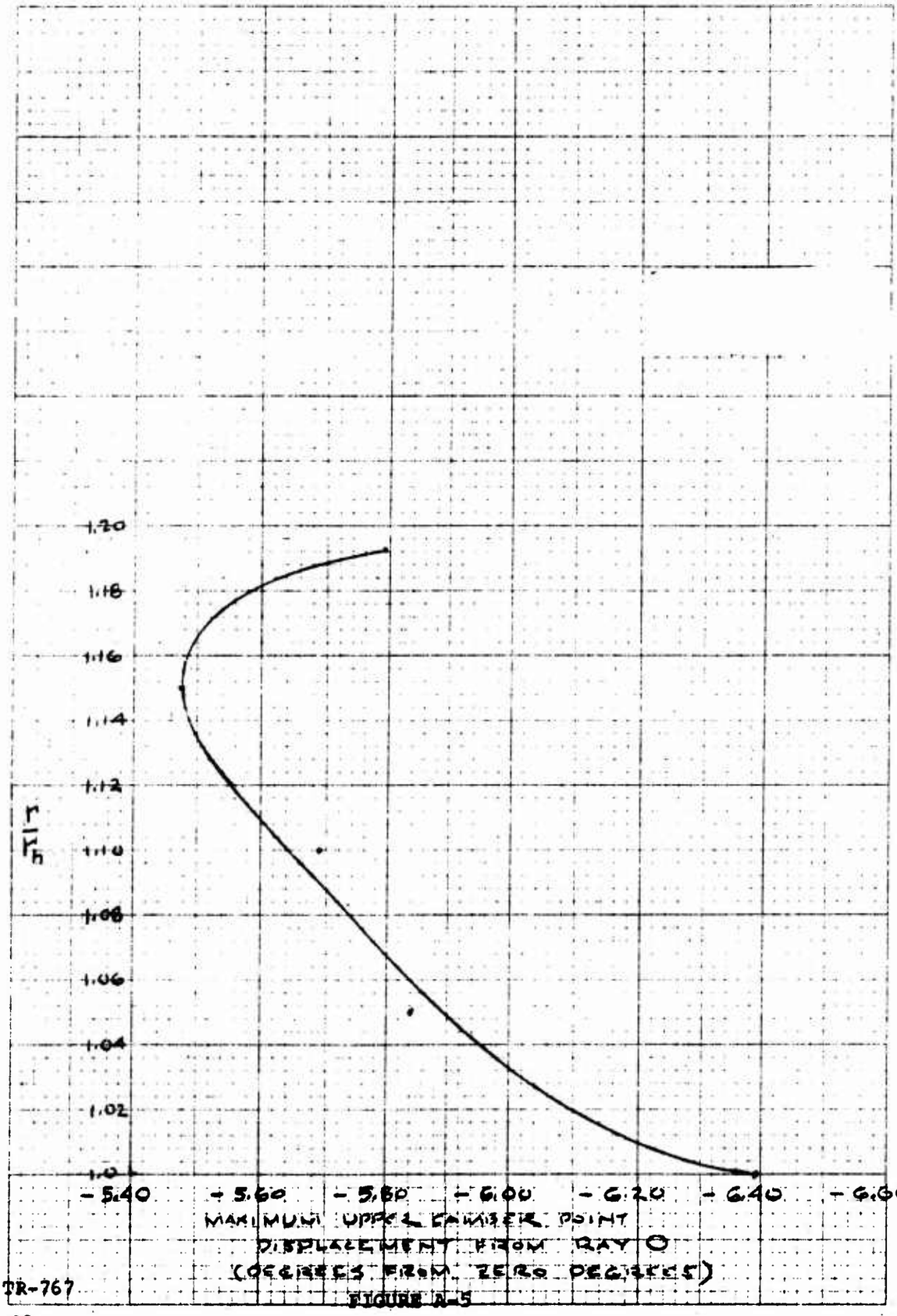
1.20
1.18
1.16
1.14
1.12
1.10
1.08
1.06
1.04
1.02
1.0
r/rh
-5.40
-5.60
-5.80
-6.00
-6.20
-6.40
-6.60
MAXIMUM UPPER CANISER POINT
DISPLACEMENT FROM RAY O
(DEGREES FROM ZERO DEGREES)

FIGURE A-5

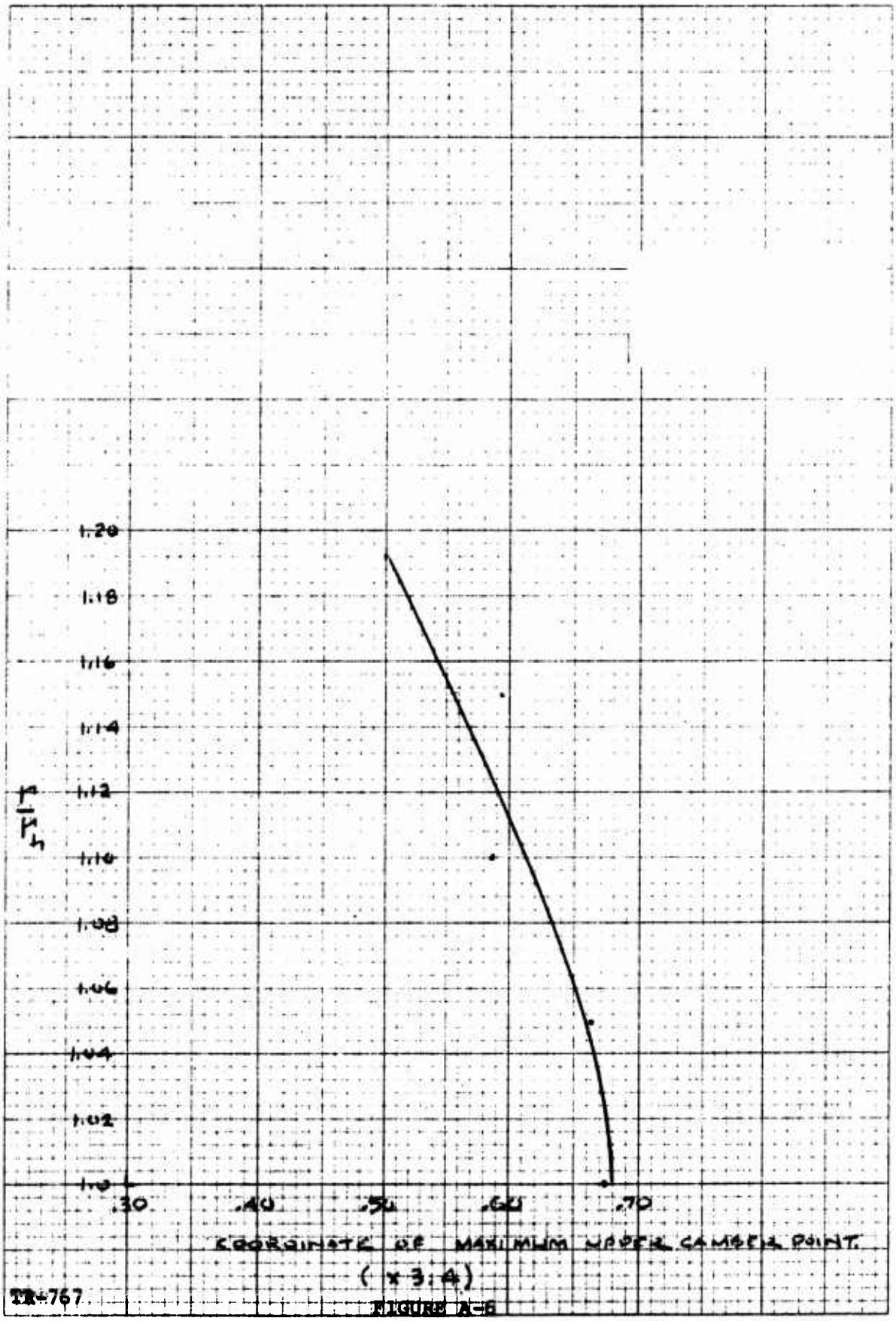

TR-767

FIGURE A-6

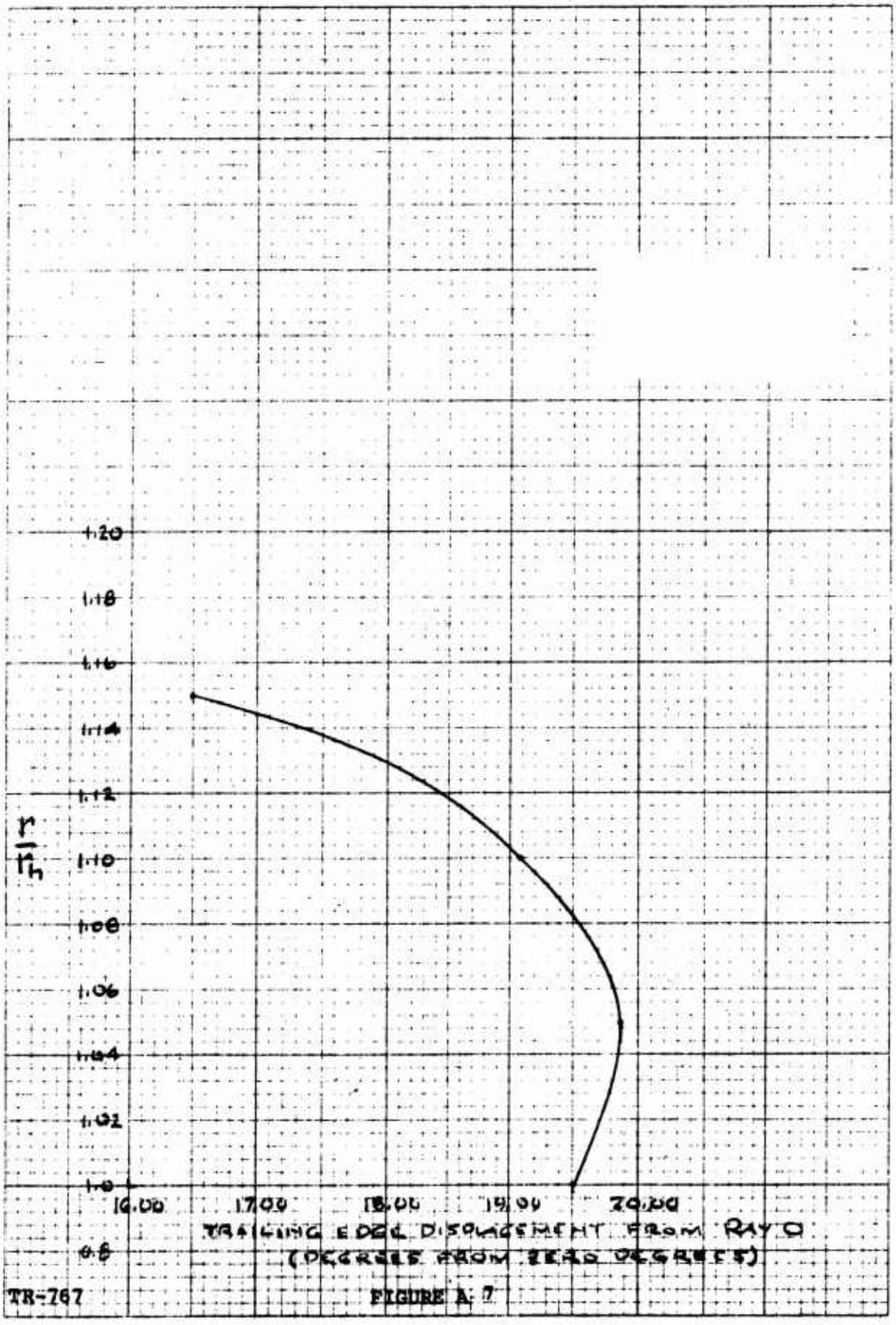

TR-767 FIGURE A-7

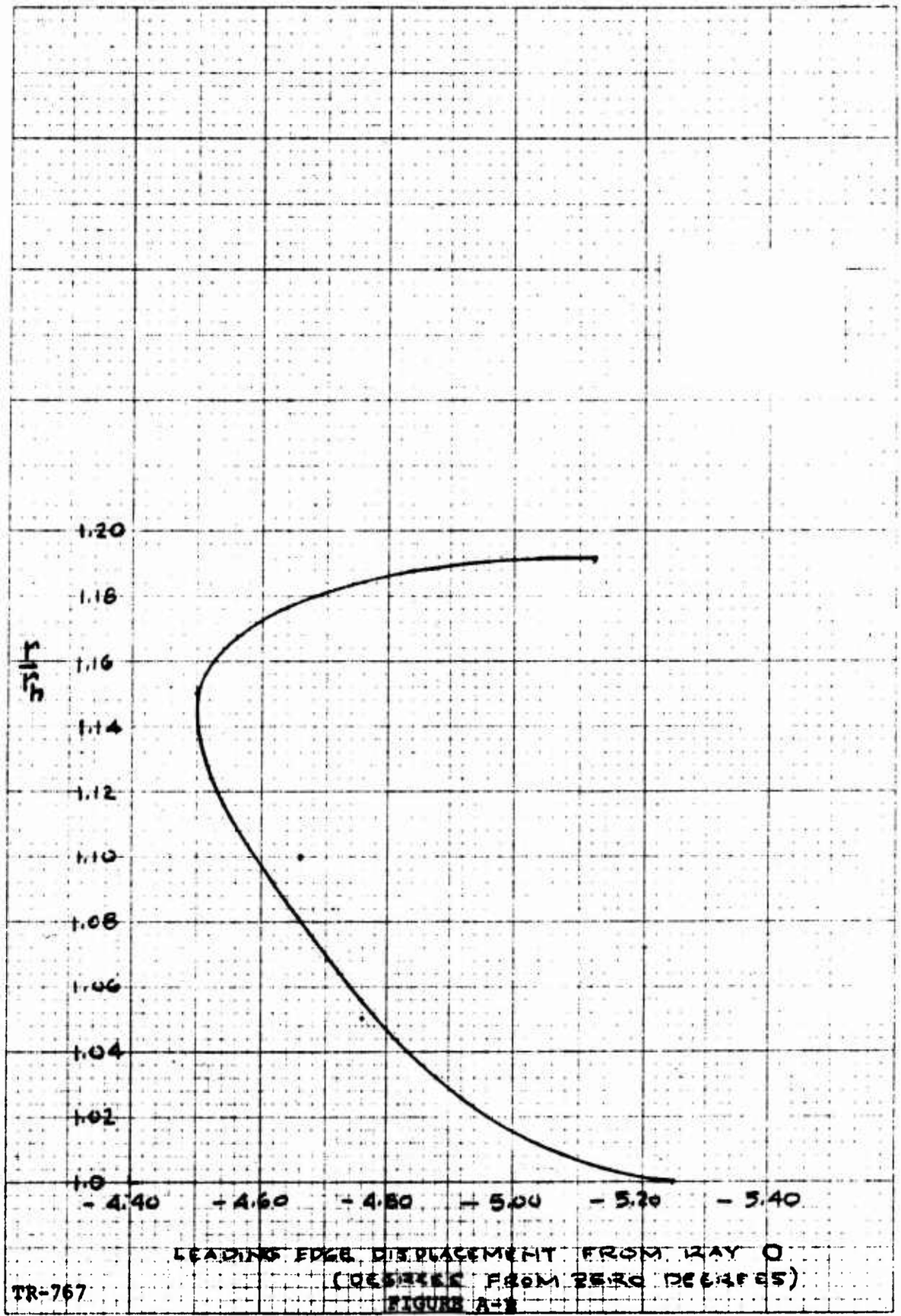

TR-767

FIGURE A-8

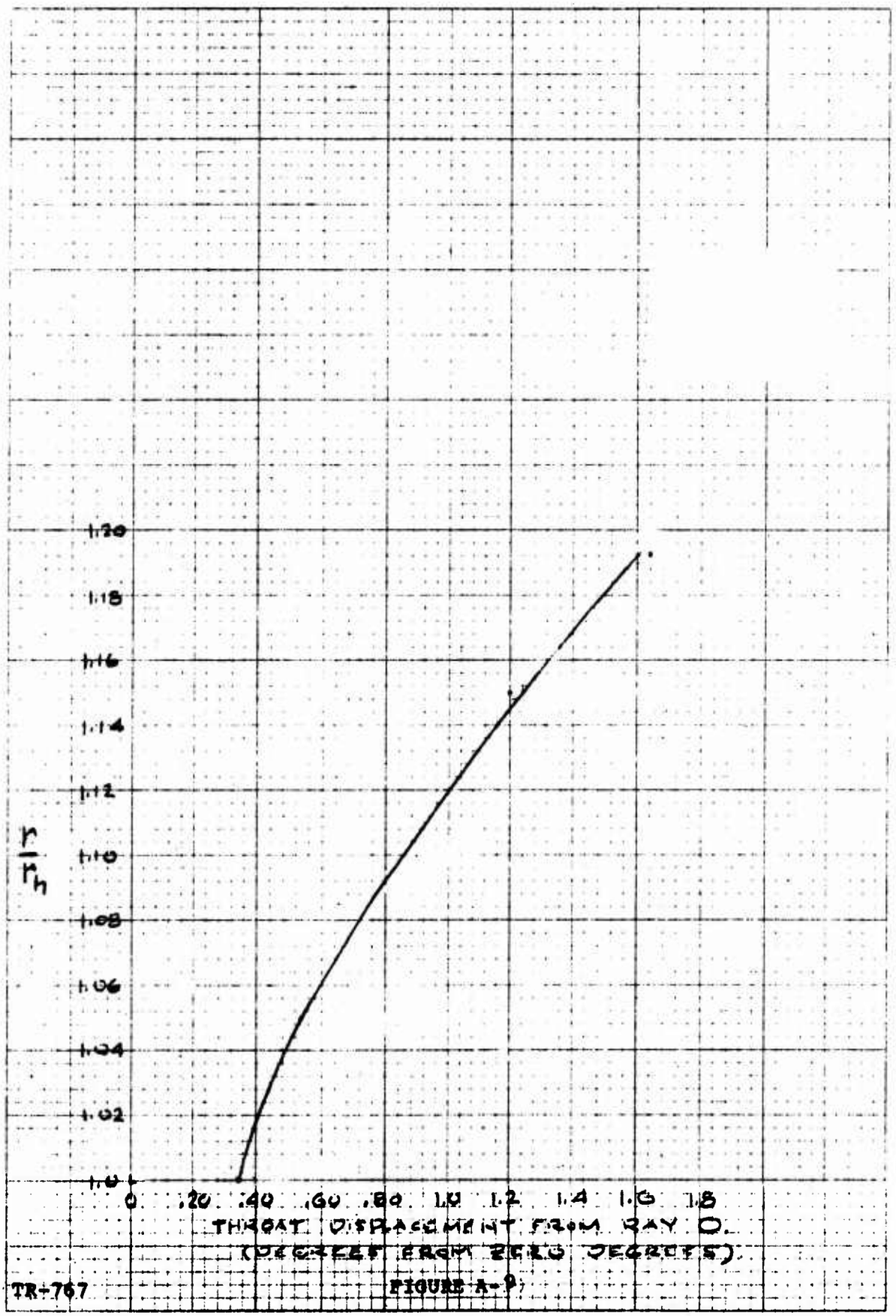

TR-767 FIGURE A-9

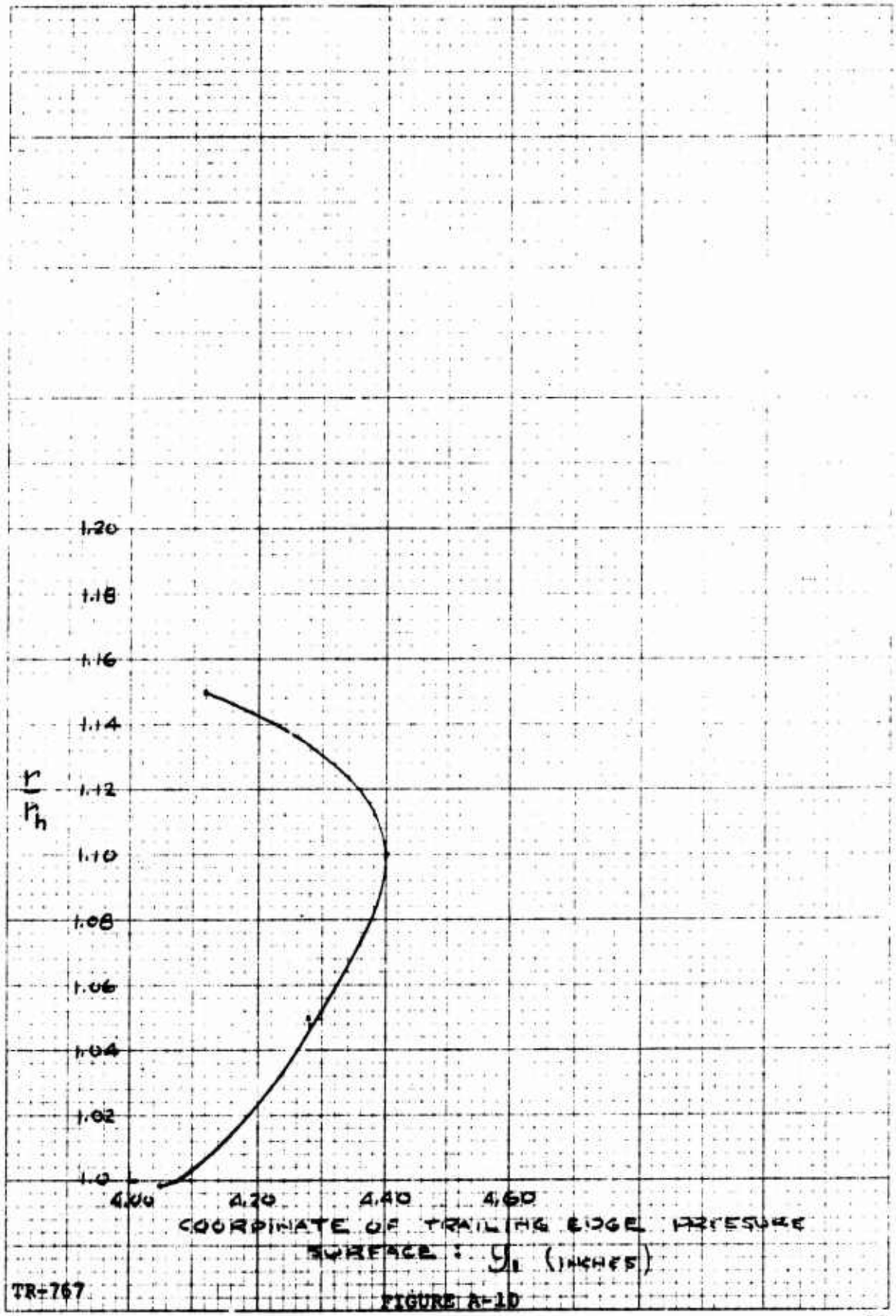

TR-767

FIGURE A-10

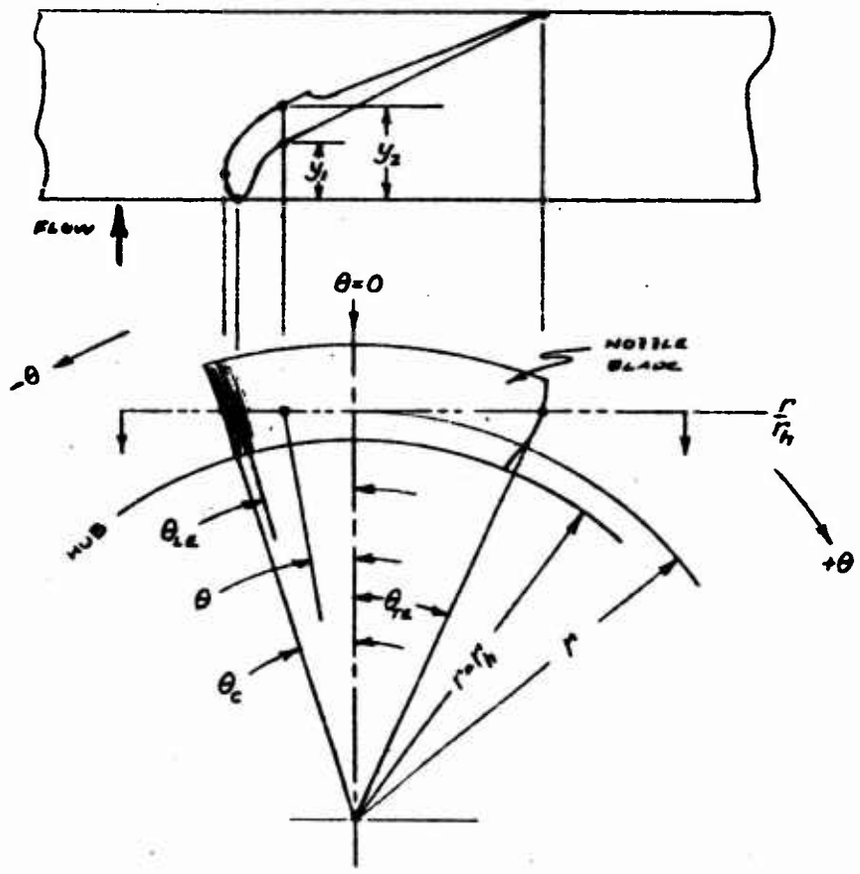

PITCH AT HUB, g_h = 1.31

NR. OF BLADES = 24

ANGULAR DISPLACEMENTS MEASURED FROM $\theta=0$ (REF.):

θ_c = TANGENT TO MAX. UPPER CAMBER

θ_{LE} = BLADE LEADING EDGE

θ_{TE} = BLADE TRAILING EDGE (ON y_1 OR PRESSURE SURFACE)

θ = POINTS ON SURFACES OF BLADE

y_1 = PRESSURE SURFACE

y_2 = SUCTION SURFACE

GENERAL APPLIED SCIENCE LABS.
WESTBURY, N.Y. 11590
W. PESCHKE

FIGURE A-11: Angular Displacements Measured From $\theta=0$

APPENDIX B

TRAVERSE PROBE ALIGNMENT

The problem considered here is one of deriving the geometrical relationships required to mount a traverse probe in such a way that its axis will be tangent to a stream surface of the exit flow and aligned with the swirling flow velocity vector, $\vec{V}$. The nomenclation is shown in Figure B-1.

The probe axis vector $\vec{T}$ is tangent to $\vec{V}$ at point a, which lies on the stream surface. The probe is to be traversed in the radial direction along the axis of its stem which is displaced downstream some distance z from the sensing head at point a. The stem axis vector $\vec{n}$ is thus normal to the cylindrical stream surface at point b. The desired result is the angle ψ between $\vec{n}$ and $\vec{T}$, which is given by

$$\cos \psi = \frac{\vec{n} \cdot \vec{T}}{|n| \; |T|}$$

Defining a rectangular coordinate system in the plane of $\vec{T}$, we first of all require that $\vec{T} \perp \vec{r}$ at a, or $\vec{T} \cdot \vec{r} = 0$. This is satisfied when $\vec{r}_a = (o, r, o)$ and $\vec{T}_a = (t \sin \varphi, o, t \cos \varphi)$. It is important to note that φ, the flow exit angle is defined as a spherical angle, since the original layout of the blading was along cylindrical stream surfaces.

Next, at point b, the normal $\vec{n}$ is given by $(r/\tan \theta, r_o, o)$ and $\vec{T}$ by $(t \sin \varphi, o, t \cos \varphi)$. Then

$$\vec{n} \cdot \vec{T} = \frac{r}{\tan \theta} t \sin \varphi$$

and

$$\cos \psi = \frac{\vec{n} \cdot \vec{T}}{|n| \; |T|} = \sin \varphi \sin \theta$$

The angle θ is given by $\frac{t \sin \varphi}{r}$, by its definition as seen in Figure B-1, and the final result is

$$\cos \psi = \sin \varphi \sin\left(\frac{t \sin \varphi}{r}\right)$$

For a probe length of 3.5 in. and an exit flow angle of 67°, this resulted in an angle between probe and stem of 120°, rather than the usual 90°.

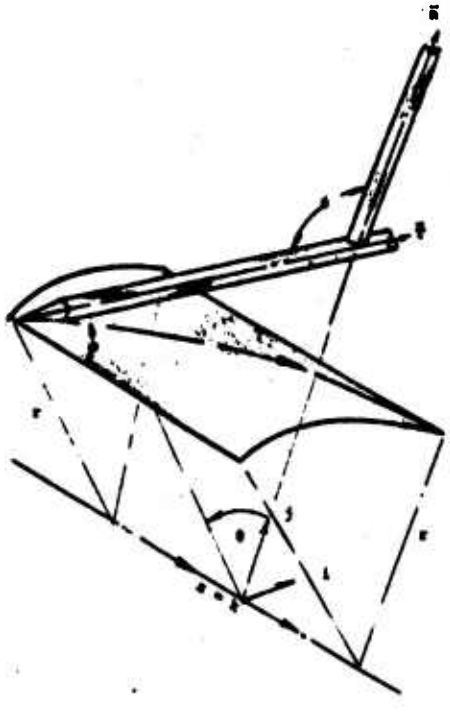

Figure B-1. - Traversing Probe Alignment Geometry

REFERENCES

1. Fruchtman, I., "Aerodynamic Design of Supersonic Turbines," GASL TR-731, (Final Report on Contract N00019-68-C-0598) Sept. 1969.

2. Lipfert, F. and Fruchtman, I., "Application Study for Supersonic Turbine," GASL TM-176, May 1970.

3. Fruchtman, I., "Cascade Performance of the Cooled Supersonic Turbine Blade," GASL TR-747, (Final Report on Contract N00019-70-C-0219), Nov. 1970.

4. Fruchtman, I., "The Supersonic-Turbine, A Design and Cascade Study," ASME Trans. 70-42.

5. Schlesinger, A. J., "Application of Linearized Characteristics to a Three-Dimensional Nozzle Flow," PIBAL Report No. 866, AF ARL 66-0107.

6. Goldman, L. J., "Experimental Investigation of a Low Reynolds Number Partial-Admission Single-Stage Supersonic Turbine, NASA TM X-2382, Oct. 1971.

7. Dunavent, J. C. and Erwin, J. R., "Investigation of a Related Series of Turbine-Blade Profiles in Cascade," NASA TN 3802, Oct. 1956.

8. Shapiro, A. H., The Dynamics & Thermodynamics of Compressible Fluid Flow, Vol. I, Ronal Press Co., 1953.

9. Vanco, M. R. and Goldman, L. G., "Computer Program for Design of Two-Dimensional Supersonic Nozzles with Sharp Edge Throat," NASA TM X-1502, January 1968.

10. Back, L. H. and Cuffel, R. F., "Turbulent Boundary Layer and Heat Transfer Measurements Along a Convergent-Divergent Nozzle," ASME Paper 71-HT-4.

11. Back, L. H., et al., "Some Observations on Reduction of Turbulent Boundary Layer Heat Transfer in Nozzles," AIAA J. 4, No. 12, Dec. 1969, pp. 2226-2229.

12. Ruptash, "Supersonic Wind Tunnels - Theory Design and Performance," UTIA Rev. 5, 1952.

13. Lipfert, F. and Genovese, J., "An Experimental Study of the Boundary Layer on Low Temperature Subliming Ablators," GASL TR-688, Feb. 1968.

14. Vahl, W. A. and Weirich, R. L., "Calibration of 30° Inducted-Angle Cone for Determining Local Flow Conditions in Mach Number Range of 1.51 to 3.51," NASA TN D-4679, Aug. 1968.

15. Foster, A. D., "A Compilation of Longitudinal Aerodynamic Characteristics Including Pressure Information for Sharp and Blunt Nose Cones Having Flat and Modified Bases," Sandia Monograph, SC-R-64-1311, Jan. 1968.

UNCLASSIFIED

Security Classification

DOCUMENT CONTROL DATA - R & D

(Security classification of title, body of abstract and indexing annotation must be entered when the overall report is classified)

1 ORIGINATING ACTIVITY (Corporate author) General Applied Science Laboratories, Inc. Merrick & Stewart Avenues Westbury, New York 11590	2a. REPORT SECURITY CLASSIFICATION UNCLASSIFIED 2b. GROUP n/a

3 REPORT TITLE

DESIGN AND DEVELOPMENT OF SUPERSONIC TURBINE NOZZLES

4 DESCRIPTIVE NOTES (Type of report and inclusive dates)

FINAL ENGINEERING REPORT for the Period October 1970-October 1971

5 AUTHOR(S) (First name, middle initial, last name)

FREDERICK W. LIPFERT
IRVING FRUCHTMAN

DISTRIBUTION LIMITED TO U.S. GOVERNMENT AGENCIES ONLY;

- ☐ FOREIGN [illegible]ATION
- ☐ PROPRIE[illegible]
- ☒ TEST A[illegible]ALUA[illegible]ON
- ☐ CONTRACT[illegible]

DATE: 7-14-72

OTHER REQUESTS FOR THIS DOCUMENT MUST BE REFERRED TO COMMANDER, NAVAL AIR SYSTEMS COMMAND, AIR-3308

6 REPORT DATE FEBRUARY 1972	7a. TOTAL NO. OF PAGES 92	7b. NO. OF REFS 15
8a. CONTRACT OR GRANT NO. N00019-71-C-0194 b. PROJECT NO. c. d.	9a. ORIGINATOR'S REPORT NUMBER(S) GASL TR-767 9b. OTHER REPORT NO(S) (Any other numbers that may be assigned this report)	

10 DISTRIBUTION STATEMENT Distribution of this report is controlled and each transmittal outside the DOD requires prior approval of the Commander, Naval Air Systems Command, Department of the Navy, Washington, D. C., 20360.

11 SUPPLEMENTARY NOTES	12. SPONSORING MILITARY ACTIVITY Department of the Navy Naval Air Systems Command Washington, D. C. 20360

13 ABSTRACT A nozzle (stator) component for a supersonic turbine stage has been designed and tested. The design was three-dimensional, with the nozzle exit Mach number varying from 1.68 at the hub to 2.23 at the tip, according to simple-radial-equilibrium theory. The hub/tip ratio was .83, and the aspect ratio .35, with a 1-inch blade height. The supersonic contour was based on the Busemann sharp-edged-throat concept.

The nozzle was tested over a range of pressure ratios from 1.9 to 10.5 and Reynolds numbers from $.65 \times 10^6$ to 3.8×10^6, based on exit conditions and the blade chord. A blow-down wind tunnel was used, with atmospheric discharge. The performance of the nozzle corresponded well to theoretical predictions in the regions of the exit flow that were traversed and along the walls where pressure taps were installed. The test program was terminated before a complete map of the exit flow had been obtained, because of vibratory cracks in some of the blades.

DD FORM 1 NOV 65 1473

UNCLASSIFIED

Security Classification

14 KEY WORDS	LINK A		LINK B		LINK C	
	ROLE	WT	ROLE	WT	ROLE	WT
Supersonic Nozzle						
Turbine						
Wind Tunnel Testing						
Annular Cascade						
Radial Equilibrium						